Fabrication of Plasmonic Probes and Composites for Surface Enhanced Raman Scattering (SERS) Investigation of Commercial Inks and Food Contaminants

by

Abeer Alyami

Ollscoil na hÉireann

NATIONAL UNIVERSITY OF IRELAND

A thesis submitted to the Faculty of Science, Engineering and Food Science for the degree of Doctor of Philosophy in Chemistry

University College Cork

May 2019

Head of School Dr. Humphrey Moynihan

Supervised by Dr. Daniela Iacopino

Tyndall National Institute

University College Cork

Declaration

The work presented in this thesis is my own work except for the fabrication of the vertical arrays of Au nanorods stamped on SiO_2 substrate of **Figure 54** ***a,*** which has been done by Dr. Alfonso Martin. This is to certify that the work I am submitting is my own and has not been submitted for another degree, either at University College Cork or elsewhere. All external references and sources are clearly acknowledged and identified within the contents. I have read and understood the regulations of University College Cork concerning plagiarism. The present thesis is submitted for the degree of Doctor in Philosophy at University College Cork.

Head of the UCC Chemistry Department	Dr. Humphrey Moynihan
External examiner	Dr. Katherine Curran
Internal Examiner	Dr. Lynette Keeney
Supervisor	Dr. Daniela Iacopino

Signature _____

Date _____

Table of Contents

Abstract

This thesis investigates the use of different Surface Enhanced Raman Scattering (SERS) substrates for commercial inks analysis and food contaminants detection. Metal nanostructures with different plasmon frequencies have been used as SERS nanoinks for identification of dye content in blue ball-point pens. Excitation wavelengths 514 nm and 785 nm were applied with Ag nanosphere inks and Au nanorods, respectively, providing complementary information and showing significantly enhanced SERS signals compared to Raman analysis. Dense plasmonic Ag nanopastes are another kind of SERS probe that was fabricated in this thesis and used in the SERS investigation of different color ball-point pen inks. Colored ballpoint pens were analyzed using Raman bench instrumentation with 514 nm laser illumination and handheld Raman instrumentation with 785 nm laser illumination in order to elucidate the dye content in the pen ink mixtures. Other complementary analytical techniques such as UV-Vis spectroscopy and thin layer chromatography (TLC) were used for the dyes identification and to confirm results of SERS investigation. Finally, immobilized Ag particles on rigid and flexible substrates (glass and PDMS) were used as minimally invasive SERS composites, and model molecule 4-aminobenzenethiol (4-ABT) was used to test their SERS enhancement. The Ag NPs/PDMS flexible composites were applied to the in-situ SERS analysis of food contaminants and as micro-extraction films to extract pollutants from fish and fruit surfaces for ex-situ analysis. The SERS results reveal great potential for easy sampling of objects with irregular surfaces or samples with matrix that shows strong background signal. While the non-invasiveness of such probes for heritage conservation applications was not extensively tested, preliminary promising non-destructive results on mock up paper drawings were achieved, showing great potential for in situ SERS analysis of arbitrary analytical surfaces..

Acknowledgements

I would like to thank everyone who supported and assisted me throughout this project, especially my supervisor Dr Daniela Iacopino for her guidance and help with the project and by giving me the opportunity to attend and present my work at international conferences. Also, I would like to express my gratitude to Dr Aidan Quinn for adapting me in the Nanotechnology group in Tyndall National Institute. Also, I want to thank my colleagues in the nanotechnology group and in the chemistry department in UCC.

Thanks to my beloved husband Yousef, who was the only family for me in Ireland, for his support and being always there for me, without you I would not have been able to go the journey. Also, I would like to thank my brothers, my sisters and my sweet niece Alzahra, for all their support and love.

Finally, I want to express my thanks to my dear uncle Mohammed, your support has been invaluable to me.

Abeer Alyami

This dissertation is dedicated to my parents Yousef and Fatimah, and I hope that this achievement will complete the dream that you had for me all those many years ago when you chose to give me the best education and support you could.

Chapter 1

Introduction

In this chapter an overview of the previous literature on which the thesis is based is given. Specifically, an initial overview of plasmonic particles and their properties is given. Chemical methodologies for synthesis and phase transfer of Ag nanoparticles and Au nanorods are presented, along with different methods for assembling of nanoparticles into substrates are covered. This chapter also presents an overview of Raman spectroscopy and Surface Enhanced Raman Scattering (SERS) and applications of both techniques in commercial inks characterization and food contaminants detection. Finally, objectives of thesis are outlined and described in detail.

1.1 Noble metal nanostructures

Noble metal nanoparticles have been used since ancient times to obtain beautiful colors in cups, stained glass and potteries. The first known example of use of such nanomaterials is the Lycurgus cup (IV century). The cup is green when illuminated from the outside and red when illuminated from the inside, due to the presence of gold nanoparticles. The colour of stained glass in medieval churches across Europe (**Figure 1**) was also obtained by adding metal nanoparticles to glass in its molten state. The early alchemist were also fascinated by these materials and tried to produce potable gold, ‘‘the elixir of life’’ as they considered gold as indestructible and to have enormous medicinal importance. Between 1493 and 1541 alchemist Paracelsius claimed to have invented Aurum Potabile (drinking gold). In1856, Faraday hypothesized that the colour of ruby glass and its aqueous solutions of gold (mixed with either SO_3 or phosphorus), was due to finely divided gold particles. The term “colloid” was invented later in 1861 by T. H. Graham. In 1925 Richard Zsigmondy was awarded the Nobel prize for his work on the synthesis and interpretation of gold nanoparticle properties. [1, 2]

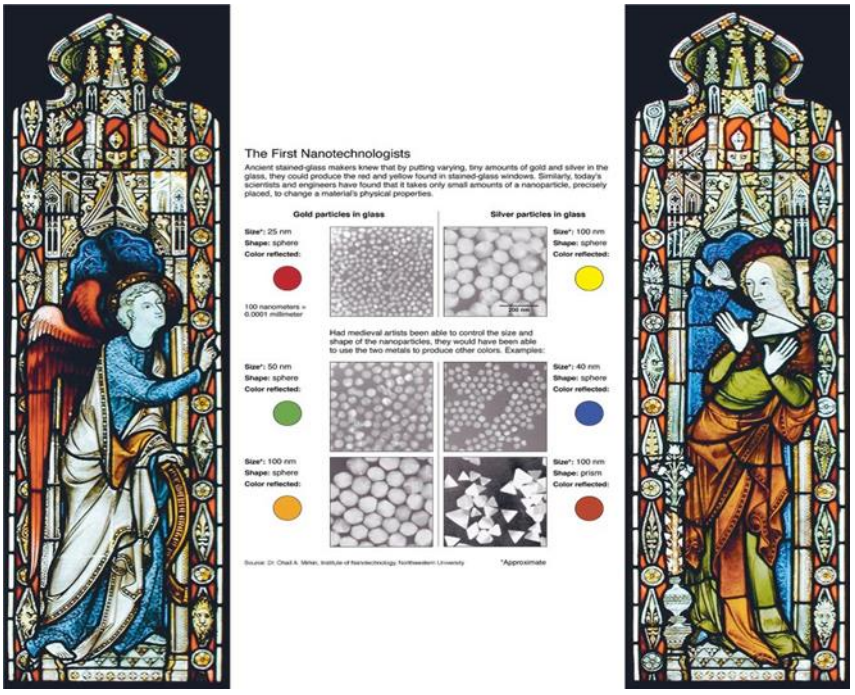

Figure 1. *Picture of stained-glass windows glass in medieval churches, adapted from The New York Times, February 22, 2005.*

However, the systematic investigation of nanomaterial optoelectronic properties started

later. Gustav Mie's 1908 paper represents the first rigorous theoretical investigation of the optical properties of spherical metal particles[3, 4]. Mie's theory yielded extinction coefficients for nanoscopic gold particles which compared well with the experimental spectra of gold sols and unlike Maxwell Garnett theory, was applicable to spheres of any size. Mie scattering theory is still applied today.

1.1.1 Localized surface plasmon resonance

Metal nanostructures gained scientific attention following developments in the understanding of their unique properties. In such small size particles the conduction band free electrons of the metal undergo displacement relative to the nuclei as result of interaction with the resonant electromagnetic field of incident light. Such displacement causes the metal core to create Coulomb restoring forces (the attraction between valence electron and the positively charged ionic core) which results in generation of oscillating electric fields (surface plasmon).The oscillating electrons on the particle surface create surface plasmon polaritons (SPPs) or localized surface plasmon resonance (LSPRs). The former be created at planar surfaces and the latter at the surface of small particles (smaller than the wavelength of light)[5]. There are many factors that can affect LSPR property, including nanoparticle shape, size, aspect ratio, composition, and the refractive index and local dielectric environment of the medium particles imbedded in[6, 7].

While spherical particle have one oscillation mode appearing in the visible region of the spectrum (**see Figure 2 a**), asymmetrical metal nanostructures having axes of different lengths such as rods, are characterized by two plasmonic modes (**see Figure 2 b**): longitudinal associated to electron oscillations along the long axis and appears in the near infrared region of the UV-Vis absorbance spectrum, and transversal associated to electron oscillations along the short axis and appears in the visible region of the spectrum.

Half a century after Faraday discovery, Gustav Mie [8] published paper in 1908 to explain change in gold solutions' colors related to their sizes. That paper included the theoretical explanation of Maxwell's equation which allowed understanding the interaction between light and small spherical particles. Although, Mie himself did not consider his theory at that time more than application of Maxwell equation, his theory constituted a breakthrough in mathematical physics[9].

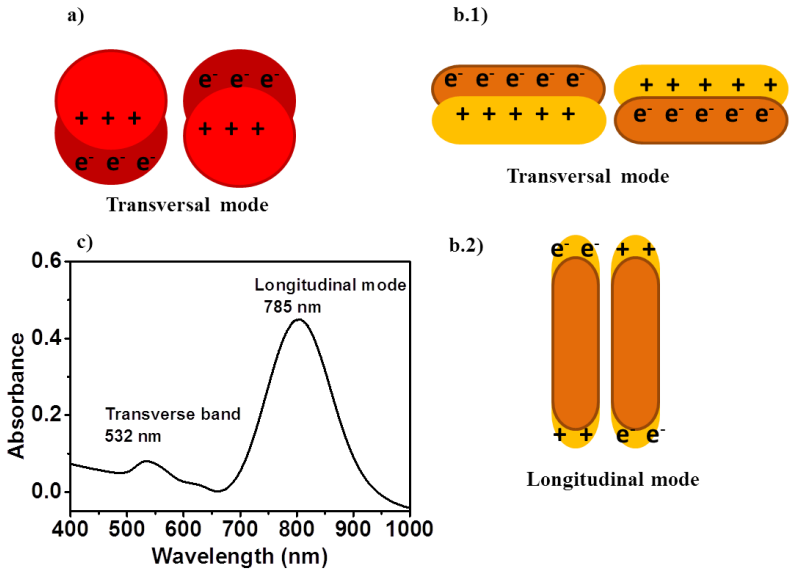

Figure 2. *Schematic of the plasmonic electron oscillations of* ***a)*** *nanoparticles and* ***b)*** *nanorod ;****c)*** *UV-vis absorbance spectra of gold nanoparticles.*

By following Maxwell computation, surface plasmon resonance can be calculated for spherical particles.

Considering that nanoparticles have dimensions much smaller than the wavelength of light (dipole approximation), scattering and extinction cross sections σ_{Sca} and σ_{ext} can be readily calculated by the equations 1and 2 below:

$$\sigma_{ext} = \frac{18\pi\varepsilon_m^{3/2}V}{\lambda} \frac{\varepsilon_2\,(\lambda)}{[\varepsilon_1(\lambda) + 2\varepsilon_m]^2 + \varepsilon_2(\lambda)^2} \qquad \text{(eq 1)}$$

$$\sigma_{Sca} = \frac{32\pi^4\varepsilon_m^2V^2}{\lambda^4} \frac{(\varepsilon_1 - \varepsilon_m)^2 + (\varepsilon_2)^2}{[\varepsilon_1 + 2\varepsilon_m]^2 + (\varepsilon_2)^2} \qquad \text{(eq 2)}$$

- where λ = the incident wavelength,
- ε_m= the dielectric constant of the medium
- $\varepsilon_1$and ε_2 are the dielectric functions of the metal
- V= the volume of the spherical particles

Then the absorption cross section can be calculated using the extinction and the scattering cross-section of the nanoparticle equation:

$$\sigma_{abs} = \sigma_{ext} - \sigma_{sca} \quad \text{(eq 3)}$$

In equation 1 and 2, it can be seen that σ_{sca} is proportional to the nanoparticle volume square V^2 (i.e. large particles scatter the incident light mostly) while σ_{ext} is proportional to V (i.e. small particles absorb the incident light mostly). As well as the volume, the dielectric function of the complex environment of the metal nanoparticles impact the scattering and absorbance values (abilities). The dielectric function of metal nanoparticles is represented in equation 4, where ε_1 is the real part of the complex permittivity and ε_2 is the damping coefficient:

$$\varepsilon(\lambda) = \varepsilon_1(\lambda) + i\varepsilon_2(\lambda) \quad \text{(eq 4)}$$

In addition, the dielectric function of the medium ε_m where the particles are embedded in is an important part of the dielectric environment and it does affect the plasmon resonance. The extinction is maximized at the resonance wavelength, when the denominator in eq. 1 is minimized, i.e. when the equation is fulfilled.

$$\varepsilon_1(\omega) = -2\varepsilon_m \quad \text{(eq 5)}$$

Therefore ε_1 (the real part of the complex permittivity) determines the wavelength at resonance conditions while ε_2 determines the width of the plasmon band. The plasmonic band is determined by both $\varepsilon_1\varepsilon_2$ values which are dependent on the refractive index and the absorption coefficient. (ω) is the resonance frequency that can be calculated from equation (5). Mie's theory can be used to calculate the plasmon resonance of spherical particles. However, for non-spherical particles such as nanorods, Gans' module [10] (derived from Mie's theory) is followed. Considering that nanoparticles have dimensions much smaller than the wavelength of light (dipole approximation), the σ_{Sca} and σ_{ext} for ellipsoid particles will be[10]:

$$\sigma_{abs} = \frac{2\pi V}{3\lambda}\varepsilon_m^{3/2}\sum_{j=1}^{3}\frac{\left(\frac{1}{P_j^2}\right)\varepsilon_2}{\left[\varepsilon_1 + \frac{(1-P^j)\varepsilon_m}{P^j}\right]^2 + {\varepsilon_2}^2} \quad \text{(eq6)}$$

$$\sigma_{sca} = \frac{8\pi^3 V^2}{9\lambda^4} \varepsilon_m^2 \sum_{j=1}^{3} \frac{1}{{P_j}^2} \frac{(\varepsilon_1 - \varepsilon_m)^2 + {\varepsilon_2}^2}{\left[\varepsilon_1 + \frac{(1-P^j)\varepsilon_m}{P^j}\right]^2 + {\varepsilon_2}^2} \qquad \text{(eq 7)}$$

The depolarization factors P_j along the main axes of the ellipsoid is defined by:

$$P_A = \frac{1-e^2}{e^2}\left[\frac{1}{2e}\ln\left(\frac{1+e}{1-e}\right) - 1\right] \qquad \text{(eq 8)}$$

$$P_B = P_c = \frac{1-P_A}{2} \qquad \text{(eq 9)}$$

W the eccentricity E calculated from the length l and diameter d of the ellipsoids:

$$e = \left(\frac{L^2 - d^2}{L^2}\right)^{\frac{1}{2}} \qquad \text{(eq 10)}$$

In case of a spherical particle the eccentricity is zero and the polarization factors for all axes become 1/3, which leads back from *eq. 6* and *eq. 7* to *eq. 1* and *eq. 2*.

1.2. Approaches to synthesis metal nanostructures

The synthesis of metal nanostructures with controlled shape, size and chemical composition is of paramount importance as the optical, electronic, chemical and physical [11-13] properties of the fabricated nanoparticles are completely dependent on those parameters. The focus of the next few paragraphs will be on the description of the most used chemical methods for synthesis of metal nanostructures. In particular, the seed mediated method for Au nanorods synthesis and the chemical reduction approach for Ag particles will be described.

1.2.1. Seed mediated synthesis of Au nanorods

Reduction conditions of Au nanorods formation enabling the size control of nanorods

were first discovered in 2002 by Murphy et al.[14] and developed by El-Sayed et al.[15] .The fabrication of Au nanorods through the seed mediated method (**Figure 3**) is performed in two steps. First, a Au precursor (chloroauric acid) is reduced by the addition of strong reducing agent sodium borohydride to obtain gold seeds (Au^0 nanoparticles 4 nm in diameter) in presence of CTAB capping agent. The capping agent is adsorbed on the surface of the seeds (or nanoparticles in general). Its role is to control particle growth and final particle size; also the capping agent keeps particles in solution by preventing particles to collapse into each other. In the second step a growth solution of chloroauric acid is reduced to Au^I by mild reducing agent (ascorbic acid) in the presence of CTAB and Ag ions (silver nitrate). As will explain in more detail in the next paragraph, Ag ions play a fundamental role in regulating the size of the final nanorods. Finally, Au^0 seeds are added to the growth solution and lead to the formation of Au nanorods (7 × 14 nm).

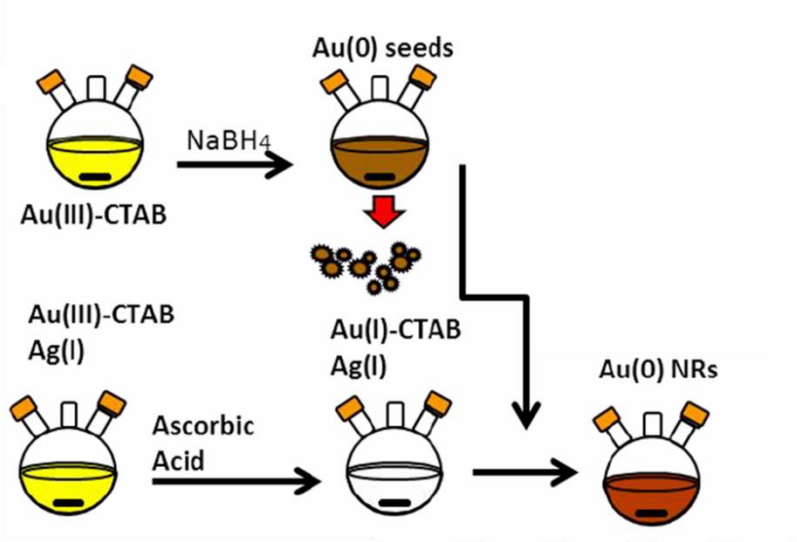

Figure 3. *Schematic of the two steps seed mediated synthesis of Au nanorods.*

In the developed method control of the nanorod's length was achieved by control of the Ag ion content. The mechanism by which Ag^+ controls the shape of nanorods is not fully understood yet. However, one reported hypothesis[14] suggests that Ag^+ formed AgBr with the CTA^+ counter ion (Br^-) and adsorbed on the Au rod surface restricting its growth. The second and most accepted theory[16] suggests that Ag^+ undergo an under-potential deposition on the {110} crystallographic facets of the seeds leading to an anisotropic growth of the {111} facets (see **Figure 4**).

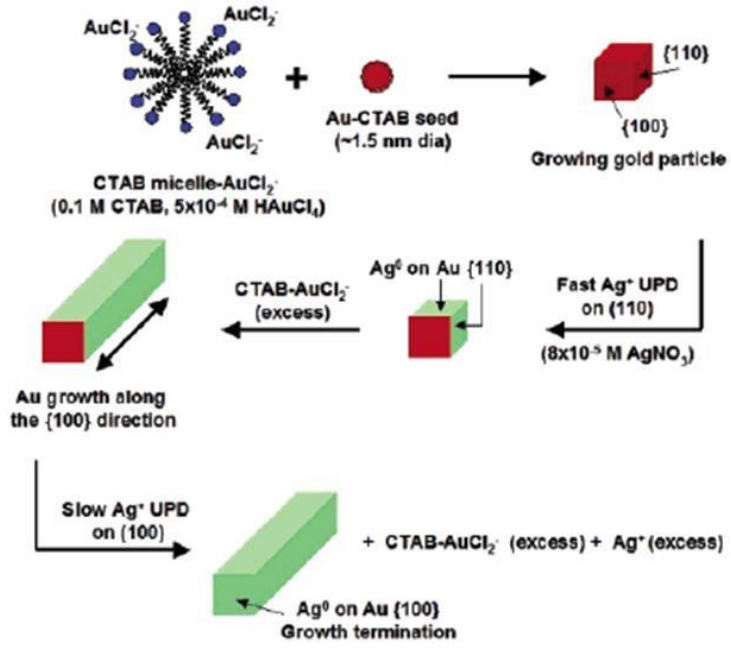

Figure 4. *Hypotetic underpotential deposition of the Ag^I cations in the {110} facets of the seeds leading to the synthesis of Au nanoords by anisotropic growth.*[17]

Although, Ag^+ is essential for formation of Au nanorods of controlled aspect ratio, it is also a double-edged sword. In fact, an excess amount of $AgNO_3$ (more than 0.12 mM) can lead to a decrease of nanorod length[15], whereas its absence results in low yield of rod formation (10-20% of total particles).[14] The controlled use of CTAB capping surfactant and Ag^+ resulted in less than 1% formation of by-products in the developed seed mediated method.

1.2.2. Chemical reduction synthesis of Ag nanoparticles

The method of obtaining Ag colloids from chemical reduction of Ag salts in the presence of sodium citrate was first proposed back in 1887 by M. C. Lea [18] through a photochemical method. In 1951 Turkevich[19] reported the synthesis of Au nanoparticles by reduction of Au salts in boiling aqueous solution with citrate anions, which were used both as reducing and capping agents. Following Turkevich's method, Ag nanoparticles fabrication was achieved with a similar approach [20-22].

Ag particles are fabricated by chemical reduction of Ag salts using tri sodium citrate as the reducing agent in two phases: nucleation and growth (**Figure 5**). The process includes the use of metal precursor, reducing agent and stabilizing or capping agent. Silver ion Ag^+ is reduced to Ag^0 in the presence of reducing agent. Nucleation phase begins when the

concentration of Ag^+ increases, the dissolved ions tie together and fabricate a steady surface. The larger the surface, the more stable i.e. energetically favorable due to the low surface to volume ratio. Nucleation step ends when no more Ag^+ is supplied in the solution and as a result the dissolved ions in the solution diffuse through solution and adsorb on the initial nucleus resulted in the growth step (Ostwald ripening) [23]. Then the reduced Ag particles need to be surface stabilized to avoid further growth and aggregation formation and that is achieved by addition of stabilizing/capping agent, which adsorbs on the nanoparticle surface preventing further particle adsorption and stopping further growth by reduction of surface energy[24, 25]. By modifying the reducing agent and the stabilizing/capping agent quantities, different degree of size and shape control is achieved.

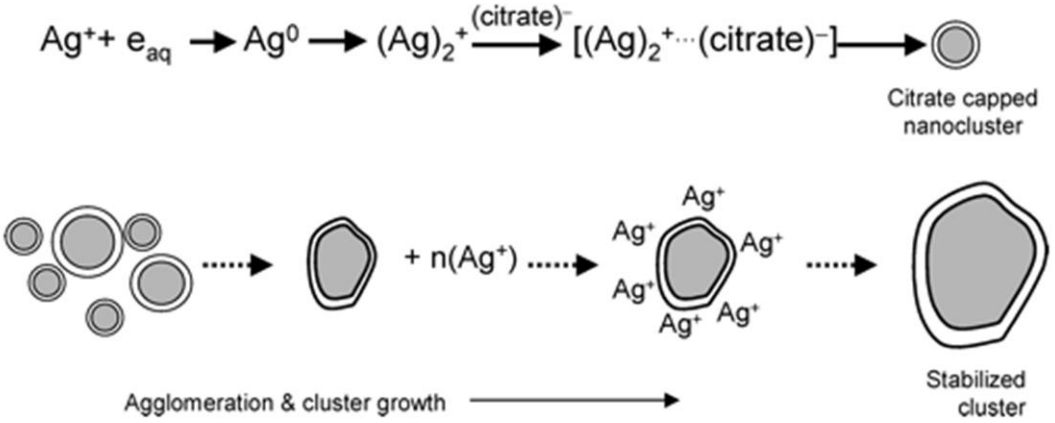

Figure 5. *Nucleation and growth steps in the formation of Ag nanoparticles.* [21].

The role of the reducing agent in size and shape distribution control can be attributed to the resulting reduction rate. By using weak reducing agent such as citrate the reduction rate is low and that enables simultaneous Ag nuclei formation and old nuclei growing resulting in low monodispersity. To the contrary, the time between new nuclei formation and old nuclei growth is significantly reduced with a strong reducing agent as sodium borohydride, due to the higher reduction rate created.

On the other hand, the initial concentration of Ag salt plays an important role in the resulting concentration of Ag nanoparticles. In **Figure 6**, Lee *et al.*[26] illustrate the relationship between the concentrations of the Ag precursor and the resulting Ag nanoparticles: the higher the concentration of $AgNO_3$, the higher the concentration of the formed Ag nanoparticles.[27-29]

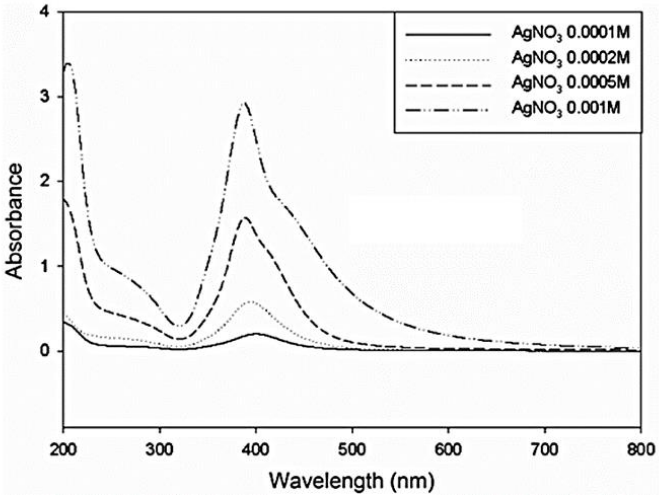

Figure 6. *UV/vis absorption spectra of Ag nanoparticles prepared via reduction of $AgNO_3$ with different initial concentrations.*[26]

1.3. Phase transfer of Ag nanoparticles and Au nanorods

Transferring metal nanostructures from aqueous phase into organic phase is often needed to achieve many properties: avoiding consuming expensive organic precursors and chemicals, obtaining better dispersion and deposition of nanostructures for better self-assembly formation purposes, due to the low interaction forces provided by the lower surface tension and dielectric properties of organic solvents.[30]

Different methods have been developed to transfer Au and Ag nanostructures from water to different organic solvents. Chen et al.[31] reported a method to transfer positively charged Au rods synthesized through seed-mediated method. In this approach the surface of Au nanorods was modified by mercaptosuccinic acid (MSA) and subsequently the amphiphilic tetraoctylammonium bromide (TOAB) was added, which promoted the passage of nanorods into organic medium by formation of an ionic interaction with MSA. **Figure 7** shows the successful transfer of Au nanorods into organic phase. On the other hand, when Au nanostructures were capped with negative charge surfactants (e.g. tiannic acid), the need for using bridge molecules (MSA) was eliminated as the positively N group of TOAB was able to attach on the negatively surface of the nanorods and its four hydrophobic alkane chains were capable pull the Au nanostructures onto the organic phase easily.

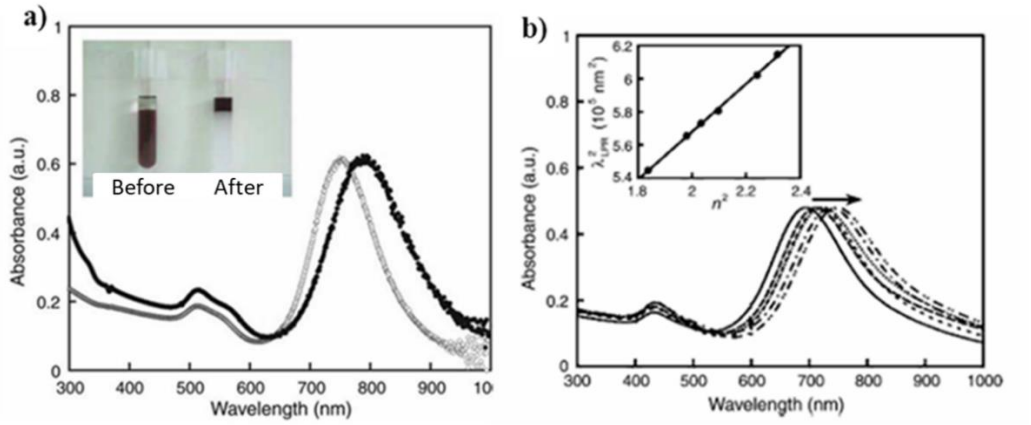

Figure 7. a) *UV–vis absorption spectra of Au nanorods before (grey)and after (black) phase transfer (toluene). The inset is photography of Au nanorods before (left tube) and after (right tube) phase transfer.* ***b)*** *UV-vis absorption spectra of Au nanorods in different organic solvents. Solid line, ether; long dashed line, tetrahydrofuran; short dashed line, cyclohexane; dotted line, chlorotoluene. The pointer shows the direction of increasing refractive index of solvent. The inset shows a typical plot of* λ_{LPR}^2 *vs. n2. n is the refractive index.* [31]

Phase transfer of metal nanostructures is dependent on many factors: size of metal nanoparticles[32], charge of metal nanoparticles [33], and surfactant used to cap the metal nanostructures[34]. **Figure 8** shows reported experimental results[35] confirming that the phase transfer by interaction of TOAB with the negatively charged Au nanoparticles was size-dependent, as the smaller the particle, the higher the transfer efficient was. The failure of transferring of large size (10 nm) Au nanoparticles into toluene organic phase was attributed to the surface area to volume ratio effect, as the large particles possess lower surface to volume ratio resulting in less adsorption of TOAB molecules i.e. less hydrophobic forces and vice-versa.

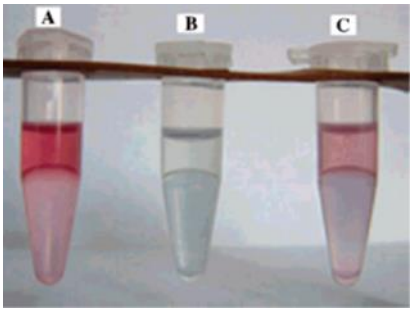

Figure 8. *Photography of phase transfer of different sizes of Au nanoparticles from water (top layer) into toluene (bottom layer);* ***a)*** *Au nanoparticles 5 nm* 10^{-4} *g/ml in TOAB 0.13 M;* ***b)*** *Au nanoparticles 10 nm* 10^{-4} *g/ml in TOAB 0.13 M;* ***c)*** *Au nanoparticles 5 nm* 10^{-4} *g/ml and 10 nm* 10^{-4} *g/ml in TOAB 0.13 M.* [35]

On the other hand, water-based Ag particles were transferred to organic solvents through fatty amine or alkanethiol molecules molecules, where the phase transfer occurred by either, covalent interaction [36]or coordination bond formation[37]. **Figure 9** illustrates the transfer of Ag nanoparticles into organic solvent (hexane) and illustrates the stability of the transferred particles over time [37]. The phase transfer process was done easily through the hydrophobization of Ag nanoparticles resulting from electrostatic interaction between tetraoctylammonium cations and citrate anions forming surface ion pairs. The hydrophobic Ag nanoparticles were extremely stable even one month after the phase transfer, as no precipitation occurred. In addition, the reported method illustrates that the transferred Ag particles can be re-dispersed in different organic solvents by separating the octadecylamine-stabilized Ag nanoparticles from hexane in the form of a powder and then dispersing them in the preferable non-polar solvent.

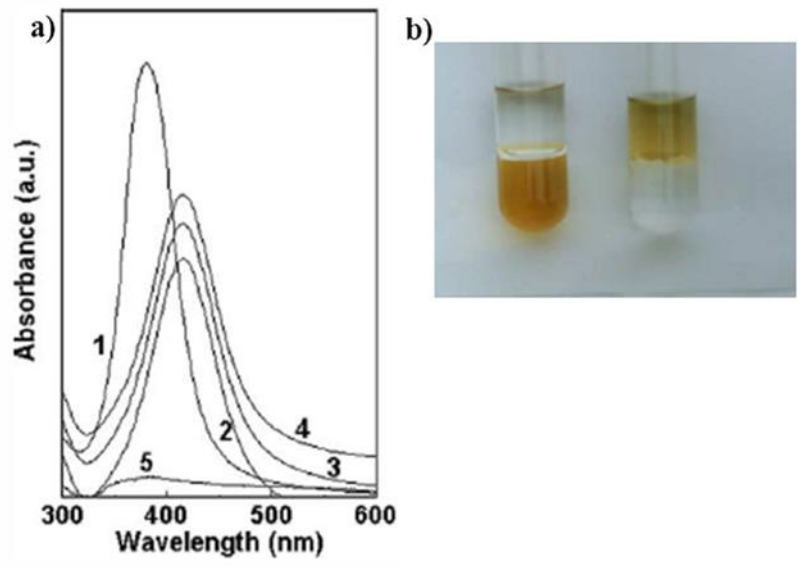

Figure 9. *a) UV–vis spectra of the Ag sol before and after phase transfer: curve 1, as-prepared Ag sol in aqueous phase; curve 2, hexane phase immediately after phase transfer of Ag nanoparticles; curve 3, Ag nanoparticles in hexane phase after 24 h of transfer; curve 4, Ag nanoparticles in hexane after 36 h of transfer; curve 5, spectrum of the aqueous phase after phase transfer of Ag nanoparticles into hexane; b) photography of Ag nanoparticles before (left tube) and after (right tube) transfer.[37]*

1.4. Applications of metal nanoparticles to molecular detection

The application of noble metal nanostructures to molecular sensing is quite well known. The mechanism relies on the interaction between localized surface plasmons and molecules[38], being Surface Enhanced Raman Spectroscopy (SERS) among the most investigated application. Substrates with reproducible high SERS enhancement factors (EFs), thus appear to be highly desirable and are a prerequisite for a wider application of SERS beyond fundamental studies. However, before going into details of molecular SERS detection, a brief introduction of Raman spectroscopy and the basics of SERS will be given.

1.5. Raman spectroscopy

Raman spectroscopy is an analytical technique based on the inelastic scattering of incident light photons on an atom or molecule. The concept of Raman spectroscopy is that when a photon of incident monochromatic light interacts with the electron of a molecule, the electron gains energy and jumps to a virtual energy state. Then, the electron in the excited state releases energy and falls back to a different lower energy level (Raman inelastic scattering), or to the same energy level of the incident photon (Rayleigh elastic scattering (**Figure 10**). The inelastically scattered photon is either scattering with lower energy than incident photon (stokes Raman shifts), or with higher energy than incident photon (Anti-Stokes Raman shifts). Raman stokes scattering is stronger than anti-stokes one as most of molecules are in the ground vibrational state and the photon is scattered at lower energy.[39]

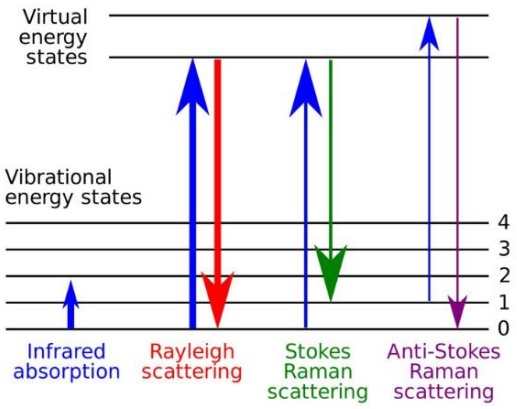

Figure 10. *Energy-level diagram of Rayleigh scattering, stokes and anti-stokes Raman scattering.*

Rayleigh scattering in which photon scatter elastically where no change occurs in the energy of incident and emitted photons (impractical in molecule vibrational characterization) is the dominant scattering, while Raman inelastic scattering occurs only on $1x10^{-7}$ of the scattered photons. [40]

1.6. Surface Enhanced Raman Scattering (SERS)

The SERS effect is a phenomenon by which the Raman scattering of a molecule in close proximity of a rough metal substrate is enhanced by several orders of magnitude[42]. SERS was discovered in 1970 by Fleischmann et al. [41] who observed SERS from pyridine adsorbed on electrochemically roughened Ag electrode. Following this initial discovery, it was found that noble metal nanostructures were able to amplify Raman signals up to 14 orders of magnitude[42] [43],due to their plasmon frequency in resonance with visible and near infrared wavelengths of the applied lasers.

The SERS enhancement is attributed to two mechanisms: an electromagnetic effect (EM) and a chemical effect (CE). In the electromagnetic mechanism enhancement occurs because of an enhancement in the electric field provided by the roughened surface, due to the interaction between laser irradiation and the surface LSPRs. The SERS effect is so pronounced because the field enhancement occurs twice. First, the field enhancement magnifies the intensity of incident light, which will excite the Raman modes of the adsorbed molecule. The Raman signal is then further magnified by the surface due to the same mechanism that excited the incident light. At each stage the electric field is enhanced as E^2, for a total enhancement of E^4.[43] The field enhancement is only maximized when the plasmon frequency ω_p of metal nanostructures is in resonance with the wavelength of the applied laser.

On the other hand, the chemical effect enhances the Raman signal when adsorption of the molecule on metal nanostructure involves chemical reaction between the conduction electrons of the metal and ion pair of the adsorbed molecule, resulting in chemical bond formation i.e. charge transfer. Chemical enhancement is achieved when the Fermi level of the metal surface is localized between the HOMO (highest occupied molecular orbital) and LUMO (lowest occupied molecular orbital) of the molecule. In this situation the energy requirement for a HOMO/LUMO transition is lowered and light of half the energy can be employed to make

the transition, where the metal acts as a charge-transfer intermediate (**Figure 11**).[44]

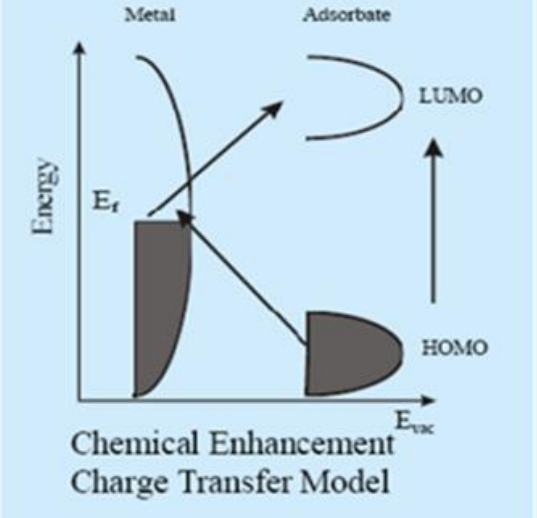

Figure 11. *Scheme of the charge transfer mechanism between the HOMO and LUMO orbitals of the molecule and the electrons at the Fermi level of the metal surface.*[44]

1.7. Coupling of metal nanostructure plasmons

The oscillations of conduction band electrons in nanoparticles are responsible for the creation of an electric field around the nanoparticle surface. In asymmetric particles, the intensity of the field is also asymmetric. For example, in metal nanorods electric fields are particularly pronounced at the rod tips; in metal nanostars the fields are pronounced in the spikes. These structures are particularly suitable for SERS, as they induce strong enhancements. In addition, when two or more nanoparticles are brought in close proximity to each other (< 5 nm) the electric fields of neighboring particles couple creating so-called hot spots, areas of strongly enhanced electric fields. Molecules adsorbed in hot spots experience the strongest SERS effects. Plasmon coupling depends on many factors: the interparticle gap, the size and the shape of the metal nanostructures. Strong electric fields are observed in closely spaced nanoparticles (< 10 nm) compared to dispersed nanoparticles (**Figure 12 *a-c***). This phenomenon is highly enhanced in non-spherical nanostrucutres consisting at least of two resonance modes (hexagons, cubes, rods, etc.) (see **Figure 12 *d***). Electric field around the nanostructures enhanced with an increase in the metal nanostructrures size that creates more hot sites.[45, 46]

For this reason research interest has focused on the development of SERS substrates with nanoparticles of controlled shape, size and spacing, in order to promote high and reproducible SERS signals.

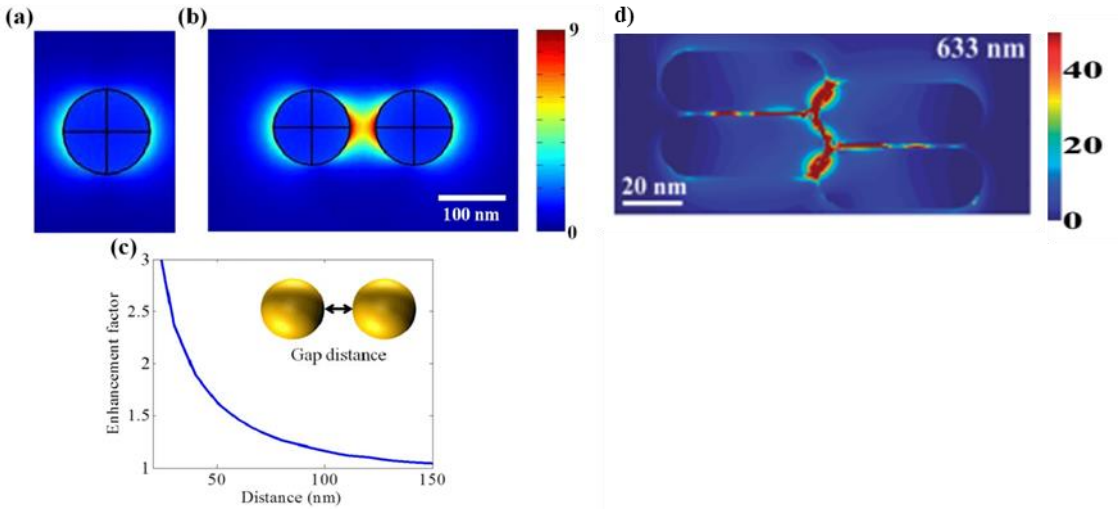

Figure 12. *Electric field intensity profile of* ***a)*** *single nanoparticle;* ***b)*** *adjacent two spherical nano particles;* ***c)*** *The relationship between the interparticle distance of two spherical nanoparticles and the enhancement factor;* ***d)*** *electric field intensity profile of neighboring Au nanorods. a) b) and c) are adapted from [47] (d is adapted from [48]*

1.8. Fabrication of SERS substrates

SERS substrates can be fabricated by top-down approaches (i.e. lithographic approaches) whereby nanostructures are placed on rigid substrates with predictable geometry and inter-particle spacing. The advantage of these methods relies on the reproducibility of analysis provided by the fabricated structures. The main disadvantages are the high cost of production and the restricted use of rigid substrates. Alternatively, bottom up approaches are used whereby chemical synthetic processes are used to fabricate nanoparticles, which are subsequently assembled and immobilized on rigid or flexible substrates. The main advantage of bottom up approaches is that they are more versatile and lower-cost. However, they are overall a lower reproducible method compared to top down approaches. Bottom-up methods are related one to this research and therefore they will constitute the focus of this chapter. Development in immobilizing fabricated metal nanostructures on very diverse solid substrates was expedited due to their important role in chemical sensing as SERS probes. Different SERS

analysis necessitate different probe specifications that may include: portability, flexibility, transparency, rigidity, stickiness, delicacy, non-invasiveness, applicability to be in-situ and/or ex-situ, substrate material with none or little background response to SERS enhancement. As these requirements vary enormously, many efforts have been devoted to the development of different nanoparticle immobilization methodologies. [23, 38, 49]

Self-assembly of metal nanoparticles on solid substrates provides high density of hot sites that result in an increase of the SERS magnitude. Moreover, immobilized nanoparticles on solid substrates are more stable than dispersed nanoparticles in solution, which can only be stored for short periods[38]. In addition, portability of SERS substrate can be achieved through stabilization of nanoparticles on solid substrates, thus enabling both the ex-situ and in-situ detection of the target analyte. Finally, non-destructiveness or micro-destructiveness are important features in the design of SERS substrates for many applications; immobilization of plasmonic colloids on solid substrates can also lead to minimization of the analyte contamination.

Direct deposition of nanoparticles on solid substrates has been developed and the resulting enhancement has been investigated by many groups. One of the most advanced method in SERS fabrication was reported by Liz.Marzán *et al.* [22] who used a commercial fountain pen filled with plasmonic nanoparticle inks to write SERS arrays directly on paper substrates (**Figure 13**). Au and Ag nanoinks were used as "pen-on-paper" SERS substrates, which exhibit highly efficient detection, depending on the excitation wavelength, dye molecule and the type of nanoparticles used.

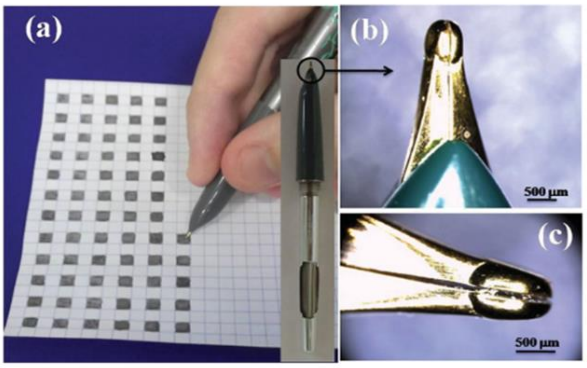

Figure 13. a) *Photograph of a fountain pen loaded with plasmonic nanoparticle ink and writing of SERS substrates on paper (the inset shows the inner part of the pen);* ***b),c)*** *Optical microscopy images of the pen nib at two different magnifications.* [22]

Another important method of metal nanostructure deposition as SERS substrate is developed by Shah *et al*.[50] who used Ag colloidal pastes for SERS analysis of samples of different vegetal and animal fibers dyed with cochineal and historical textiles. Ag nanopastes were exploited for the fiber analysis (**Figure 14**) as they allowed homogeneous coating of the three-dimensional fibers and enabled sensitive SERS detection. It should be pointed out that this analysis was performed by micro-extraction of fiber material from historical textiles followed by deposition of nanopastes, as deposition of nanopastes in situ would result in permanent staining of the historical object. Therefore development of non-invasive SERS probes would be extremely relevant for analysis of historical textiles.

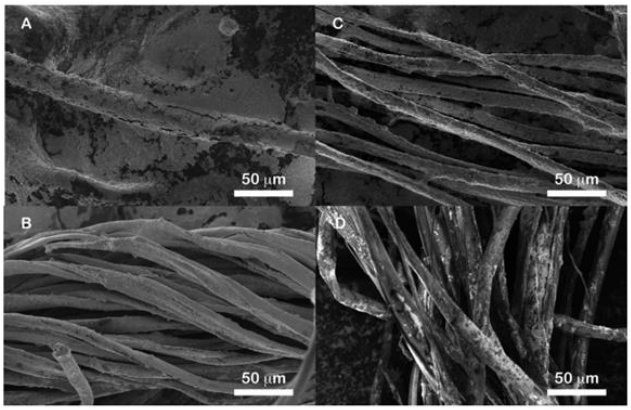

Figure 14. *SEM micrographs of natural fibers coated with Ag colloidal paste: A) wool; B) silk; C) cotton and D) flax.* [50]

SERS substrates also have been fabricated by stabilizing metal nanostructures on rigid substrates such as glass [51],quartz [52], alumina [53],soda-lime silica glass [54] and SiO_2 [55].Although, these types of SERS substrates lack in flexibility, they are suitable to analyze analytes ex-situ after extraction and can even be used sometimes as both in-situ (at the point-of-need) and ex-situ SERS substrates. Moreover, stabilizing metal nanostructures on rigid substrate enables non-invasive or minimal invasive SERS analysis which is of paramount importance in historic object analysis where saving the integrity and reducing the metal nanostructures contamination of textile samples are required. For example, Ag nanoparticles were stabilized on glass slides by deposition of metal colloids left to dry and self-assemble by solvent evaporation in oven at 130^0C [56]. **Figure 15** illustrates two types of application of the fabricated SERS substrates: a) where the laser penetrates from the front side and passes through

the molecule and the metal particles (ex-situ application); b) the laser penetrates from the back side and passes through the glass slide, molecule and the metal particles (in-situ application). The SERS analysis provides good quality and reproducible SERS signal of alizarin dye, where consistent three SERS measurements were collected on different parts of the substrate.

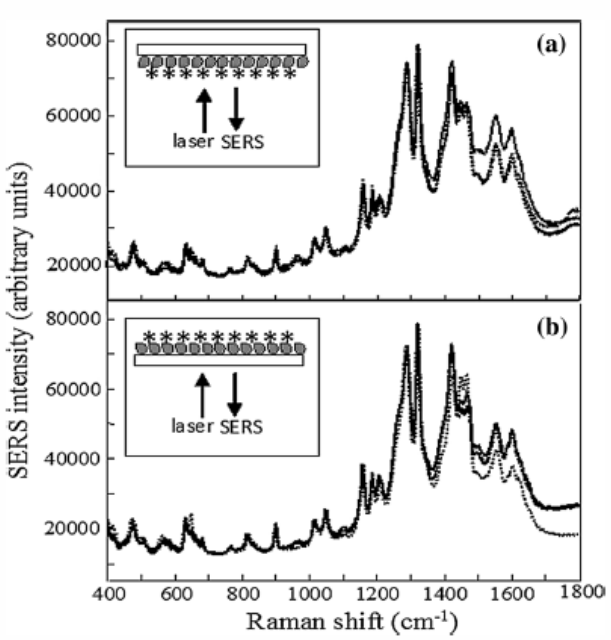

Figure 15. *SERS spectra of a 10^{-3} M of alizarin deposited onto Ag nanoparticles stabilized on glass slide. a) front side SERS analysis, b) backside SERS analysis. [56]*

Polymers also have been exploited to immobilize metallic nanoparticles such as PDMS (Polydimethylsiloxane) [57], PMMA Poly (methyl methacrylate) [58], PE (Polyethylene) [59] and hydrogel[60], due to their flexibility and transparency. Also elasticity features shown by polymers enable different SERS applications as in-situ, ex-situ analysis and analyte trace extraction. For example, SERS slime was fabricated by encapsulated Ag nanoparticles into poly (vinyl alcohol) hydrogels (**Figure 16**) and used to extract the target analyte for further ex-situ SERS analysis[60]. Other literature [59, 61] applied plasmonic polymers as in-situ and ex-situ substrates for direct SERS analysis.

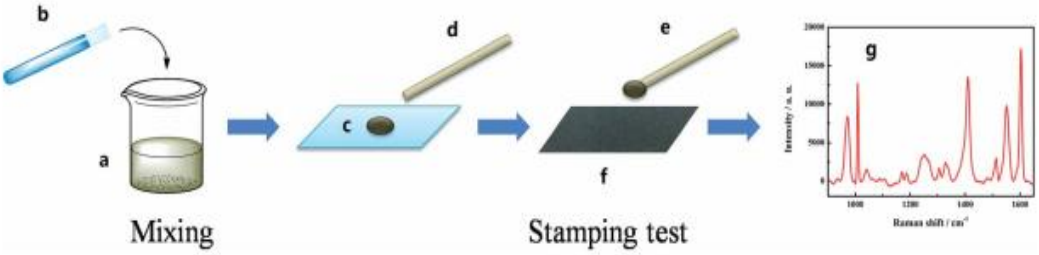

Figure 16. *Schematic representation of the preparation of the slime SERS substrate and the stamping analysis;* ***a)*** *Ag NPs–PVA mixture;* ***b)*** *sodium borate****; c)*** *SERS slime;* ***d)*** *wood stick;* ***e)*** *SERS slime on a wood stick;* ***f)*** *contaminated surface;* ***g),*** *SERS of the surface contaminant.* [60]

1.9. Ink Characterization

The analysis of commercial ballpoint pens towards the identification of dye content in ink composition has been the object of forensic investigation for many years. However, this field of research is also increasingly becoming relevant for art conservation applications. In fact in the last 80 years artists have used ballpoint pens for the production of artworks nowadays found in many museum collections all over the world. Unfortunately, such artworks are rapidly deteriorating, due to the fast color fading caused by exposure of the ink to light and air. The answer to this problem requires the establishment of novel long-term preservation approaches which in turn can only be developed if the chemical composition of fading dyes and their interaction with light are well-known and understood.

Ballpoint pen inks are complex mixtures of several dyes and pigments constituting up to 50% of the total ink formulation contained in either a glycol-based solvent or benzyl alcohol.[62, 63] Additional components (vehicle) include fatty acids, softeners and polymeric resins, designed to improve the consistency, flow or drying characteristics of the ink.[64] Many analytical methods, including chromatographic techniques [65-68] and mass spectrometry, [69, 70] have been used for investigation of ink composition in the field of forensic analysis, mainly aiming at development of reliable protocols towards the establishment of the source or authenticity of a questioned document. Recently, preference has been given to spectroscopic techniques such as Fourier transform infrared (FTIR), [71, 72] X-ray fluorescence,[73] Raman spectroscopy[74] due to their inherent non-destructive nature. In fact, spectroscopic techniques require a small amount of analyte, little or no manipulation of the specimen, are simple to perform and therefore allow preservation of the integrity of the analyzed object, which is a strong requisite for both forensic and art conservation applications.

Among spectroscopic techniques, Surface Enhanced Raman Scattering (SERS) has been recently successfully applied to the analysis of inks, where strong Raman signals were obtained, due to the ability of SERS to quench the fluorescence interference associated with Raman measurements. One of the most comprehensive studies in this field was performed by Lombardi *et al*.[75] who analyzed the discrimination capabilities of SERS with various excitation wavelengths. They found that while under normal Raman conditions only FT-Raman excitation provided good spectra, SERS spectra were obtained using diluted solutions of all dye molecules at 633 nm and 785 nm excitation wavelengths. Gooijer et al.[76] also tested the applicability of SERS for the discrimination of blue and back ballpoint pens and concluded that illumination at 685 nm was necessary for the spectra to be distinguished.

1.9.1. Application of SERS in inks characterization

In the context of ink works for art preservation and analysis, the development of non-invasive SERS substrates enabling sensitive detection while preserving the integrity and the authenticity of the analysed art work is highly relevant. Although other spectroscopic techniques such as Fourier transform infrared spectroscopy (FT-IR), near infrared spectroscopy (NIR), and X-ray fluorescence have been successfully employed for the analysis of historical inks, SERS offer unique advantages. In fact FTIR requires extraction of mg amount of material and XFR is ineffective for analysis of modern inks, constituted by organic dyes. In contrast SERS offers sensitivity and the potential for in situ analysis, which avoid extraction of sample and therefore damage of the precious analyte. In forensic analysis, Raman spectroscopy has been used for ink analysis of different colour ball-point pens and for chronological sequencing method of crossed ink lines[77]. Distinguishing between commercially available ball-point black pens of different brands (**Figure 17**) was achieved in the study using two laser lines. Black pen ink (c) showed strong characteristic Raman signals with 514nm, while with 785nm featureless spectrum was recorded. The response of the same ink of each black pen was different depending on the molecular resonance with the used two excitation wavelengths.

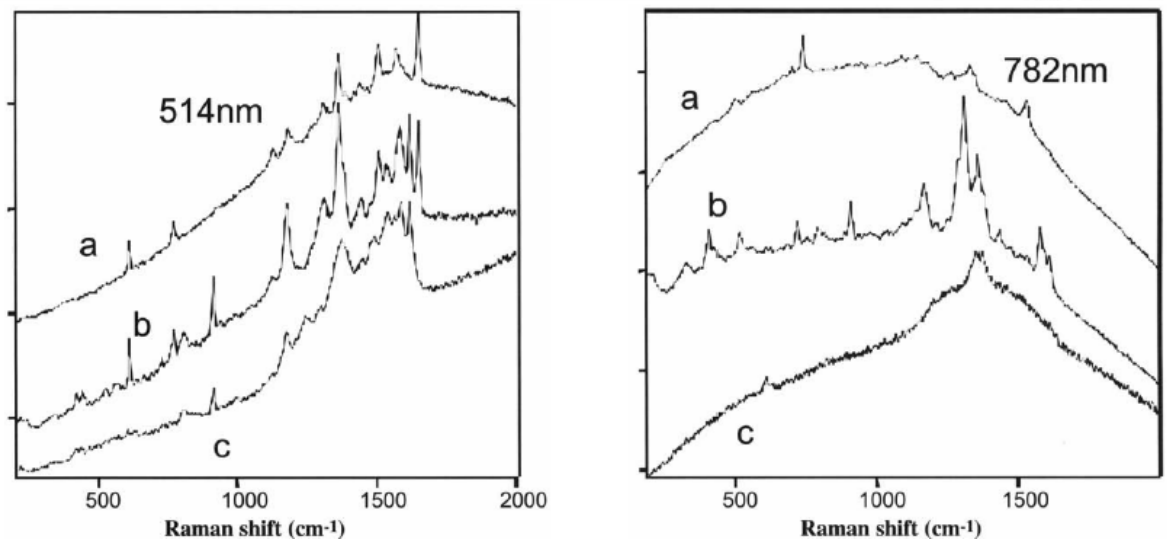

Figure 17. *Raman spectra for three black ballpoint inks taken with the 514 nm laser and the 782 nm laser* ***a)****Bic® fine;* ***b)****Pilot® BP-GP; and* ***c)*** *Schneider®.* [77]

Although, Raman spectroscopy with more than one laser line can be used to distinguish between two or more same color ink pens, SERS shows more practicality as only one laser line can be used. Moreover even with excitation wavelengths causing ink fluorescence, SERS can overcome this interference by quenching of the fluorescence and enhancement of the masked signal. For example, different ball-point pens inks dyes separated by TLC (thin layer chromatography) have been analyzed by Raman and SERS[75]. Most of the dyes analyzed with 633 nm showed high level of fluorescence (**Figure 18**), while in comparison SERS analysis with the same laser line revealed characteristic signal for all ball-point synthetic dyes, which proves the high discrimination capabilities of SERS technique.

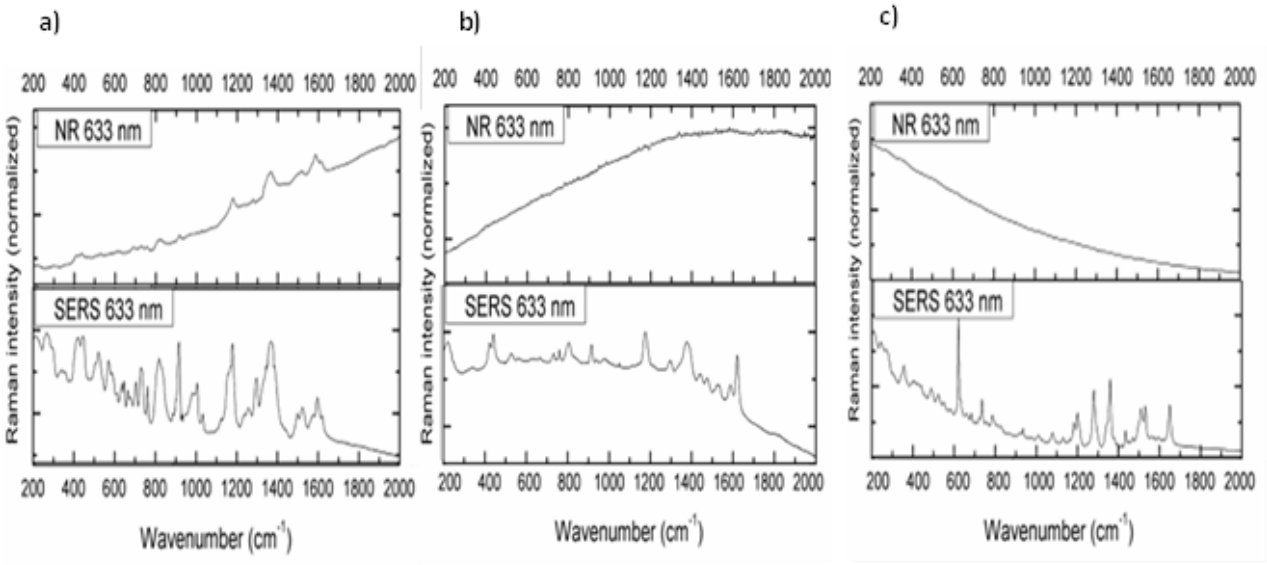

Figure 18. *Normal Raman (NR) and surface-enhanced Raman spectra of (SERS)* ***a)*** *Aniline Blue;* ***b)*** *Methyl Violet;* ***c)*** *Rhodamine B.* [75]

However, SERS investigation is dependent on the choice of the excitation wavelength i.e. resonance enhancement along with the chemical interaction between ink molecules and the metal nanoparticles. For example, in-situ SERS analysis using different laser lines was conducted on set of blue ball-point pen lines on paper was reported[76] using Ag colloids. Blue ball-point pen ink is known to consist of blue negatively charged dye (solvent blue 38 SB38) and purple cationic dye (methyl violet). The SERS signal of the latter was dominant with 514nm excitation wavelength, where the resonance effect was achieved along with the electrostatic interaction with the negatively charged Ag nanoparticles. Instead, the SERS signal of the blue dye SB38 was significantly enhanced when 685 nm excitation wavelength was applied, due to resonance enhancement and the reduction of strong signal of the dominant dye (methyl violet) by using excitation wavelength in the red region.

1.10. Food contaminants

Antibiotics such as chloramphenicol and phenylmethane dyes used as drugs because they work effectively against various fungal infections in fish, while pesticides such as dithiocarbammate compounds are used as fungicide to inhabit crop diseases in agriculture. However, drugs and pesticides are found to be common food contaminants due to their links

to genotoxicity and cancer causing after long exposure at high dose.[78, 79] Therefore, their detection is essential to regulate their existence in the environment at trace level. Although, chromatographic methods are [38] commonly used to detect the presence of food contaminants, such methods are highly costing, time consuming and require pretreatment and preparation of the samples. On the other hand, in recent years metal nanostructures have shown great potential as SERS platforms for detection of drugs and pesticides traces in food. Such methods will never compare with the sensitivity and quantitative capabilities of chromatographic methods. However, SERS performed with low-cost and disposable probes, could constitute an effective pre-screening method, which would reduce the number of samples requiring costly and lengthy chromatographic analysis.

1.10.1. Application of SERS in food contaminants detection

In literature, various nanoprobes and SERS methods are reported for the detection and monitoring of pesticides and drugs levels: solution-based nanostructures for in-situ/ex-situ analysis[80], portable solid SERS substrate for ex-sit/in-situ analysis[58, 59], and portable SERS substrate to extract contaminants as ex-situ method[81] to ensure food safety.

For pesticides detection, an in-situ SERS method has been developed using bimetallic nanorods (Au@Ag NRs) solutions along with pretreatment of the fruit[80]. The method was used to detect multi-pesticides residues thiram and methamidophos on apple peel (**Figure 19**). An ethanol solution was dropped on the fruit peel allowing pesticides molecules to dissolve and preconcentrate on the treated area. After the ethanol dried, the Au@Ag NRs solution was added on the peel for SERS analysis and the method was used with different pesticide concentrations which provided qualitative analytical reference for the analyzed pesticides.

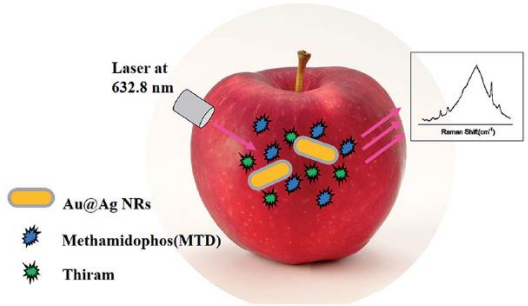

Figure 19. *Schematic illustration of the simultaneous detection of thiram and methamidophos (MTD) on apple surface based on SERS technique.*[80]

Moreover, metal nanostructures capped with silica shell through atomic layer deposition, called SHINERS, were used as in-situ in pesticides detection on real sample[82]. In the study, the gold nanoparticles capped with silica shell were deposited on contaminated orange and showed discriminative SERS analysis. The method was modified whit hollow Au and Ag particles coated with silica and used to detect pesticides traces on fruits[83].The method showed that hollow metal nanostructures were better than solid nanoparticles for SHINERS analysis.

On the other hand, less-invasive in-situ SERS detection of pesticides was reported[59] using immobilized Ag nanocubes on flexible and transparent polyethylene PE films. Significant SERS enhancement was obtained (**Figure 20**) when Ag-NC@PE was placed directly on the contaminated orange with methyl parathion through backside illumination. However, the PE film did not stick on the orange surface and had to be fixed with with band-aid to ensure close contact of the nanomaterial with the analyte.

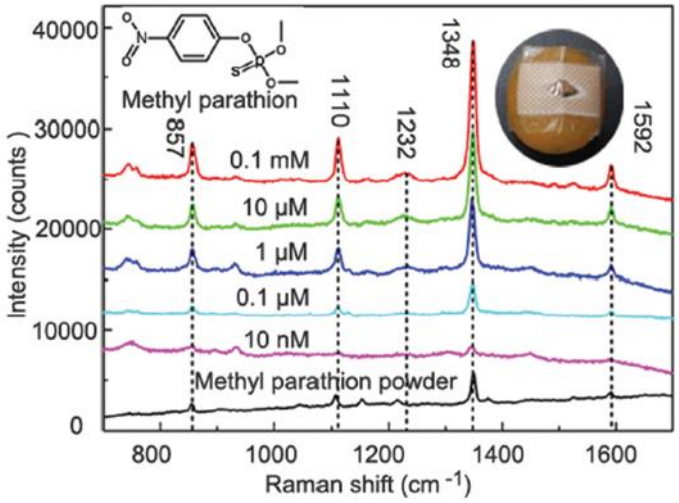

Figure 20. *SERS spectra of methyl parathion probed at different concentrations from 0.1 mM to 10 nM at the wavelength of 785 nm. The insets show the chemical structure of methyl parathion and the photograph of the Ag-NC@PE composite film integrated with Band-Aid being pasted on the contaminated orange [59]*

A similar method was introduced using Au nanostars immobilized on PDMS to detect pesticides on fruit[61]. In this method the composite attached to the analytical surface. However, nanoparticles easily detached from the sample surface during the analysis due to low adhesion of metal nanostructures onto the PDMS.

In addition, extraction method of pesticides from fruits and vegetables surfaces for further SERS analysis was reported[81] using commercial tapes (**Figure 21. 1**). Au nanoparticles solutions were dropped and left to dry on commercial tapes. The modified tape was applied to the contaminated surface by pressing gently for few seconds. Although, the method provides enhanced SERS signals with the major characteristic peaks of the analyzed pesticides (**Figure 21. 2**), more attention should be made for the tape selection as the plasmonic tape can be too sticky and extract fruit tissues along with the contaminants or be not sticky enough resulting in no extraction of the analyte.

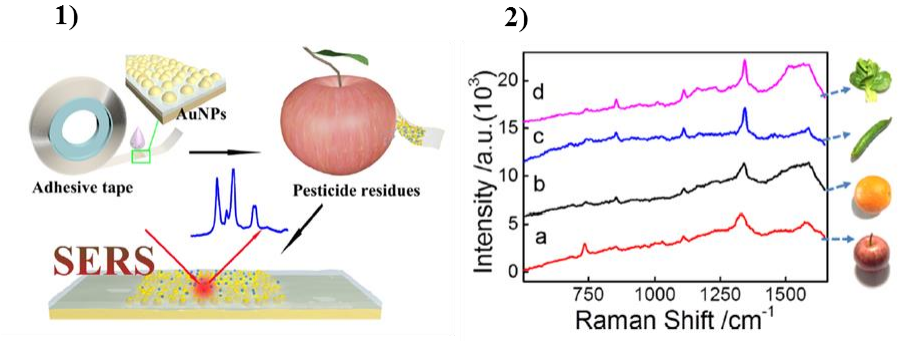

***Figure 21**. **1)** Schematic illustration of the fabrication of SERS tape and extraction of targets from fruit peel surface (apple) for SERS analysis. **2)** SERS spectra of parathion-methyl extracted from the surfaces of **a)** apples; **b)** oranges; **c)** cucumbers; **d)** green vegetables using SERS tape.[81]*

Finally, drug detection in food from the aquatic environment has been done using ex-situ SERS analysis using commercial solid surface based substrates (QSERS and SERS active Klarite) by extraction of crystal violet and chloramphenicol from fish surfaces for further SERS analysis[84] . On the other hand, in-situ analysis of drug detection in fish using portable SERS substrate that offers good flexibility and transparency was developed[58]. Au nanoparticles fixed on PMMA polymer were placed directly on contaminated fish skins with different concentrations of crystal violet; SERS results showed high sensitivity with backside laser penetration (**Figure 22**).

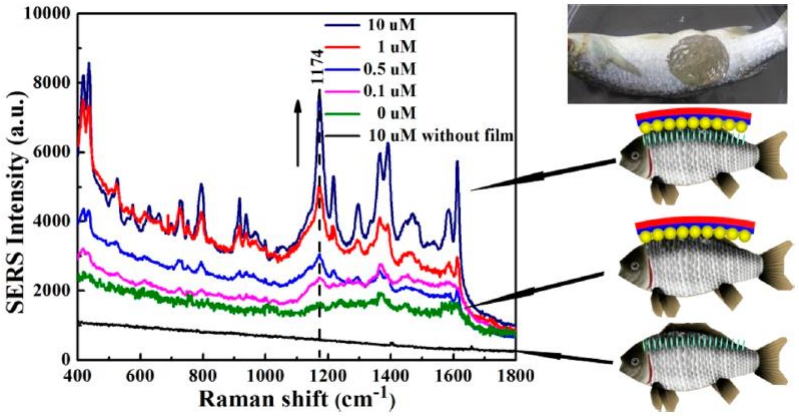

Figure 22. *In situ SERS detection of MG with different concertation on fish surface.* [58]

1.11. Scope and novelty of this thesis

The aim of this thesis is to investigate the applicability of Raman spectroscopy and SERS for identification of dye content in commercial inks and for the identification of food contaminants directly on the surface of food products. The emphasis and novelty of this work was the fabrication of suitable SERS probes able to overcome the challenges associated to the target applications. Regarding the analysis of commercial inks, the application of Raman and SERS spectroscopy is becoming increasing relevant for art conservation purposes. Modern and contemporary artists increasingly use commercial pens (ballpoint, gel pens, felt tip pens etc) for their artistic productions, due to their low cost, bright colors and easy availability. However, the color stability of commercial inks is low and colors fade upon exposure to ambient light. The preservation of such objects requires knowledge of the chemical ink composition, to date largely unknown due to patent protection. SERS has been largely used for the investigation of artworks and identification of natural colorants. However, so far SERS has been used on micro-extracted materials and very few examples of in situ applications are available. The novelty of this work relies on the development of SERS probes including metal nanopastes and nanoinks, for the direct, in situ analysis of colored drawings. In contrast to previously used diluted colloidal solutions, concentrated nanopastes and nanoinks SERS probes could be deposited directly on the colored paper without causing dissolution of the water-soluble analytical ink underneath. Such SERS probes evenly covered the colored paper fibers, ensuring occurrence of strong SERS effects and leading to the effective detection and identification of ink constituent dyes. Another important development was the fabrication of Ag NPs/PDMS composites for the non-invasive SERS analysis of artworks. These probes were only completed at the end of the thesis and could not be extensively tested. However, proof-of-concepts of their applicability has been obtained.

Regarding the application of food contaminants, the novelty of this work relies on the development of flexible and transparent sticky SERS probes that can be applied to the surface of food for the easy and direct SERS investigation of surface contaminants. Compared to previously developed SERS probes, our material could be stuck and un-stuck from the analytical surface and did not require additional tapes to be held in place. This was due to the high conformability of PDMS. The developed Ag NPs/PDMS probes offered versatility of analysis (in situ, ex situ upon micro-extraction) and constitute a valid screening alternative to

cumbersome chromatographic techniques.

Details of all developed SERS probes and their applications are below:

1) Plasmonic nanoinks constituted by Ag nanoparticles and Au nanorods and concentrated Ag pastes for in situ investigation of Bic pens.

2) Rigid SiO_2 substrates with deposited ordered arrays of Au nanorods for ex situ investigation of BIC pen inks.

3) Films of self-assembled Ag nanoparticles on PDMS for in situ investigation of food surfaces.

4) The stabilized Ag nanoparticles on PDMS were also used for micro-extraction of a desired analyte for ex-situ food contaminant analysis.

Plasmonic nanoparticles inks with different resonance enhancement (Au nanorods and Ag nanoparticles) were fabricated to control SERS investigation of mixture of dyes in blue ball-point pen with different laser lines. Complementary information about the pen inks' compositions using Au nanorods with 785 nm laser excitation and Ag nanoparticles inks with 514 nm laser excitation was obtained and details of fabrication/characterization of metal nanostructures and SERS performance in blue pen inks identification are presented in Chapter 2 and Chapter 3 respectively.

Formation of high density and high uniformity nanoparticle area was introduced by concentration of Ag nanoparticles inks to obtain plasmonic Ag paste. SERS investigation of different color ball-point pens was conducted through combination of Ag paste and the use of portable and bench Raman instrumentation. The Ag paste fabrication/characterization and SERS enhancement obtained is presented in chapter 2 and Chapter 4 respectively.

Ag nanoparticles immobilized on different solid substrates obtained by self-assembly of organic Ag nanoparticles into 1) rigid glass slide substrate, 2) flexible and transparent polymers PDMS and PMMA were fabricated and used as in-situ and point-of–need SERS probes for samples with irregular surface (fish and fruit). The strong adhesion of nanoparticles to the solid substrate and a developed cleaning process promote the minimal invasiveness feature of the obtained SERS substrates. The transparency feature of these substrates was exploited to conduct back illumination where the nanoparticles are in contact with the analyte, and the laser penetrates from the other side to enable in-situ SERS analysis. Characterization

of the minimal invasive substrate and SERS performance in food pollutant detection are reported in details in Chapter 2 and Chapter 5 respectively.

Micro-extraction of target molecule from complex surfaces using the flexible and transparent Ag nanoparticle/PDMS substrate for ex-situ SERS analysis was introduced. The extraction efficiency of drug form fish and pesticides from fruit was investigated to evaluate the potential of SERS film in easy sampling of real object with irregular surfaces. The characterization and applicability of extraction method is described in details in Chapter 2 and Chapter 5 respectively.

CHAPTER 2

Fabrication of Highly-Sensitive and Multi-Purpose SERS Probes

The fabrication of various SERS substrates is presented in this chapter for in-situ, ex-situ, minimally invasive/in-situ and micro-extraction/ex-situ SERS analysis. The first SERS probe was fabricated following literature procedures: Ag and Au nanoinks with different plasmon resonance bands were used in combination with resonant excitation wavelengths as SERS analysis for in-situ/ex-situ applications. Another SERS probe was fabricated using thick paste of concentrated Ag nanoinks, that gave a quite dense and uniform coverage of plasmonic moiety on the analytical surface and were used for either in-situ or ex-situ SERS applications. A third SERS probes for ex-situ applications was constituted by Au nanorods ordered in monolayer vertical superstructures on SiO_2; the advantage of such probes relied on their highly-sensitive and reproducible capabilities for SERS analysis. For in-situ and minimally invasive SERS analysis, Ag particles immobilized on rigid substrates (glass) and on flexible substrates (PDMS and PMMA) were fabricated. As a result of the high level of transparency, such probes were investigated for in-situ SERS analysis at the point-of-need: SERS probes were applied on the analytical surface and analysis performed in situ by laser back illumination through the probe. Assembled Ag particles on flexible PDMS substrates were also used to perform SERS analysis ex situ on micro-extracted analytes. Full characterization of each type of SERS probes including electron microscopy and UV-vis spectroscopy and investigation of their SERS capabilities are reported in this chapter.

2.1. Introduction

SERS has been attracting researchers' attention due to its valuable role as sensitive and effective tool in enhancing weak analyte Raman signals for various applications. Different types: Au, Ag, Pt and Cu, etc., and various shapes: rods, spheres, hollow spheres, , cubes and stars, etc., of metal nanostructures have been synthesized and developed in literature. Developments are not exclusive to the metal nanostructures synthesis, but also to their application as SERS substrates using many different preparation methods.

Plasmonic nanostructures were fabricated to be used as inks[22], solutions[80], pastes[50], and to be applied directly on real samples or on target analytes extracted with organic solvents for further detection[85]. Metal nanostructure deposition method, either directly on the sample or on the analyte after extraction, enables the easiest and lowest-cost SERS analysis, although lacks in reproducibility, due to the random aggregation of drop deposited colloids on the analytical surface. On the other hand, the drop deposition method is not suitable for delicate samples requiring no extraction or contamination-free methods of analysis. Therefore, recent efforts have been made to immobilize metal nanostructures on various low cost substrates. Among these substrates filter paper soaked in plasmonic solutions[86], or office paper with deposited plasmonic solutions [87] have been widely investigated. Solid transparent substrates have also been used to immobilize metal nanostructures for in-situ applications[51, 56]. For some applications, transparent but rigid substrates (glass) with deposited nanoparticles can be sufficient for SERS analysis (object has regular surface and rigid glass can be deposited on its surface). However, for many other applications such as work of art and food analysis, etc., where the analyzed objects has irregular or complex surfaces, some level of substrate flexibility is crucial point for SERS in-situ analysis. In recent years several authors have reported fabrication of plasmonic flexible, transparent substrates for in-situ SERS investigation using polymers such as PMMA, PDMS, and PE, which have been used to immobilize metal nanostructures for realization of in-situ SERS probes [58, 59, 61]. In addition, alternative methods of analyte extraction from sample surface with organic solvents in combination with SERS analysis with flexible probes have been developed by many authors [60, 81, 85].

In this chapter, several methods of SERS probe fabrication are presented. Ag and Au nanoinks were fabricated following Liz- Marzán *et al*.[22] with slight modification to achieve different plasmonic resonances that were used with two excitation wavelengths 514 nm and

785 nm for complementary blue BIC pen SERS investigation. The second probe was constituted by Ag nanopaste and was prepared to achieve denser and homogeneous coverage of plasmonic layer on the analyzed sample (BIC colored paper fibers) for in-situ and ex-situ SERS analysis. The third SERS probe was constituted by stamped Au vertical arrays on SiO_2 for high sensitive ex-situ analysis of BIC pen composition. The fourth SERS probe was constituted by deposited Ag nanoparticles on rigid and transparent (glass) or flexible and transparent (PDMS and PMMA) substrates and were used for SERS analysis of food contaminants. In addition, Ag nanoparticle/glass and Ag nanoparticle/PDMS SERS probes were investigated for potential minimal invasive SERS analysis on works of art.

Ag nanoparticle/PDMS were also applied to food surfaces to perform micro-extraction of contaminant for subsequent ex situ SERS analysis. For all plasmonic SERS probes, 4-ABT molecule was used as model analyte to investigate SERS applicability and feasibility before moving into real analysis.

2.2. Experimental Section

Materials

Tetrachloroauric acid ($HAuCl_4$ $3H_2O$), silver nitrate ($AgNO_3$), trisodium citrate ($Na_3C_6H_5O_7$), sodium borohydride ($NaBH_4$), ascorbic acid ($C_6H_8O_6$), cetyltrimethyl-ammoniumbromide (CTAB), octadecylamine (ODA), chlorobenzene (C_6H_5Cl), methanol (MeOH), Tetraoctylammoniumbromide (TOAB) with a purity equal or greater than 99.9%, Mercaptosuccinic acid ($C_4H_6O_4S$) with purity bigger or greater to 99% HPLC grade and 4-aminobenzenethiol (4-ABT) were purchased from Sigma-Aldrich. All glassware was cleaned with aqua regia prior to nanoink synthesis. Milli-Q water (resistivity 418 MΩ/cm) was used throughout the experiments. Poly(methyl methacrylate) (PMMA, MW = 996000, CAS 9011-14-7), and SYLGARD 184 Silicon Elastomer Kit for polydimethylsiloxane (PDMS) were also purchased from Sigma-Aldrich. All chemicals were used as received.

Characterization

Scanning electron microscopy (SEM) images of metal nanostructures were acquired using a field emission. SEM (JSM-6700F, JEOL UK Ltd) operating at beam voltages of 3 kV. UV-vis spectra were acquired using an Agilent/HP 8453 UV-vis Spectrophotometer (200 nm to1100 nm).

Raman and SERS measurements were obtained from a Renishaw inVia Raman system equipped with a 514 helium–neon laser. The laser beam was focused onto the sample through a Leica 20X objective with 0.4 N.A. Acquisition time was usually 10 s and measured power was 3 mW. Also, Raman and SERS spectra at 785 nm were obtained from a Pelkin Elmer Raman station. The laser beam was focused onto the sample through a 50 objective (MPlan Achromat) with 0.75 N.A. The laser power was around 35mW and typical acquisition time was 10 s. Hand held Raman spectra at 785 nm were obtained from an InPharma spectrometer. The laser power was 50 mW at sample and acquisition time was between 7 and 20 s.

2.3. Fabrication of Ag Nanoparticle and Au Nanorod Nanoinks SERS probes

Au nanorod nanoinks (Au NR Nis) were synthesized by a modification of the seed mediated growth reported by Liz- Marzan et al.[22] Specifically, a seed solution was prepared by adding 0.3 mL of an ice-cold aqueous sodium borohydride ($NaBH_4$, 0.01 M) solution to an aqueous solution of 4.7mL hexadecyltrimethylammonium bromide (CTAB, 0.1 M) and 25 mL of gold(III) chloride trihydrate ($HAuCl_4$, 0.05 M) at 30^o C. An aliquot of 0.36 mL of the seed solution was added to a growth solution prepared by mixing 150 mL of CTAB (0.05 M), 1.5 mL of $HAuCl_4$ (0.05 M), 0.225 mL of silver nitrate ($AgNO_3$, 0.01 M) and 5.0 mL of ascorbic acid ($C_6H_8O_6$, 0.1 M) at 30 °C. The solution color changed from colurless to brownish-bluish after the addition of the seed solution to the brown solution. The obtained aqueous solution of Au nanorods was centrifuged twice and redispersed in water (1 mL) to achieve the nanorod ink. The resulted gold nanorods inks are stabilized with overall positive charge dispersed in aqueous solution. **Figure 23a** shows the UV-vis spectrum of Au nanorods inks dispersed in aqueous solution with absorbance bands at 780 nm (longitudinal) and 517 nm (transversal). SEM images of Au NRs NIs (10 μL) deposited on silicon dioxide substrate with high and low magnifications are shown in **Figure 23*c,d***.

Ag nanoinks were fabricated following the Lee and Meisel method reported by Liz-Marzán *et al*.[22] Briefly, trisodium citrate solution (4.5 mL, 1.00 wt%) was added to an aqueous boiling solution containing $AgNO_3$ (200 mL, 42 mg) under vigorous stirring. The reaction was boiled for another 1 hr and then cooled to room temperature. The obtained Ag nanoparticles in water (200 mL) were centrifuged at 7000 rpm for 20 min and then redispersed in water (2 mL) to obtain Ag nanoinks (3 mg/mL). The resulted silver particles inks are negatively charged with maximum absorbance band at 420 nm (**Figure 23 *e***). The SEM images of 10 μL Ag NPs NIs deposited on silicon dioxide substrate with high and low magnifications are shown in **Figure 23*g,h***.

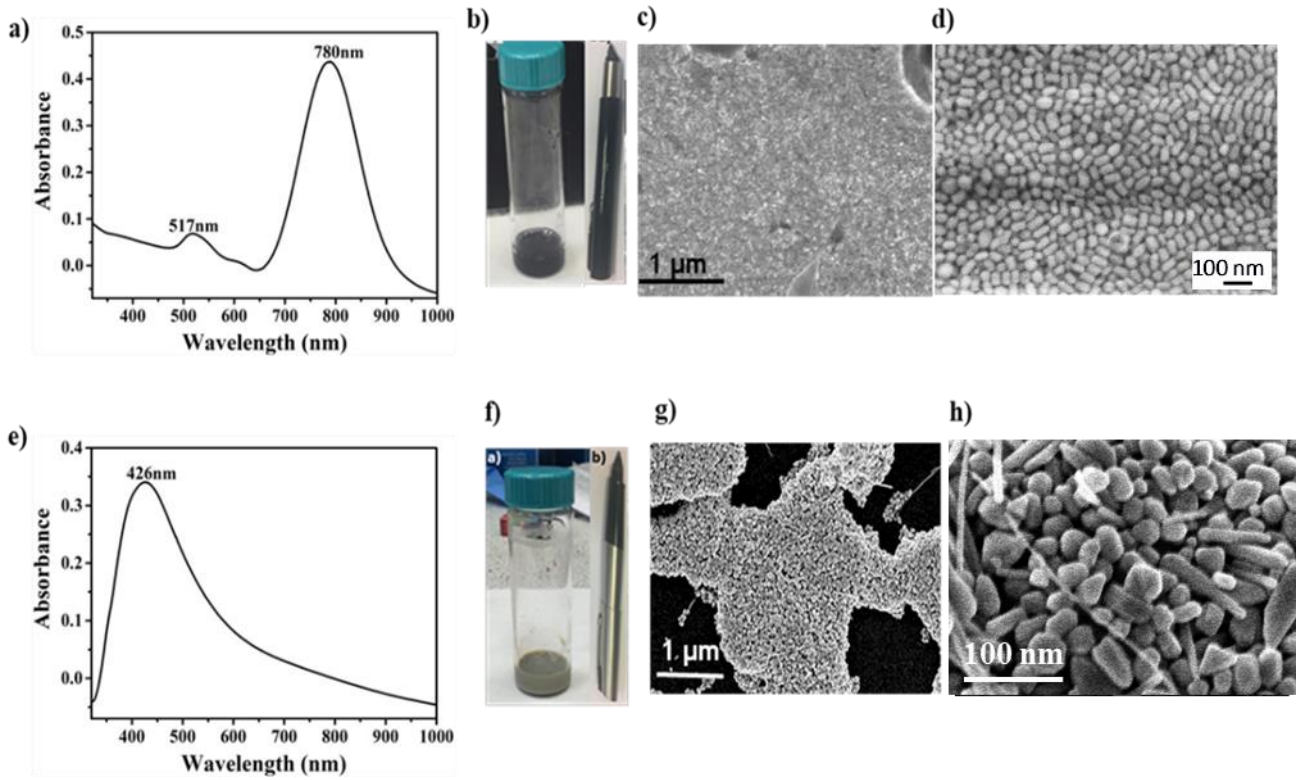

***Figure 23**. **a)** UV-vis spectrum of Au NR NIs solution; **b)** Photography of Au NIs; **c), d)** SEM images of the synthesized Au NIs aqueous solution deposited on SiO_2 substrate; **e)** UV-Vis spectrum of Ag NIs solution; **f)** Photography of Ag NIs; **g), h)** SEM images of Ag NIs deposited onto SiO_2 substrate.*

The Au NR NI mean diameter and length were 15 and 50 nm, respectively. An aspect ratio (AR) = 3.3 was measured from SEM images averaging the size of over 300 nanorods (**Figure 24*a,b***) by the use of Image J software. SEM images were used to measure the dimensions of the nanostructures using the software and then the aspect ratio was calculated at the average ratio of the highest to the lowest dimension over 300 of similar particles. The mean average size of the obtained Ag NP NIs was 90 nm, measured from SEM images averaging the size of over 300 nanoparticles (**Figure 24*c***).

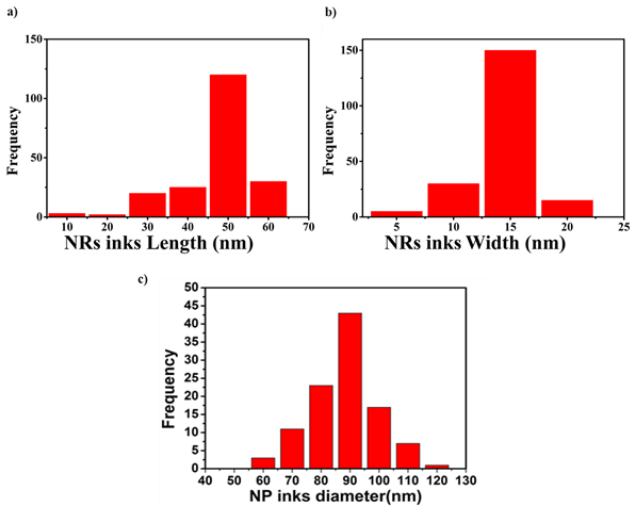

Figure 24. *Histogram of metal nanoinks* ***a)*** *length,* ***b)*** *width of Au NR NIs obtained by statistical measures over 300 nanorods, and* ***c)*** *Ag NPs NIs diameter obtained by statistical measures over 300 nanoparticles.*

SERS feasibility was evaluated using 4-aminobenzenethiol (4-ABT) molecule, by depositing 10 µL of aqueous 4-ABT solutions (0.01mM) onto a clean glass slide and left to dry at room temperature. Subsequently, 5 µL of Au nanorod NIs were deposited on the dried 4-ABT (0.01mM). **Figure 25*b*** shows the Raman spectrum of 4-ABT obtained by illumination at 785 nm. Two main Raman peaks at 1087 and 1592 cm^{-1}, related to the C-S stretching mode and C-C stretching modes were observed. Additional peaks were observed in the SERS spectrum (**Figure 25*c)*** at 1137, 1388 and 1430 cm^{-1}, associated to vibrational modes of symmetry *b2*. Such peaks are only observable under SERS conditions as they are associated to interactions between 4-ABT and the plasmonic substrates, resulting in chemical charge transfer processes.[88-92]

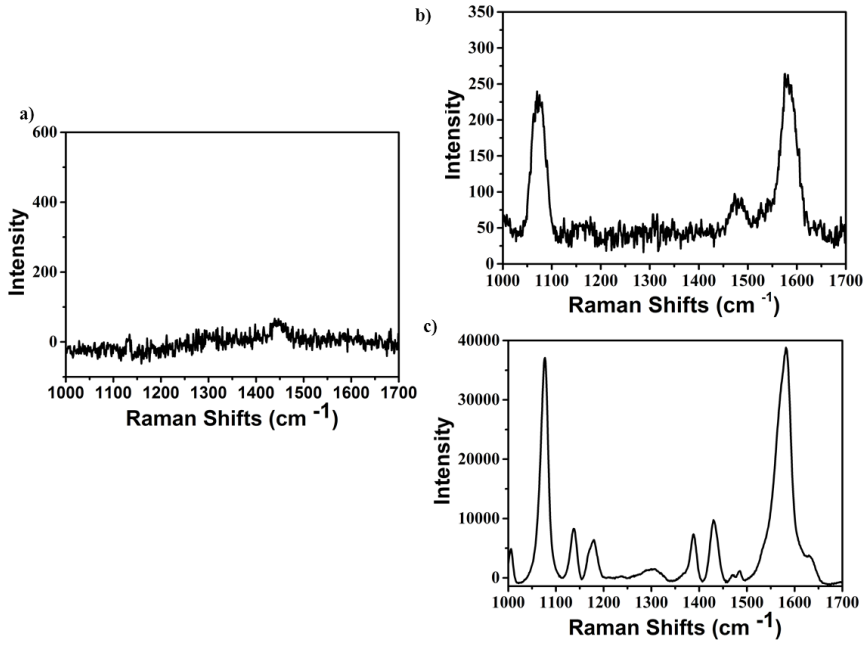

Figure 25. a*) Blank Raman signal of Au nanorod NIs on deposited on glass substrate,* ***b****) Raman signal of 4-ABT deposited on glass substrate and* ***c****) SERS signal of 4-ABT deposited on glass substrate with Au nanorod NIs. All spectra were recorded using 785nm excitation wavelength.*

Similarly, Ag nanoparticle NIs were deposited (5 μL) onto a dry droplet of 4-ABT (10 μL, 0.01mM) onto a glass substrate in order to evaluate the SERS capability of such probes. As the plasmonic peak of Ag NP NIs was centered at 426 nm (broad band) an illumination excitation at 514 nm was selected to test this SERS probes. The SERS spectrum of **Figure 26*c*** showed characteristic SERS peaks of 4-ABT at 1137, 1388 and 1430 cm^{-1}, assigned to *b2* in plane, out of phase vibrational modes and attributed to metal-molecule charge transfer related to a chemical enhancement process[44, 93]. The blank signal for both inks was featureless, indicating no spectral response from the capping agents used in the synthesis.

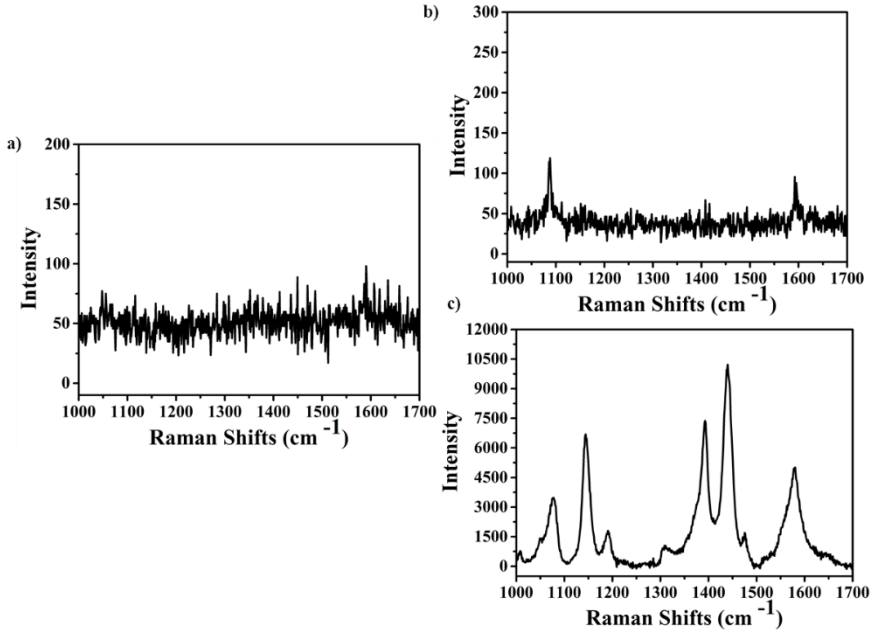

Figure 26. a) *SERS blank signal of Ag nanoparticle NIs on glass substrate;* ***b)*** *NR signal of 4-ABT on glass substrate and* ***c)*** *SERS signal of 4-ABT on glass substrate using Ag nanoparticle NIs using 514nm excitation wavelength.*

2.4. Fabrication of Ag NP pastes as in-situ/ ex-situ SERS probes

Ag nanoparticle paste were synthesized by a modification of the synthesis of Ag NP NIs reported by Liz- Marzán *et al*.[22].This method started with the synthesis of high volume nanoparticle solutions, which were subsequently concentrated up to 200 times in order to obtain highly viscous, paste-like colloids. The obtained Ag NP paste showed a maximum absorbance band at 445 nm (**Figure 27** ***a***). **Figure 27** ***c*** shows SEM images of the Ag nanopaste deposited on SiO_2 substrates. The Ag NPs pastes were mostly spherical in shape and had an average size of 90 nm (**Figure 27** ***d***).

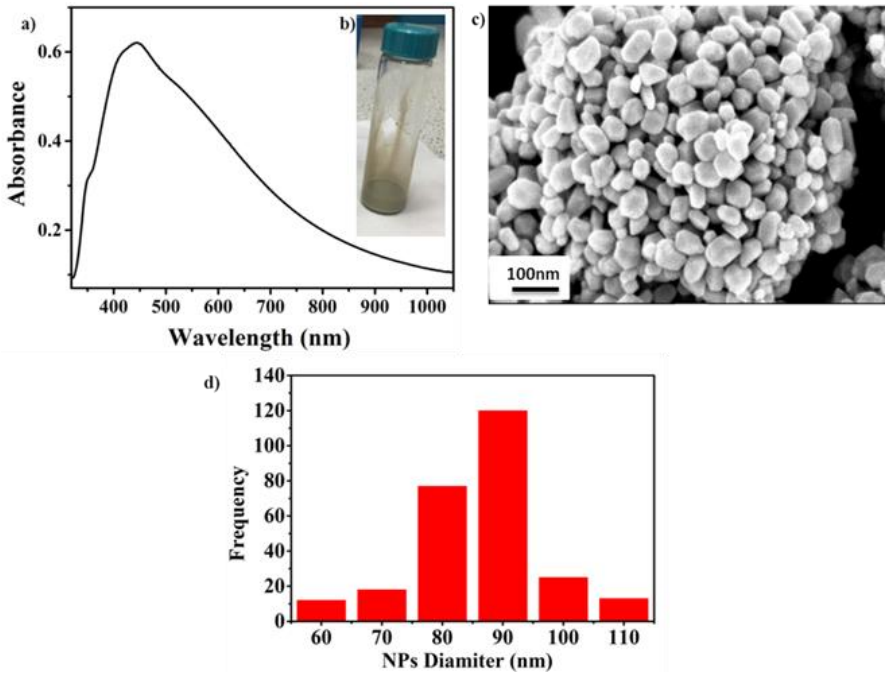

Figure 27. a) *UV-vis spectrum of Ag NP pastes;* ***b)*** *Photography of Ag NP pastes;* ***c)*** *SEM images of the synthesized Ag NP pastes deposited on SiO_2 substrate;* ***d)*** *Histogram of Ag NP pastes diameter obtained by statistical measures over 300 nanoparticles.*

4-ABT was also used as the model molecule to investigate the SERS potential of the fabricated Ag pastes, by depositing 10 µl of Ag NP paste on dried 4-ABT molecule (0.01mM, 5µl) on glass slide. All characteristic SERS peaks of 4-ABT (**Figure 28 *c***) using Ag pastes were collected and compared with the low intensity signals of the Raman spectrum (**Figure 28 *b***), which proved the strong enhancement of the SERS probe using 514nm excitation wavelength. The blank signal of Ag nanopastes deposited on glass slide showed no spectral interference from the citrate molecule used as stabilizer for the nanopaste (**Figure 28 *a***).

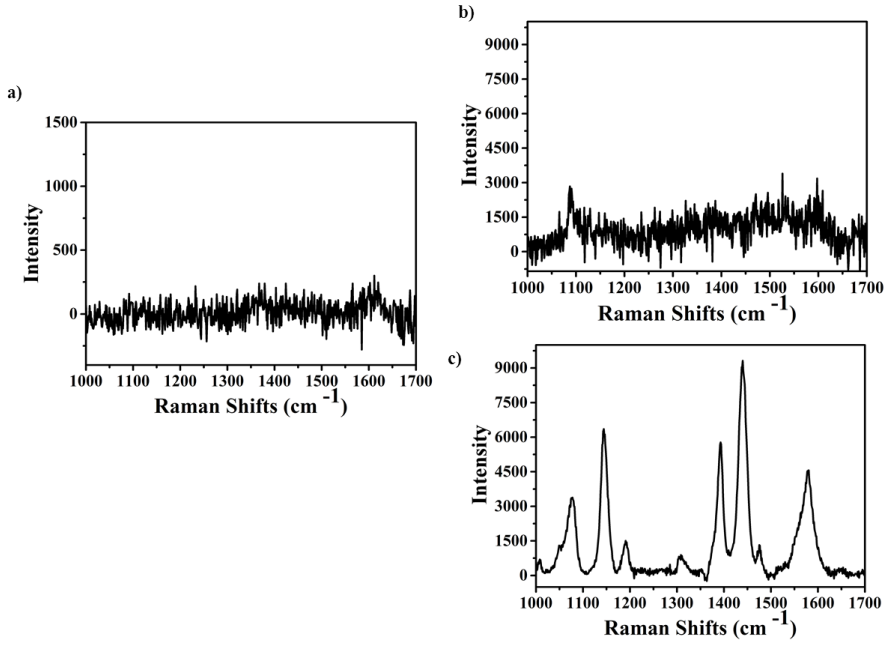

***Figure 28**. **a**) SERS blank signal of Ag NP pastes on glass substrate, **b**) Raman signal of 4-ABT on deposited on glass substrate and, **c**) SERS signal of 4-ABT deposited on glass substrate using Ag NP pastes with 514 nm excitation wavelength.*

SEM images of the Ag pastes compared to as synthetised Ag nanoparticles are shown in **Figure 29.** Different magnification of SEM images of Ag nanopastes on A4 paper show (**Figure 29 *a, b***) even distribution of the nanopaste over the paper fibers. It was clear that the colloids evenly covered large areas of the paper substrate and wrapped uniformly around the paper fibers. In addition, the high SEM magnification of the deposited colloids (**Figure 29 *b)*** showed preservation of their original spherical shape while forming dense coverage on the paper's fibers. **Figure 29 *c,d*** shows an analogous figure displaying the low density coverage obtained by direct droplet deposition of Ag nanoparticles on A4 paper. The SEM images either with high or low magnification shows low density of the diluted silver colloide, therfore, less hot spots on the paper fibers compred to that of nanopastes.

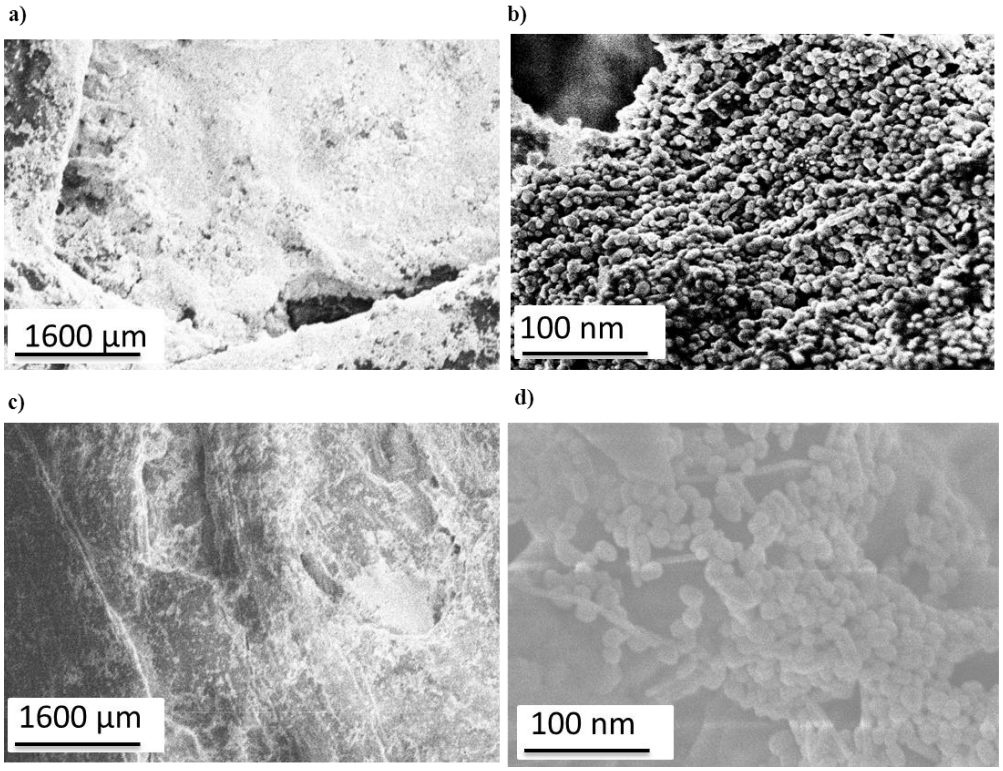

Figure 29. *SEM images of* ***a)****,* ***b)*** *Ag nanopastes deposited on A4 paper with low and high magnifications respectively;* ***c)****,* ***d)*** *Ag nanoparticles deposited on A4 paper with low and high magnifications respectively.*

Although, the SERS measurements performed so far enable in-situ measurement, they are highly invasive as the nanostructures are deposited on the analyte surface of interest and stain the surface where they are deposited. Moreover, the direct deposition of Ag nanoparticles from aqueous solutions on solid substrates is known to create non-homogeneous particle deposition, due to so-called coffee stain effects. This very well-known effect causes the accumulation of nanoparticles into the periphery of concentric rings as the droplet evaporates. [94] In addition, deposited Ag nanoparticles are not tightly bound to the substrate and can detach and transfer to the analytical surface making the analysis of invasive nature. In contrast, work previously carried in our group, showed that nanoparticles dispersed in organic solvents form more homogeneous deposits on solid substrates and can also be transferred from one substrate to another [95].Particles transferred to host substrates resulted tightly bound and displayed strong and reproducible SERS signals. Therefore, in this research efforts have been focused on development of such SERS substrates removable from the analytical surface.

2.5. Fabrication of immobilized Au nanorods on glass slide as SERS composites for ex-situ analysis

Synthesis of Au nanorods

Au nanorods were synthesized by the seed-mediated method reported by El-Sayed et al.[15] **Seed solution:** a CTAB solution (3.75 mL, 0.15 M) was mixed with 1.25 mL of 1mM $HAuCl_4$ at 30°. To the stirred solution 0.3 mL of ice-cold $NaBH_4$ of concentration 0.01 M was added under vigorous stirring, which resulted in the formation of a pale brown solution. Stirring of the seed solution was continued vigorous for 1 min and gentle after further use. **Growth solution:** 0.91 g of CTAB was dissolved in 12.5 ml of deionized water at 30 °C. Once all the CTAB just solved 1 mL of $AgNO_3$ (4 mM) and 12.5 mL of $HAuCl_4$ (1mM) dissolved in deionized water were added. After gentle mixing of the solution 0.175 mL of ascorbic acid (0.0788 M) were injected in once. Upon addition of ascorbic acid, the solution colour changed from intense orange to colourless as a result of the reduction of the Au^{III} ions (yellow-orange colour) to Au^{I} ions (colourless). Finally, 35 μL of seed solution and the colour of the solution gradually changed from colourless to intense brown-red (10-20 mins) as a result of the reduction of the Au^{I} ions (colourless) into Au^{0} nanorods.

Characterisation of the resulted Au nanorods is shown in **Figure 30**, where the UV-Vis spectra shows the maximum absorbance band at 835 nm and transversal band at 510 nm (**Figure 30** ***a).*** High magnification SEM image of the Au nanorods deposited onto a SiO_2 substrate (**Figure 30** ***b)*** illustrates the fabricated Au nanorods with dimensions 55 × 30 nm Aspect Ratio:1.9, which was obtained by statistical measurement of over 100 rods (**Figure 30** ***c,d).***

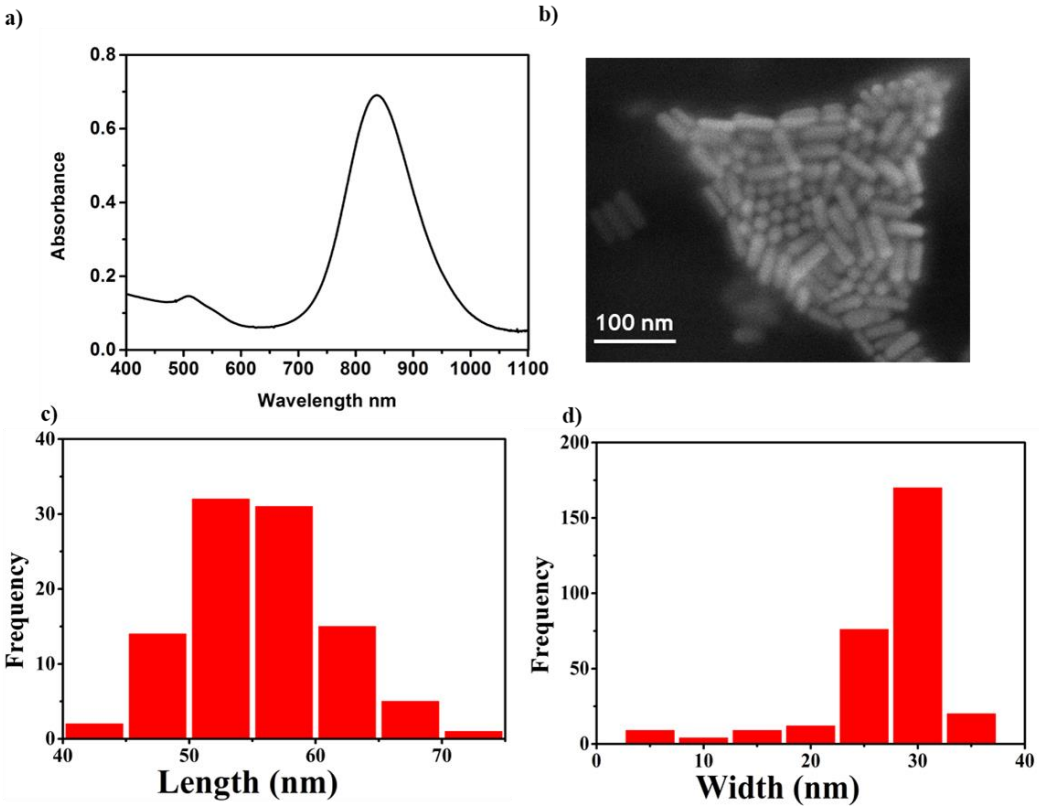

Figure 30. a) *UV-Vis spectrum of Au nanorods in water;* ***b)*** *SEM images of the synthesized Au nanorods deposited on* SiO_2 *substrate;* ***c)*** *and* ***d)*** *Histogram of Au nanorods length and diameter obtained by statistical measures over 300 nanoparticles respectively.*

Overgrowth and Phase transfer of Au nanorods

Overgrowth: Au nanorods were overgrown by reduction of the $Au^{(I)}$ remaining in solution after a typical seed mediated synthesis, according to a method described by Liz-Marzán *et al.* [96]. The process consisted of stepped additions of reducing agent ascorbic acid to the solution of Au nanorods. The excess ascorbic acid reduced the $Au^{(I)}$ ions left unreacted in the nanorod solution leading to a growth of the nanorod. The overgrowing process was monitored by the gradual increase in intensity of the longitudinal plasmon band in combination with a slight blue shift (775 nm) (**Figure 31**). The suspension was stirred until no unreacted $Au^{(I)}$ ions were left in the solution, as estimated by the absence of further changes in the UV-vis spectrum upon addition of ascorbic acid.

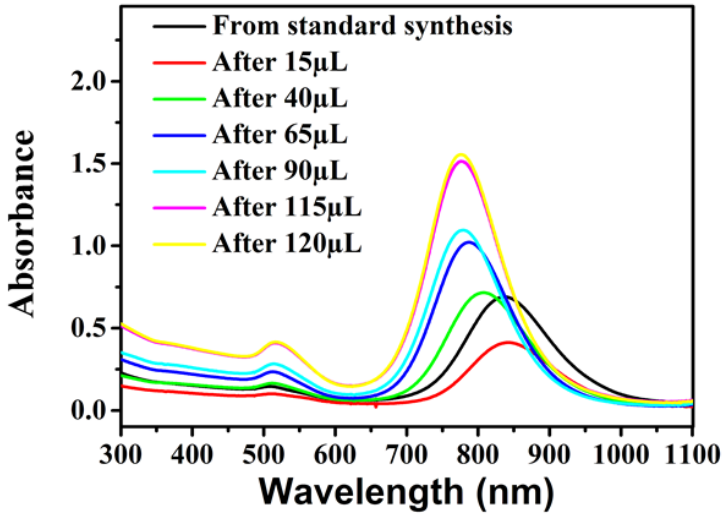

Figure 31. *UV-vis spectra of of AuNRs in water and the overgrowth process after stepped addition of Ascorbic acid.*

Transfer to organic phase: nanorods were transferred into chlorobenzene following the method described by Chen et al.[31]. Briefly, As-prepared overgrown Au nanorods in water solution were centrifuged and redispersed into water, in order to maintain the final CTAB concentration to lower than 0.2 mM. Then, Mercaptosuccinic acid (3 mL, 10 mM) was added to 3 mL of aqueous nanorod solution (pH = 9) under vigorous stirring. To this solution 1.5 mL of a 50 mM solution of TOAB in chlorobenzene was added. The resulting mixture was left under vigorous stirring for 30 min until the water phase discolored and the organic phase became intense red, indicating the transfer of Au nanorods into chlorobenzene with maximum absorbance band shifted to 824 nm (**Figure 32 *a***).

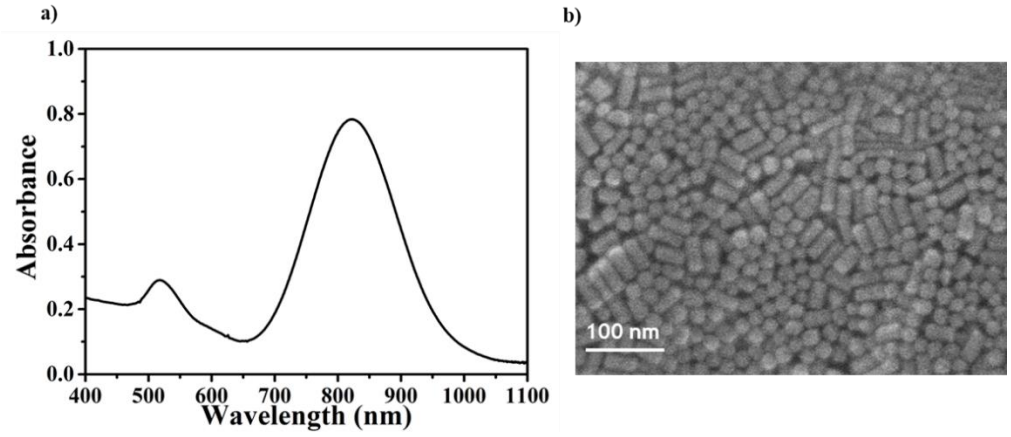

Figure 32. a) *UV-vis spectrum of Au nanorods dispersed in chlorobenzene;* ***b)****. SEM image of hydrophobic overgrown Au nanorods deposited on* SiO_2 *substrate.*

Immobilized Au nanorods on SiO_2 substrate

Schematic of **Figure 33** shows the process of immobilizing Au rods a SiO_2 support. A small aliquot (10 μL) of Au nanorod cholobenzene solution 15 × 40 nm ([Au] = 10 nM) was deposited on a SiO_2 support, covered with a petri dish, and then left to evaporate at room temperature over a time of 3 hrs, resulting in vertical arrays formation. Fabricated arrays were transferred intact onto transparent supports by placing a glass coverslip on the original SiO_2 support and pressing the two surfaces together for 30 s. Excess organic matter was removed by multiple rinses with fresh isopropanol.

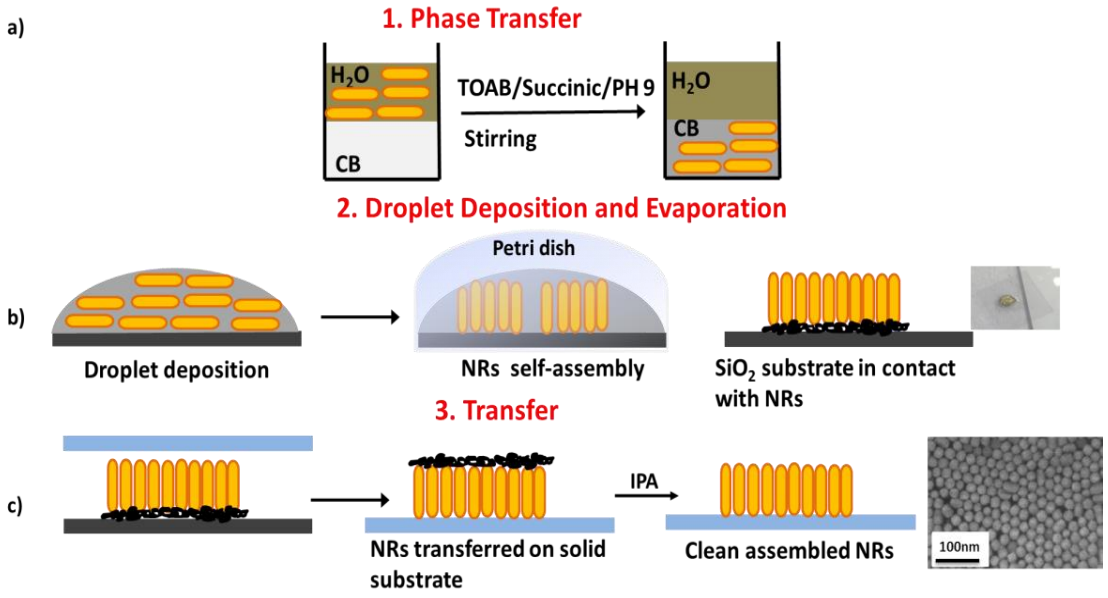

Figure 33. *schematic representations of* ***a)*** *phase transfer of Au nanorods into cholorbenzene;* ***b)*** *droplet deposition and evaporation process. Inset is photography of Au nanorods in chlorobenzene deposited on glass slide before stamping;* ***c)*** *transfer processes to SiO_2. Inset is SEM image of gold vertical arrays immobilized on SiO_2 after stamping.*

2.6. Fabrication of immobilized Ag nanoparticles on solid substrates for in-situ/ex-situ SERS analysis

Synthesis of Ag nanoparticles

Ag nanoparticles were synthesized by a modified version of a previously reported by Sheehan et al. [97]. Typically, 12 mL of a (0.2% w:w) solution of silver nitrate and 488 mL of deionized water were mixed with stirrer bar and heated to 100° C. Next, 11.6 ml sodium citrate

(0.034 M) in deionized water was added, followed 30 s later by the quick injection of 5.5 mL of a freshly prepared, ice-cold solution of sodium borohydride (0.2 M) and sodium citrate (0.03 M) in 50 mL deionized water. Then, the silver solution was cooled, centrifuged once at 9000 rpm for 20 mins and redispersed in deionized water (4 ml) and stored in the dark. **Figure 34** illustrates the optical characterization of the obtained silver particles. The maximum absorbance of the synthesized silver particles was at 388nm and a shoulder at 425 nm ***(*Figure 34 *a)***, with an average size of 15 nm was measured over 300 particles ***(*Figure 34 *b)***. The size control was important as literature showed that silver particles larger than 25 nm barely transferred to organic solvents [32].

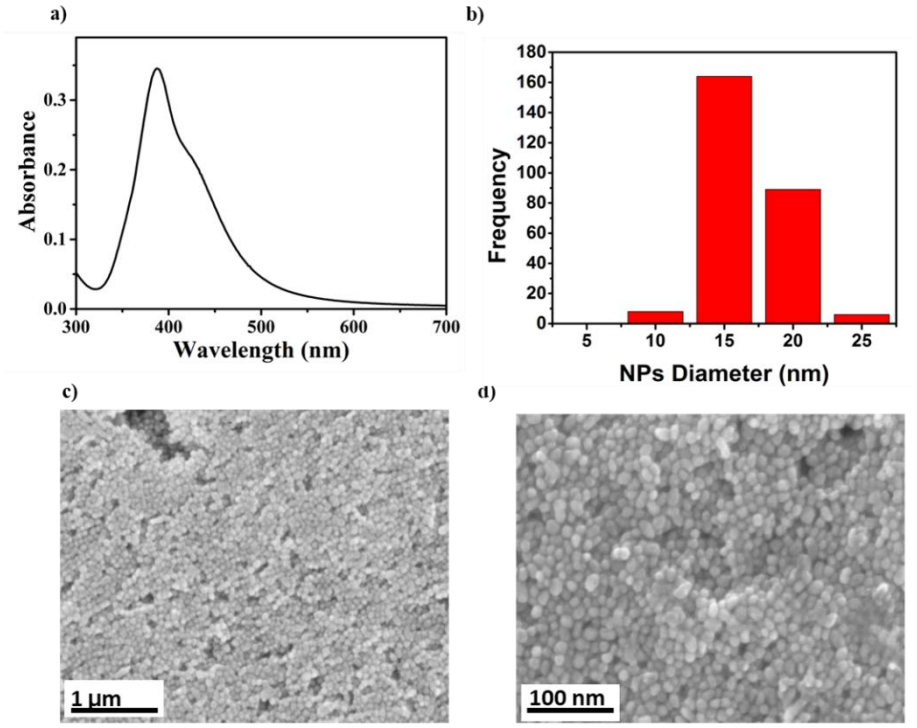

Figure 34. a) *UV-vis spectrum of Ag nanoparticle aqueous solution;* ***b)*** *histogram of Ag nanoparticle diameter obtained by statistical measures over of 300 nanoparticles;* ***c),*** *and* ***d)*** *SEM images of Ag nanoparticle in organic solvent deposited on* SiO_2 *substrate.*

Phase transfer of Ag nanoparticles into organic solvent

Ag nanoparticles were transferred to organic phase by slight modification of a method previously reported [32]. Briefly, 2 mL of the concentrated aqueous Ag nanoparticle solution were added to 2 mL of a 2×10^{-5} M solution of ODA in chlorobenzene. The two solutions were

vigorously stirred for 60 mins to facilitate the transfer of Ag nanoparticles to the organic phase. The phase transfer of silver particles was achieved by using ODA as transferring agent, due to the electrostatic interaction between the carboxylate ion on the nanoparticle surface and the ionized amine groups of ODA; therefore, the hydrophobization of Ag nanoparticles surfaces occurred and resulted in the phase transfer. The transferred silver particles in chlorobenzene have a maximum absorbance band at 415 nm (**Figure 36 a**), which was red shifted after the transfer to chlorobenzene suspension with an average size of Ag nanoparticles is 20 nm (**Figure 36 b**). SEM images of the hydrophobic silver particles deposited on SiO_2 substrate shown in **Figure 36 c,d**.

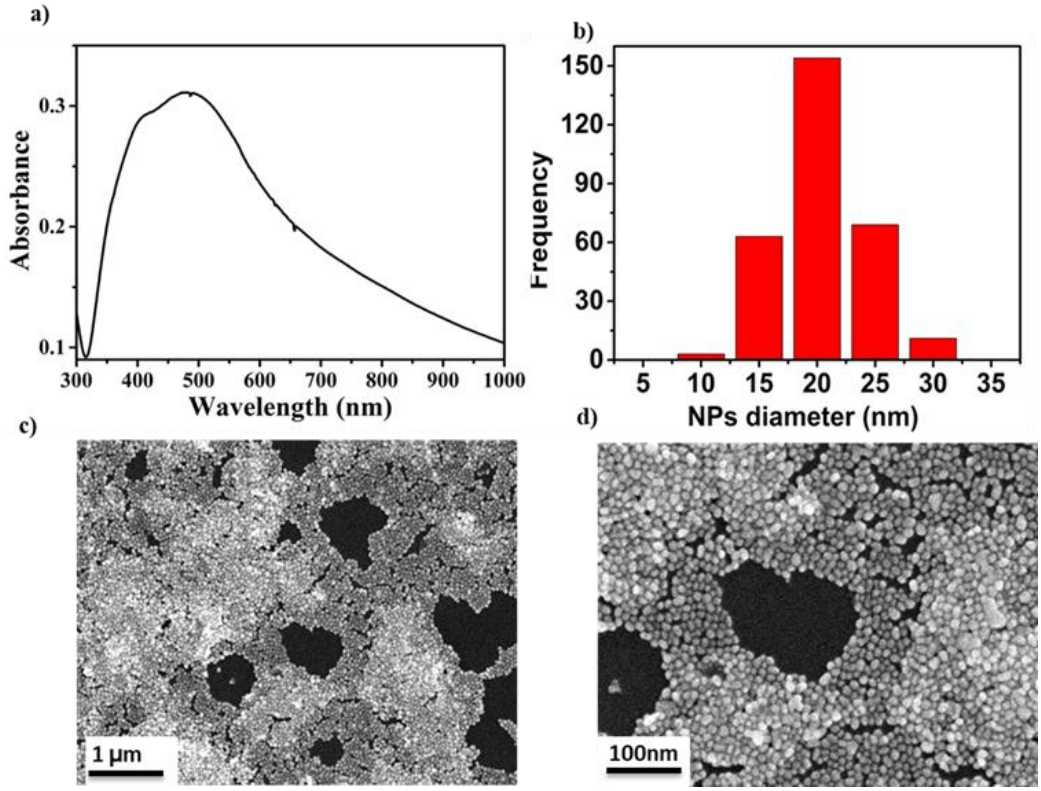

Figure 35. a) *UV-Vis spectrum of Ag nanoparticles in chlorobenzene;* ***b)*** *Histogram of Ag nanoparticles diameter obtained by statistical measures over of 300 nanoparticles;* ***c)*** *and* ***d)*** *SEM images of Ag nanoparticles in chlorobenzene deposited on* SiO_2.

Immobilized Ag nanoparticles on rigid and flexible solid substrates: fabrication of Ag NPs/glass, Ag NPs/PDMS and Ag NPs/PMMA composites.

These novel SERS probes were developed to overcome some of the obtacles associated with SERS analysis of target analytes. Specifically, transparent substrates can be applied on the analytical surface and allow in situ measurements. Transparent/flexible can mold over irregular surfaces allowing effective detection on food surfaces. The tight immobilization of Ag nanoparticles developed allowed for non-invasive measurements.

Glass substrates were used as rigid substrate after being cleaned with acetone and deionized water and dried with N_2 gun. Polydimethylsiloxane (PDMS) was fabricated by pouring 10:1 (w:w) of Sylgard 184 elastomer and curing agent in a petri dish followed by heating at 60 °C for 24 hrs. After removal from oven, the PDMS film was rinsed with isopropanol several times, dried with N_2 gun and cut to small squares of 1×1 cm. The final thickness of the PDMS film was 1 mm. Poly methyl methacrylate (PMMA) with a molecular weight of 996000 was fabricated using acetone as solvent and with concentration of 10%wt, then left to dry and subsequently cut to small squares of 1x1cm with final thickness of 0.5mm.

Ag nanoparticles were transferred onto glass or polymers (PDMS, PMMS) by using these substrates as support to retrieve assembled nanoparticles. After transfer of the Ag nanoparticles into organic solvent, a small aliquot (10 μl) of Ag nanoparticle chlorobenzene solution was deposited on an acetone-cleaned glass coverslip (**Figure 36**). The droplet was left in contact with air (5 mins) until Ag nanoparticles spontaneously self-assembled at the solvent/air interface, as shown by the formation of a metallic lustre layer. Substrates then were used to transfer the assembled nanoparticles by bringing them into contact with the nanoparticle droplet for 30 s. Excess organic matter was removed by multiple rinses with fresh isopropanol.

A number of factors were considered responsible for the self-assembly of Ag nanoparticles in chlorobenzene and their transfer to rigid and flexible substrates: i) lower surface tension of chlorobenzene compared to water, which promoted movement of particles close to each other and therefore self-assembly; ii) formation of a well-defined and high curvature droplet, due to the high contact angle of chlorobenzene on glass; iii) strong Van der Waals hydrophobic attractive forces between ODA alkyl chains which overcame repulsive electrostatic forces between nanoparticles.

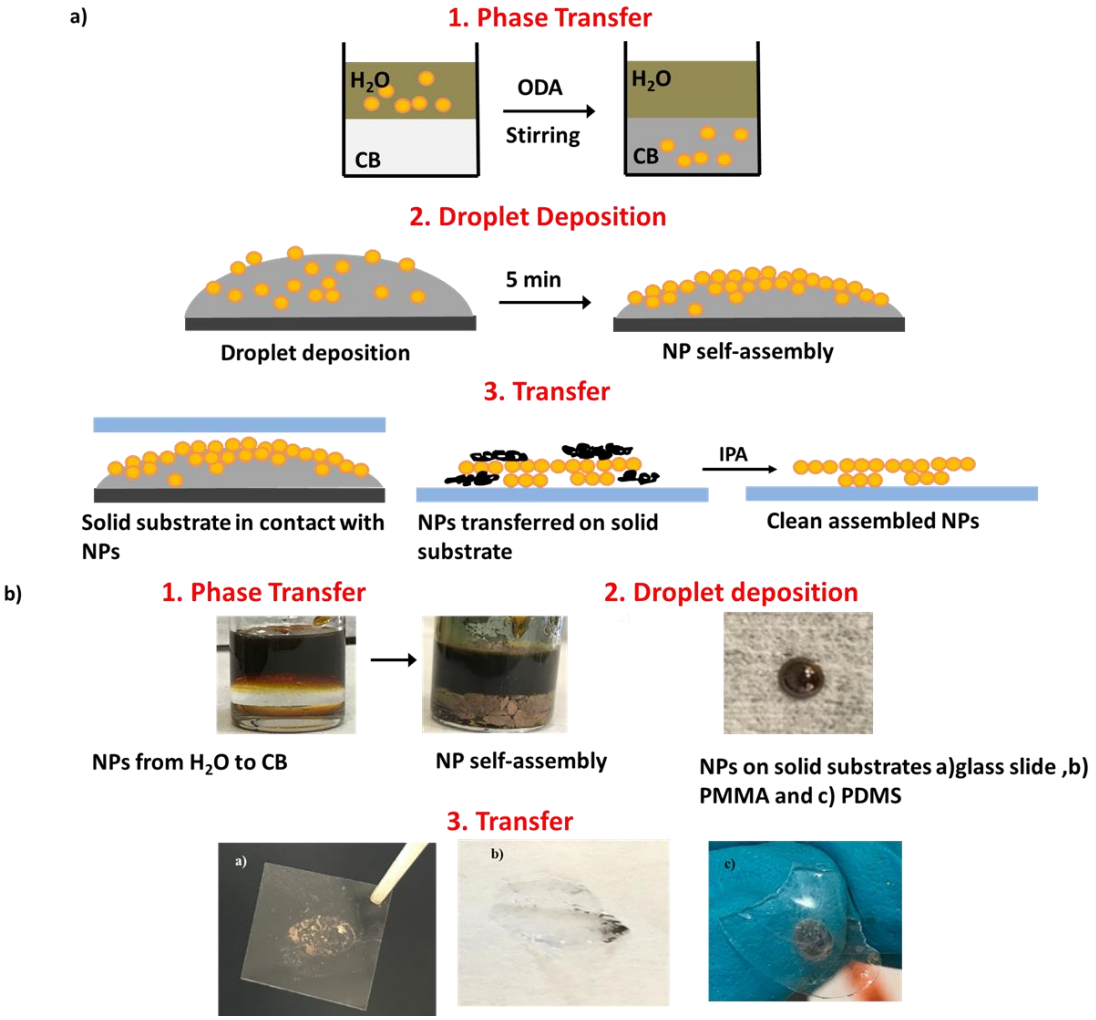

Figure 36. a) *schematic representations of phase transfer, droplet deposition and transfer processes of Ag nanoparticles into substrates;* ***b)*** *representative photographs illustrating the same processes depicted in a).*

2.7. Raman Confocal Analysis

The ability of assembled Ag/transparent substrates to perform SERS measurements in situ can open up interesting applications, whereby the SERS substrate can be applied to the surface under examination and measurement can be performed through the substrate by back illumination. Confocal Raman spectroscopy is essential to perform such analysis, in order to focus the illumination excitation at the plasmonic/sample interface where the SERS phenomenon is taking place. In order to investigate the behaviour of fabricated SERS probes, a confocal Raman spectrograph with 514 nm laser excitation was used. The SERS investigation was done by placing Ag NPs/glass, Ag NPs/PDMS and Ag NPs/PMMA SERS substrates on a dry 4-ABT in MeOH droplet (10 μL, 0.01mM) deposited on glass slide, with the side of Ag

nanoparticles facing the 4-ABT molecule for backside SERS measurements.

The importance of the focal point was investigated by a comparison between SERS signals collected at the outer surface of the SERS substrates and signals collected at the Ag nanoparticle/4-ABT molecule interface. The confocal results of Ag NPs/glass, Ag NPs/PDMS and Ag NPs/PMMA SERS substrates (**Figure 37,Figure 38, Figure 39**) show that SERS signals are clearly very different when the laser focused on the outer surface of the substrate (featureless spectra), with significantly enhanced SERS spectra with all characteristic peaks of 4-ABT obtained when the laser was moved precisely into the cross-section (intersecting) between the Ag particles and the 4-ABT.

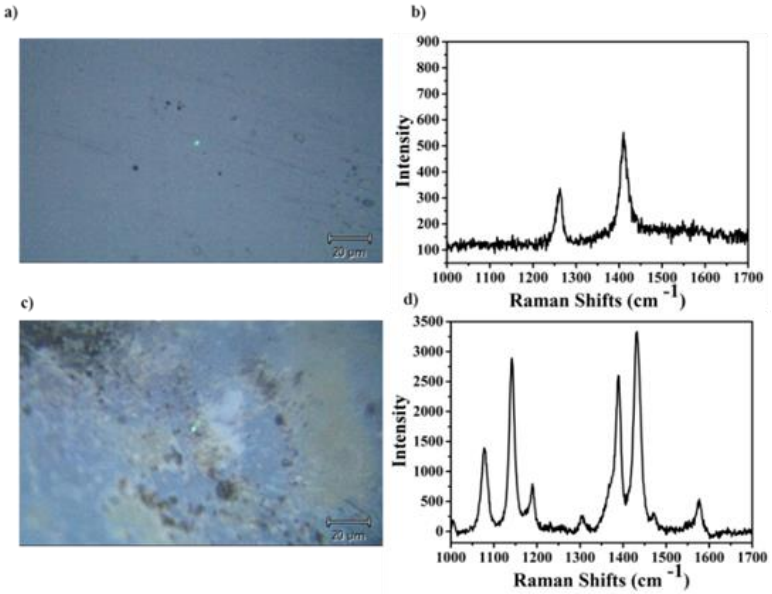

Figure 37. a) *Optical microscopic image of Ag NPs/glass composite substrate when the focus on the outer surface of the substrate;* ***b)*** *SERS spectra of 4-ABT collected when the focus on the area in image (a);* ***c)*** *Optical microscopic image of Ag NPs/glass composite substrate when the focus on the point where Ag NPs and the 4-ABT molecule in contact; and* ***d)*** *SERS spectra of 4-ABT collected when the focus on the area in image (c).*

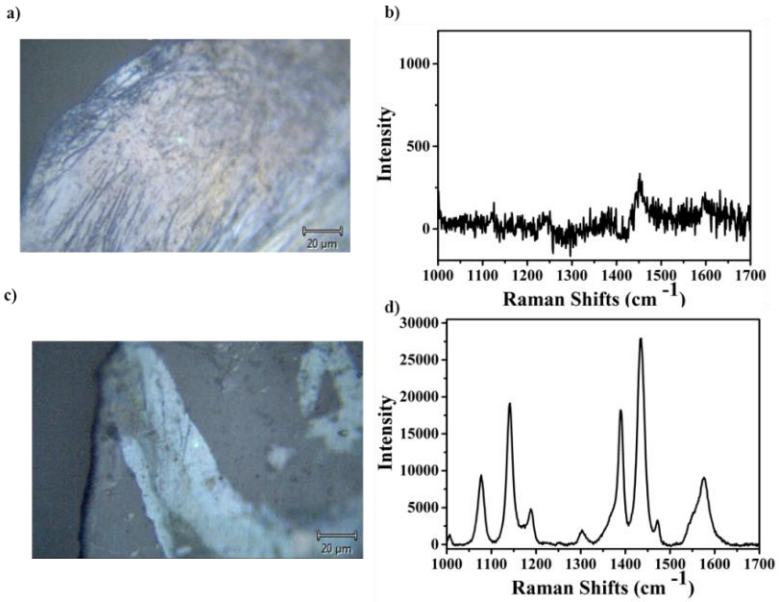

***Figure 38**. **a)** Optical microscopic image of Ag NPs/PDMS composite film when the focus on the outer surface of the film; **b)** SERS spectra of 4-ABT collected when the focus on the area in image (a); **c)** Optical microscopic image of Ag NPs/PDMS composite film when the focus on the point where Ag NPs and the 4-ABT molecule in contact; and **d)** SERS spectra of 4-ABT collected when the focus on the area in image (c).*

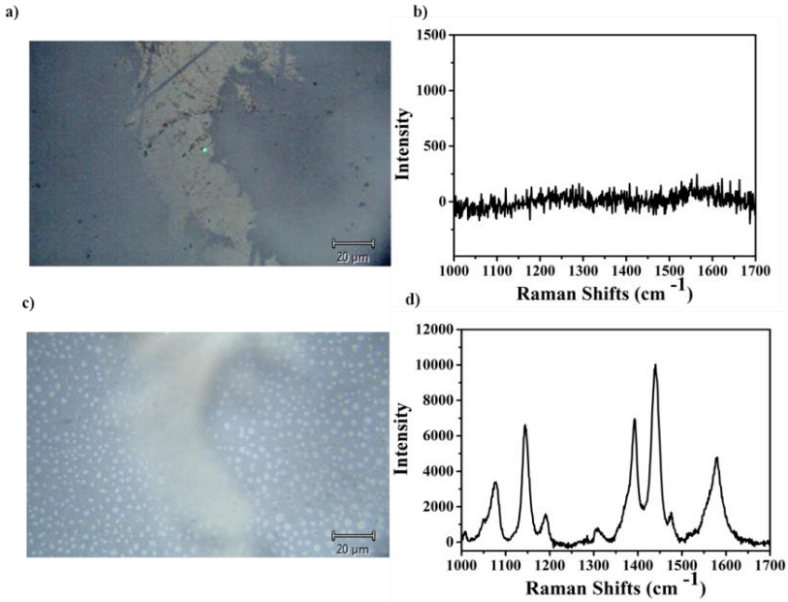

***Figure 39. a)** Optical microscopic image of Ag NPs/PMMA composite film when the focus on the outer surface of the film; **b)** SERS spectra of 4-ABT collected when the focus on the area in image (a); **c)** Optical microscopic image of Ag NPs/PMMA composite film when the focus on the point where Ag NPs and the 4-ABT molecule in contact; and **d)** SERS spectra of 4-ABT collected when the focus on the area in image (c).*

2.8. Characterization and SERS evaluation of Ag NPs/glass, Ag NPs/PDMS and Ag NPs/PMMA composites

Low and high magnifications SEM images (**Figure 40*a,b***) show successful attachment of Ag nanoparticles into the host glass substrate (photograph in the inset of **Figure 40*b***). In order to obtain SERS spectra, fabricated Ag NPs/SiO_2 substrate were deposited on a dry droplet (10 μL, MeOH) of 4-ABT 0.01 mM, with Ag particles in contact with 4-ABT and 514 nm laser penetrating from the back of the substrate. **Figure 41*a*** shows no expected interference of the blank as featureless Raman and SERS signal of the Ag NPs/SiO_2 substrate was achieved**.** Strong SERS signals with all distinctive peaks of 4-ABT (1433 cm^{-1}, 1389 cm^{-1}, and 1139 cm^{-1}) were collected (**Figure 41*c***), compared to weak Raman signals with two dominant peaks at 1592 and 1087 cm^{-1} assigned to C-C stretching mode and the C-S stretching mode, respectively.

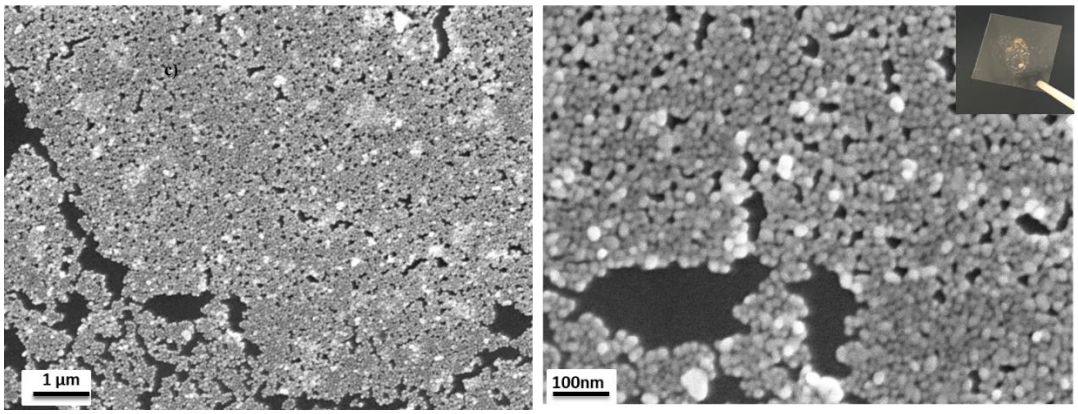

Figure 40. *SEM images of Ag NPs/glass substrate* ***a)*** *low magnification and* ***b)*** *high magnification. Inset: photography of Ag NPs immobilized on glass slide.*

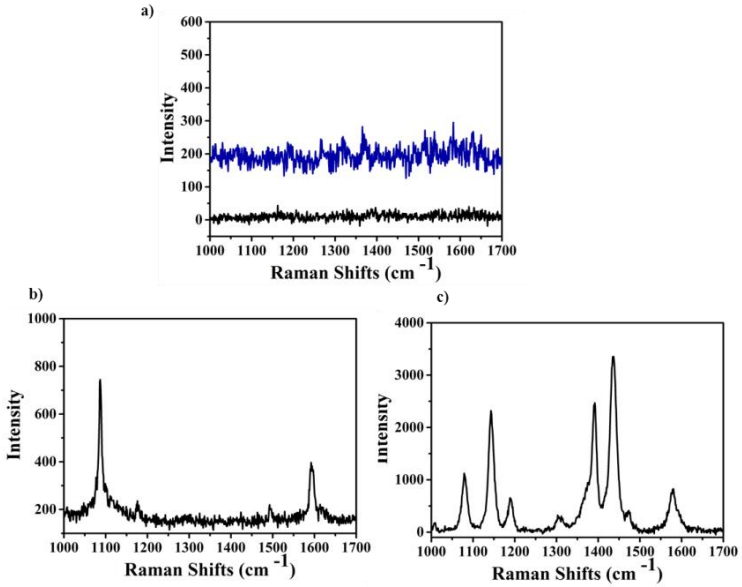

Figure 41. a) *Raman signal (black line) signal of blank SiO_2 and SERS signal (blue line) of Ag NPs/glass substrate;* ***b)*** *Raman 4-ABT deposited on SiO_2;* ***c)*** *SERS signal of 4-ABT deposited on glass slide by back illumination of Ag NPs/glass on 4-ABT (514nm).*

PMMA polymer did not show any dominant peaks either in Raman or SERS spectra (**Figure 42*a)***. **Figure 42*b,c*** illustrate the typical Raman signal of 4-ABT compared to the significantly enhanced 4-ABT SERS signal obtained using Ag NPs/PMMA with 514nm excitation wavelength. The obtained SERS enhancement resulted from careful confocal focus at the Ag NPs/4-ABT intersection point. Noteworthy, despite the flexibility of PMMA polymer, the substrate needed some support to be kept in full contact with the analyzed molecule. Two glass slides were placed at either side of the Ag NPs/PMMA substrate to promote contact.

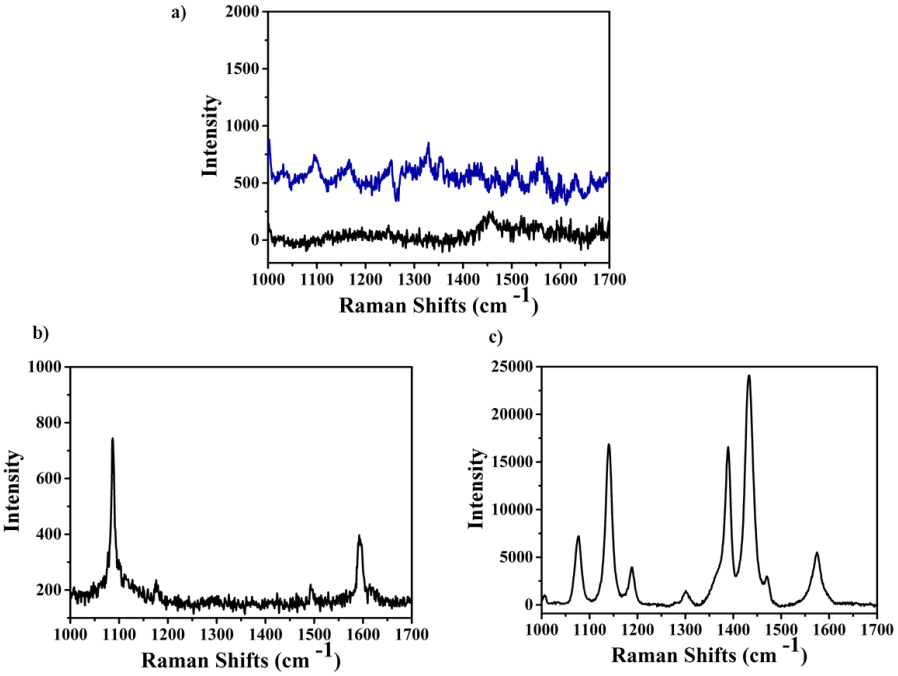

Figure 42. a) *NR signal (black line) signal of blank PMMA and SERS signal (blue line) of Ag NPs/ PMMA substrate;* ***b)*** *NR 4-ABT deposited on glass slide;* ***c)*** *SERS signal of 4-ABT deposited on glass slide by back illumination of Ag NPs/ PMMA on 4-ABT (514nm).*

A SEM image of the Ag NPs layers transferred on the PDMS film is displayed in **Figure 43*a***. Dense and high coverage of surface areas larger than 10 μm^2 was achieved. Closer observation of magnified areas (**Figure 43*b***) showed that a mixture of monolayers and multilayers formed during the process. The high resolution confirms that nanoparticle size and shape was also maintained during all the fabrication process of the Ag NPs/PDMS SERS composite. Finally, SERS analysis on 4-ABT model molecule was conducted (**Figure 44**). Raman and SERS spectra of PDMS (**Figure 45a**) show signals at 1406 cm^{-1} and 1260 cm^{-1} peaks related to CH_3 asymmetric bending and CH_3 symmetric bending, respectively [98]. However, the SERS signal of 4-ABT was strong and clean of any polymer spectral interference.

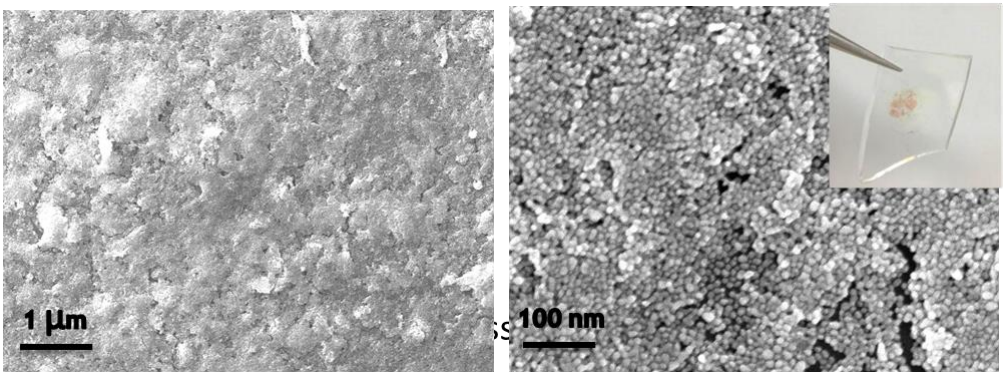

Figure 43. *SEM images of Ag NPs/PDMS* ***a)*** *low magnification and* ***b)*** *high magnification. Inset: photography of Ag NPs immobilized on PDMS.*

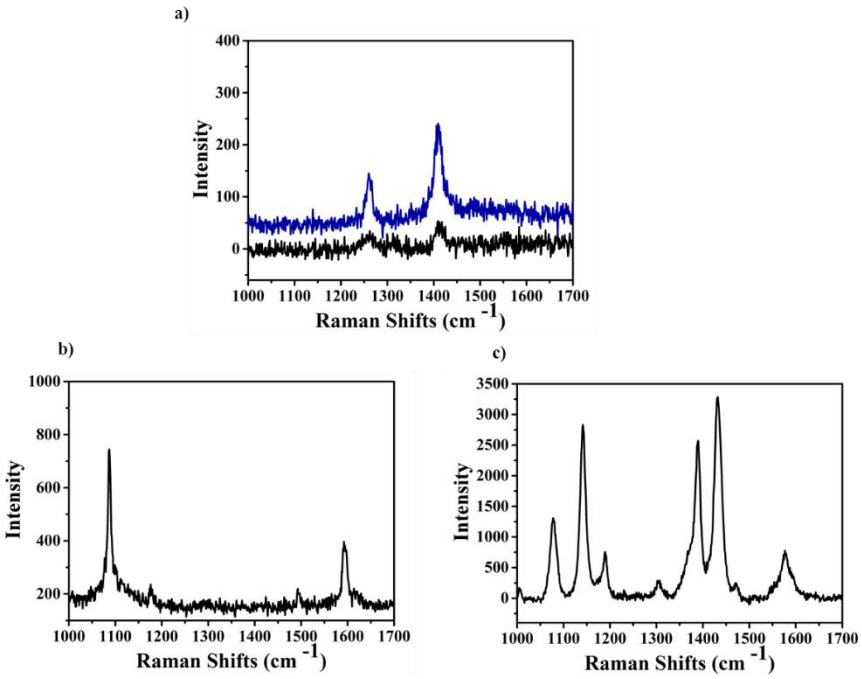

Figure 44. a) *Raman and SERS signals of blank PDMS film;* ***b)*** *Raman 4-ABT on glass slide and c) SERS signal of 4-ABT using Ag NPs/PDMS film back illumination (514nm).*

2.9. Investigation of minimal invasiveness of portable SERS probes

SERS substrates that fulfill transparency and /or flexibility and conformability to the substrate would be ideal to perform non-invasive SERS analysis in situ for example on precious drawings and paintings. For this reason the non-invasiveness of these composites was tested on white commercial paper prior testing on real samples. Ag NPs/glass as rigid substrate and Ag NPs/PDMS as flexible substrate were chosen for this investigation as both showed good contact with the analyte and high transparency features, while Ag NPs/PMMA was excluded due to its inability to contact the analytical surface without external support (glass slide or tape).

Cleaning process

Contamination of analytical surfaces could arise from detachment of loosely attached Ag nanoparticles from the glass or PDMS support during contact with the analyte. In order to prevent such contamination a cleaning process was developed. In addition, excess organic solvent and ODA residues can have their own SERS response and interfere with SERS analysis. In order to minimize such side effects Ag NP/glass and Ag NP/PDMS probes were immersed in isopropanol overnight, washed extensively with isopropanol and deionized water and dried with nitrogen gun prior use.

Pressing process

After the cleaning process, the Ag NPs/substrates were investigated for invasiveness, by gently hand pressing them on a A4 office paper followed by analysis under optical microscope to assess presence of any residue. Office paper was chosen due its clear white colour and in view of future applications on artistic drawings. **Figure 45, 1** illustrates the cleaning process under the microscope for Ag NPs/glass substrate: optical microscopy images of the A4 paper were taken before any contact with the composite and after the composite was pressed on the paper. This process showed that four contacts with paper were necessary before no Ag nanoparticle residue was observed on the paper, as shown in Figure 45.1, b-e. After the four pressure trial no more residues were observed for subsequent SERS probe depositions (Figure 45.1f) On the other hand, Ag NPs/PDMS substrate (**Figure 45, *2***) no nanoparticle traces were observed after the first and subsequent depositions.

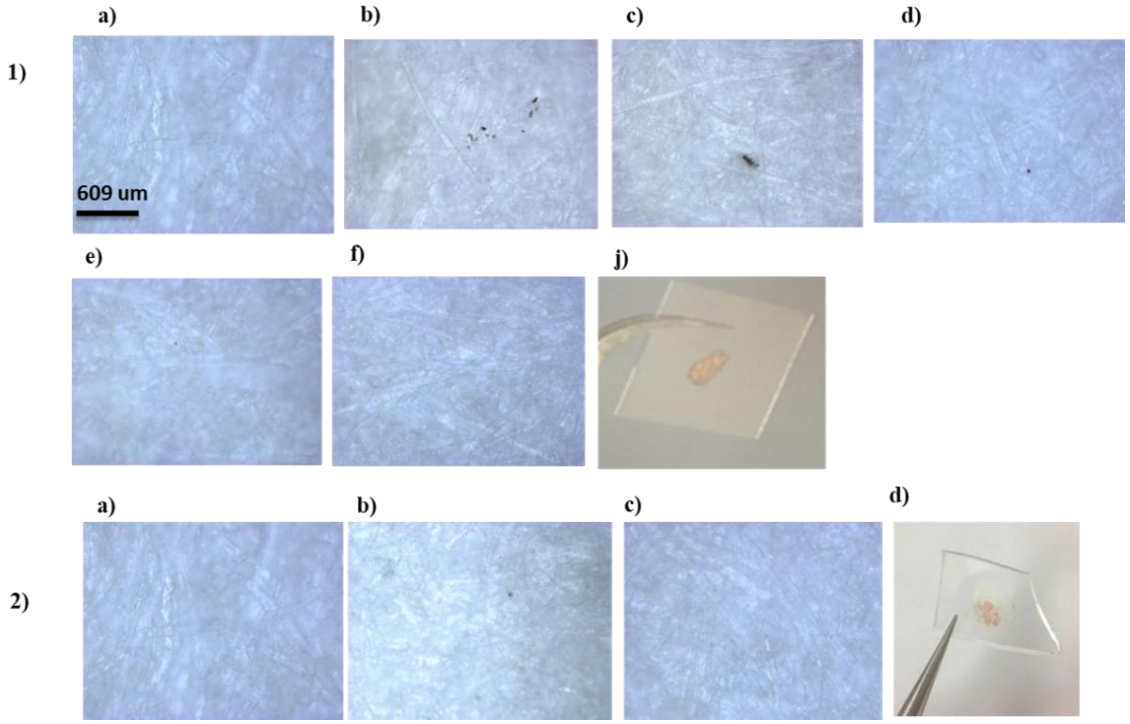

Figure 45.1. *a) Optical microscopy image of white paper before Ag NPs/glass deposition; b-f) optical microscopy images of white paper following consecutive Ag NPs/glass depositions; j) photograph of Ag NPs/glass SERS probe. Scale bar is 609 um for all images*

Figure 46.2. *a) Optical microscopy image of white paper before Ag NPs/PDMS deposition; b-c) optical microscopy images of white paper following consecutive Ag NPs/PDMS depositions; d) photograph of Ag NPs/glass SERS probe.*

Moreover, Ag particles were transferred to different organic solvents and immobilized through the same method to compare Ag NPs/glass and Ag NPs/PDMS efficiency. **Table 1** shows the number of times that different substrates must be pressed on A4 paper before it can be applied on a sample. It is clear that the immobilized Ag on PDMS substrate is the best SERS substrate in terms of cleaning as it becomes non-invasive substrate after being only cleaned once, comparing to the glass slide.

Substrates	Organic Solvents	Immobilization Method	Number of Pressing Times to Achieve Clean Paper
Glass slide	Chlorobenzene	Stamped	2-3 times
Glass slide	Cyclohexane	Stamped	4 times
PDMS	Chlorobenzene	Stamped	1 time
PDMS	Cyclohexane	Stamped	2 times
PDMS	Hexane	Deposited	More than 10 times

***Table 1**. Cleaning process using Ag NPs in different organic solvents and immobilised on glass slide and PDMS.*

2.10. Micro-extraction of analyte using immobilized Ag nanoparticles on flexible PDMS

Efficient extraction of 4-ABT model molecule deposited on glass slide using Ag NPs/PDMS film was achieved by placing the composite film on the dried molecule and performing gentle pressing for three seconds. Then, the Ag NPs/PDMS was removed for further ex-situ SERS analysis. Strong and clear SERS signals were obtained (**Figure 47**) for 4-ABT with all its discriminative SERS peaks. The blank signal of the SERS substrate illustrates two peaks at 1400 and 1250 cm^{-1} [98]which were assigned to the PDMS film and not matching any of the characteristic peaks of 4-ABT. This further use indicated great potential of SERS composites for easy sampling of real analytes without any use of organic solvents for extraction.

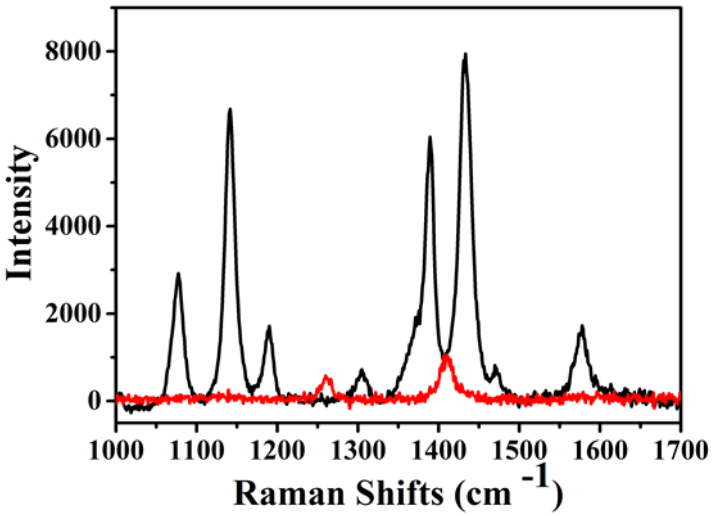

Figure 47. *SERS spectrum (red line) blank of Ag NPs/ PDMS composite compared to SERS signal of 4-ABT molecule (black spectrum) after micro-extraction using Ag NPs/PDMS substrate.*

2.11. Conclusion

In conclusion, different methods of fabricating SERS probes were developed for various SERS applications. Au and Ag nanoinks fabricated with different plamonic bands for direct in-situ SERS analysis of sample or ex-situ after extraction of target analyte were fabricated. For more homogenous and dense distribution of nanoinks, a concentration method was developed to obtain paste-like colloidal solution of Ag nanoparticles for more sensitive and strong enhancement of SERS either in-situ or ex-situ. As portable SERS probe, gold rods stamped on SiO_2 with high level of ordered arrays for more sensitive and reproducible ex-situ SERS investigation were fabricated. Finally, Ag nanoparticles were stabilized on rigid and flexible substrates for in-situ SERS analysis at the point-of-care or for minimally invasive in-situ SERS analysis. Moreover, a new solvent-free micro-extraction method was developed using immobilized Ag particles on flexible PDMS. SERS feasibility of all SERS probes was proved using 4-ABT as model molecule and optical characterization of all fabricated nanostructures showed large range of fabricated nanostructures and applications.

CHAPTER 3

Using Au/Ag nanoinks and Au vertical arrays for the SERS analysis of blue BIC ballpoint pen

Metal nanoinks constituted by Ag nanoparticles and Au nanorods were employed as probes for the Surface Enhanced Raman Scattering (SERS) analysis of a blue BIC ballpoint pen using 514 nm and 785 nm excitation wavelengths for complementary SERS analysis. Highly enhanced SERS spectra were obtained compared to normal Raman (NR) signals, with Enhancement Factors (EFs) between 5×10^3 and 3×10^6 were achieved, depending on the combination of SERS probes and laser illumination used. Furthermore, Au nanorods vertical arrays immobilized on rigid substrate SiO_2 were also used for reproducible and sensitive ex-situ SERS analysis of blue Bic pen ink traces. The self-assembly of Au nanorods into large area ordered superstructures allowed detection of BIC pen traces with good intensity and high reproducibility SERS spectra, due to the high density of hot spots and morphological reproducibility of these superstructures.[1]

---

[1] * This work has been published as: "**Metal nanoinks as chemically stable surface enhanced scattering (SERS) probes for the analysis of blue BIC ballpoint pens** ", A. Alyami,[a] D. Saviello,[a] M. A. P. McAuliffe [b] A. Mirabile, [c] L. Lewis[ab] and D. Iacopino *[a]: Phys. Chem. Chem. Phys., 2017, 19, 14652.

This work has been published as: "**Chemically stable Au nanorods as probes for sensitive surface enhanced scattering (SERS) analysis of blue BIC ballpoint pens** ", Abeer Alyami[1], Daniela Saviello [1], Micheal A.P. McAuliffe [2], Raffaele Cucciniello [3], Antonio Mirabile [4], Antonio Proto [3], Liam Lewis [2], Daniela Iacopino[1,a] AIP Conference Proceedings **1873**, 020003 (2017); doi: 10.1063/1.4997132.

3.1. Introduction

The scientific interest behind commercial ink characterisation relies to its importance for forensic examination applications. However, recently chemical characterisation of ball-point pens has gained importance for art conservation purposes as many ball point pen were found to be used in many museum collections all over the world. Ballpoint pen inks are complex mixtures of several dyes and pigments constituting up to 50% of the total ink formulation contained in either a glycol-based solvent or benzyl alcohol [62, 63]. Additional components (vehicle) include fatty acids, softeners and polymeric resins, designed to improve the consistency, flow or drying characteristics of the ink [64]. This complex composition makes the identification of dyes in inks challenging. Additional difficulties are constituted by trademark protection and periodical introduction in the market of novel products with slightly modified formulations. Nevertheless, elucidation of dye chemical composition in commercial inks is of paramount importance for the preservation of ballpoint-based artworks, currently endangered by the fast color fading induced by exposure to light[99]. The identification of inks used for artistic purposes requires the use of relatively low-cost, potentially deployable and non-destructive analytical techniques enabling in situ analysis and preservation of the analysed object's integrity. For this reason spectroscopic techniques such as Fourier transform infrared (FTIR),[71, 72] X-ray fluorescence,[73] and Raman spectroscopy[74] are nowadays preferred to (or used in combination with) more conventional chromatography techniques. Among spectroscopic methods, Surface Enhanced Raman Scattering (SERS) has proven to be particularly amenable to the identification of ink mixtures, due to its ability to overcome the fluorescence interference observed in Raman and FTIR analyses.

The SERS phenomenon is based on the enhancement of Raman signals experienced by analytes adsorbed on nanostructured metal surfaces. SERS arises from two contributions, an electromagnetic effect (EM) and a chemical effect (CE), leading to overall enhancements of up to 10^{12} compared to normal Raman (NR) signals.[100-102] The largest enhancement factors were conventionally obtained with aggregated Ag spherical colloids whereas 1–2 orders of magnitude lower enhancements were reported for aggregated Au spherical particles.[103, 104] Accordingly, to date the majority of studies applied to the identification of ballpoint pens use Ag colloids as SERS probes. However, the efficacy of Ag colloids for SERS ink identification is still under debate with authors reporting poor reproducibility due to the fast oxidation of Ag colloids[76] and others reporting good stability results.[105] In addition, the following drawbacks

were reported: measurements had to be performed within minutes of colloid deposition due to fast Ag oxidation, SERS signals were not reproducible due to inhomogeneous (coffee stain effect) evaporation of Ag colloidal droplets, and charged polymers had to be added to counter balance the negative surface charge of Ag colloids in order to promote electrostatic interaction with negatively charged dyes. In spite of this, alternative SERS probes based on more chemically stable materials have scarcely been proposed.[106]

Recently, theoretical work by Hao *et al.* calculated the greatest E-field enhancement at the end of isolated Au nanorods compared to other nanoparticle shapes, due to the high density of E-field concentrated at the nanorod tips.[107] Other authors also referred to Au nanorods as the most promising candidates for the achievement of chemically stable and high intensity SERS signals.[108] In parallel, Liz- Marzán *et al*. reported the synthesis of highly concentrated Au nanorod colloids which displayed stable and reproducible SERS spectra on paper substrates.[22]

In this chapter we report on the use of chemically stable metal nanoinks for SERS analysis of a blue BIC ballpoint pen. Metal nanoinks were constituted by Ag nanospheres and Au nanorods and were used in combination with Thin Layer Chromatography (TLC) to identify the dye components in the pen. The novelty of this work relies in the clarification of chemical stability of metal nanoinks and the role played in the SERS effect observed by measuring the enhancement factors (EFs) arising from different effects at different excitation wavelengths. While normal Raman conditions required the use of two laser wavelengths to obtain the spectra of all separated spots on the TLC, SERS illumination at either 514 nm or 785 nm was successful in obtaining enhanced spectra for all separated spots. High intensity and good signal-to-noise SERS spectra were obtained, due to the matching of laser illumination with the plasmon resonance of the used nanoinks. In addition, the contribution of molecular resonance, electromagnetic and chemical effects was evaluated by further SERS analysis carried out under non-plasmonic resonance conditions. EFs between 5×10^3 and 3×10^6 were obtained for the separated spots, allowing identification of phthalocyanine Blue 38 and triarylene crystal violet (CV) in the pen ink mixture. In contrast with what is reported in the literature, both nanoinks gave stable SERS signals for days after deposition and did not necessitate the use of additional aggregating or charge-adjustment agents.

Moreover, self-assembled Au nanorods vertical arrays immobilized on SiO_2 were used

in blue Bic pen traces detection. Highly enhanced SERS signals of the diluted blue inks deposited on the gold arrays were achieved compared to normal Raman featureless signal with EFs 1×10^5 obtained. The SERS investigation of blue inks traces using highly ordered gold arrays provides high reproducibility with 8% RSD, due to the high density of hotspots. The use of SERS probes with reproducible features also potentially enables quantitative analysis, a highly desirable feature that has the potential to enhance the analytical capabilities SERS to a degree comparable to chromatographic methods.

3.2. Experimental Section

Ag and Au NIs were synthesized by a modification of the Lee and Meisel method reported by Liz-Marzán et al. [22] Fabrication of Ag and Au NIs were reported in detail in chapter 2 section (2.5.).

Immobilized Au nanorods were synthesized by seed mediated growth reported by El-Sayed et al.[15]. Au nanorod arrays (Au NRs/$SiO_{2)}$ were fabricated as already described in detail chapter 2 in section (2.7).

Reference dyes Blue 38 and crystal violet were purchased from Sigma and used without further purification. Commercial blue BIC ballpoint pen was purchased from local stores.

Scanning electron microscopy (SEM) images of nanoinks deposited on SiO_2 substrates were acquired using a field emission SEM (JSM-6700F, JEOL UK Ltd) operating at beam voltages of 2 kV.

Thin layer chromatography was performed with silica plates 10 × 20 cm (Sigma-Aldrich). The BIC ballpoint pen and reference samples were deposited as concentrated MeOH solutions. TLC was performed in ethylacetate–ethanol–water (70 : 35 : 30 v/v) for 60 mins.

Optical characterization

UV-vis spectra were acquired using an Agilent/HP 8453 UV-vis Spectrophotometer (200 nm to 1100 nm). Raman spectra at 514 nm were obtained from a Renishaw inVia Raman system. A helium–neon laser was employed as an excitation source. The laser beam was focused onto the sample through a Leica 20X objective with 0.4 N.A. Measured power at the sampling level was controlled at about 3 mW. Acquisition time was usually 10 s. Raman spectra at 785 nm were obtained from a Pelkin Elmer Raman station. The laser beam was focused onto the sample through a 50 objective (M Plan Achromat) with 0.75 N.A. The laser power was around 35 mW and typical acquisition time was 10 s. To obtain SERS spectra, 5 mL of metal nanoinks were deposited on the TLC plate and left to evaporate for 10 minutes prior to the analysis.

3.3. Results and discussion

Metal nanoinks fabrication started with the synthesis of high volume nanoparticle solutions, which were subsequently concentrated up to 100 times in order to obtain highly viscous, ink-like solutions. **Figure 48** shows SEM images of Ag (**a**) and Au (**b**) nanoinks deposited on SiO_2 substrates. The Ag NIs were mostly spherical in shape and had an average size of 65 nm; the Au NIs displayed an elongated (rod-like) shape with an average size of 13 nm × 41 nm.

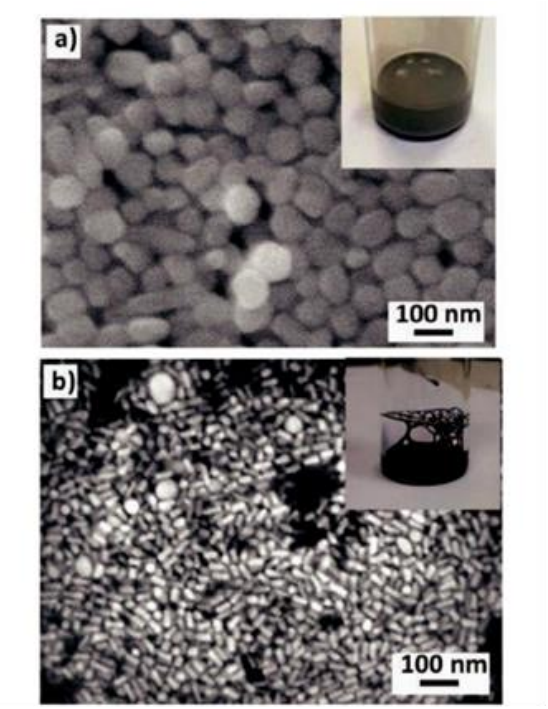

Figure 48. *SEM images of* ***a****) Ag and* ***b****) Au NIs deposited on SiO_2 substrates. Insets: Photographs of Metal colloids NI solutions.*

The separation of the dye components in the blue BIC pen ink was achieved by TLC (**Figure 49** ***a***). By using an ethylacetate– ethanol–water (70 : 35 : 30 v/v) eluent, blue spots and purple spots with retention factors (R_f) equal to = 0.44 and 0.67 formed by TLC as a result of ink mixture separation. For comparison, reference dyes solvent Blue 38 and CV were also deposited on the TLC and run alongside the pen spots. These dyes were specifically selected as triarylene dyes and phthalocyanine pigments were identified in the literature as components of the BIC ballpoint blue pen.[76, 109] Deposited Blue 38 displayed a R_f equal to = 0.44, whereas CV displayed R_f equal to = 0.67, equivalent to the R_f of the BIC blue and purple spots,

respectively. Prior to Raman analysis, absorbance spectroscopy was carried out in order to investigate the optical properties of the analytes and nanoinks. **Figure 49 d** shows the UV-vis spectrum of the BIC pen ink diluted in MeOH. The solution was intensely purple colored and showed a main peak centered at 588 nm with a shoulder at 548 nm, another peak was centered at 628 nm (buried under the CV peak in the pen solution spectrum) and 666 nm.[110] CV showed the same peak and shoulder centered at 588 nm and 548 nm as shown by the BIC pen solution spectrum, arising from the coexistence of two isomeric forms in MeOH solution.[111] **Figure 49 *e*** also shows the absorbance spectra of Ag NIs and Au NIs in water suspensions. The Ag NI solution was milky grey in color (see the inset of **Figure 48 *a)*** and was characterized by a relatively large plasmonic peak centered at 428 nm. The Au NI solution was deep blue in color (see the inset of **Figure 48 *b***) and showed two peaks at 520 nm and 787 nm, characteristic of transversal and longitudinal plasmon resonances occurring in elongated nanoparticles.[112]

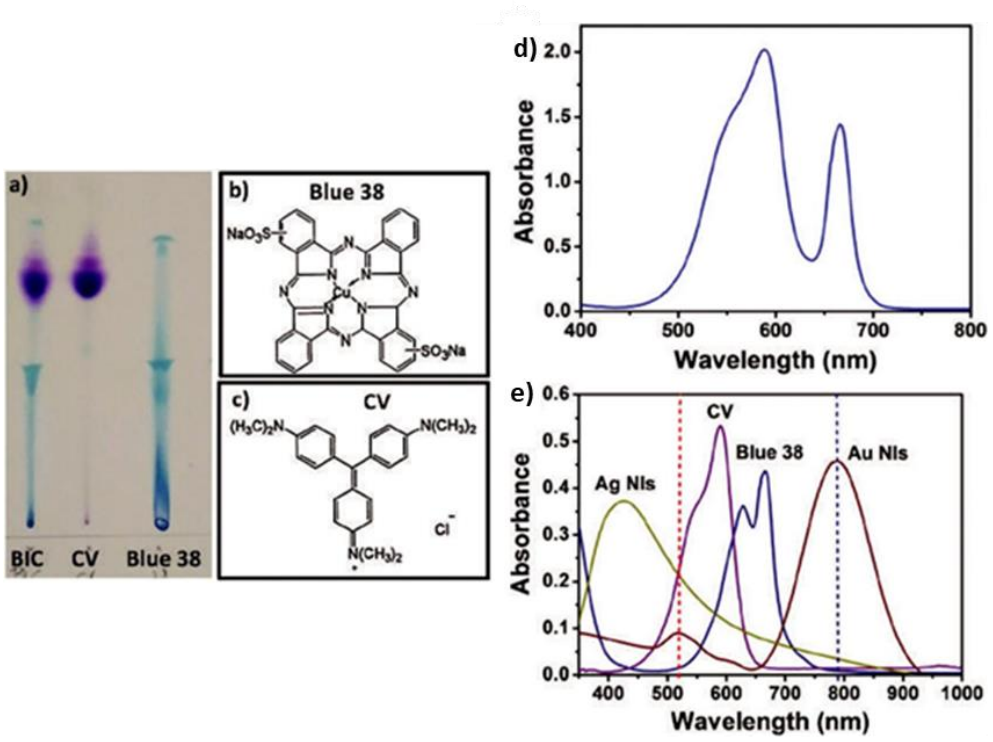

***Figure 49**. **a)** Photograph of TLC showing the BIC pen components and reference samples Blue 38 and CV; **b)** and **c)** molecular formulas of the reference samples Blue 38 and CV. **d)** UV-vis spectrum of BIC pen solution in MeOH; **e)** UV-vis spectra of Blue 38 and CV in MeOH and metal NIs in water. Dotted lines indicate the position of 514 nm (red) and 785 nm (blue) laser excitation wavelengths used for SERS analysis.*

As a result of this analysis two laser excitation wavelengths at 514 nm and 785 nm were

selected for Raman analysis, as strongly enhanced SERS spectra were expected to be obtained, due to their plasmonic resonance with Ag and Au NIs, respectively (see dotted lines in **Figure 49 *e***). **Figure 50 *a*** shows Normal Raman (NR) spectra obtained by direct illumination of the TLC separated spots with an excitation wavelength of 514 nm. All spectra at 514 nm were recorded with a laser power of 2 mW and 10 s integration time. A featureless spectrum was obtained for the blue spot (light blue curve). A low intensity spectrum was also obtained for the reference Blue 38 with only two peaks appearing at 1539 cm^{-1} and 1337 cm^{-1} (dark blue curve). In contrast, the spectra of relatively good intensity were obtained for the purple spot and the reference CV (light purple and dark purple curves, respectively). Both spectra displayed the same diagnostic peaks at 1620 cm^{-1}, 1592 cm^{-1}, and 1540 cm^{-1}, associated with stretching of the benzene rings and 439 cm^{-1} and 420 cm^{-1} associated with bending of the CNC bonds.[113]

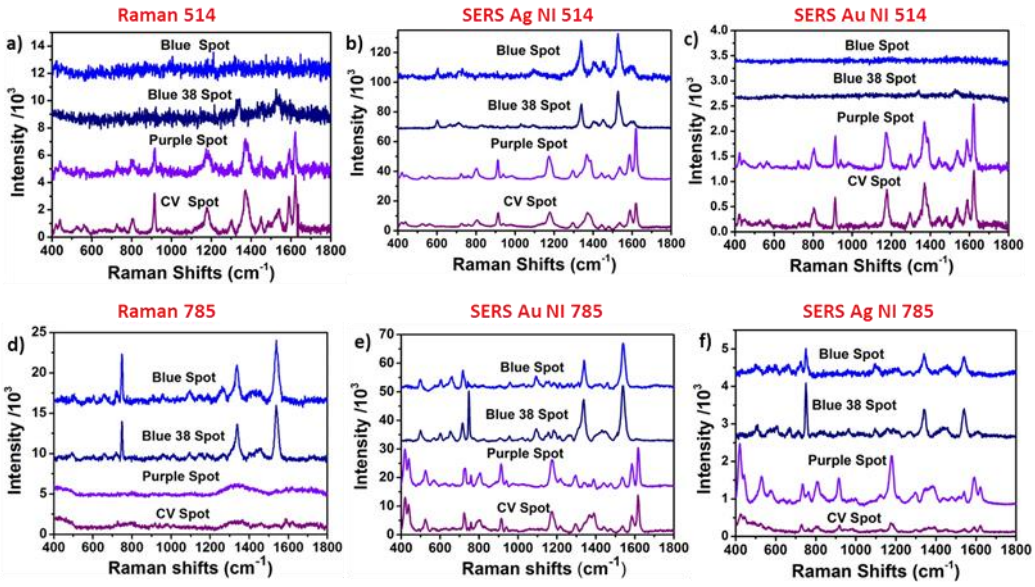

Figure 50*. NR and SERS spectra of TLC BIC pen components and reference samples Blue 38 and CV:* ***a)*** *NR taken at an illumination wavelength of 514 nm;* ***b)*** *SERS at 514 nm with Ag NIs;* ***c)*** *SERS at 514 nm with Au NIs;* ***d)*** *NR taken at an illumination wavelength of 785 nm;* ***e)*** *SERS at 785 nm with Au NIs;* ***f)*** *SERS at 785 nm with Ag NIs. Laser power was 2 mW and 35 mW for 514 nm and 785 nm lasers, respectively.*

The intensity of the observed spectra was ascribed to the occurrence of molecular resonance (MR) effects, due to the use of an illumination wavelength corresponding to a maximum in the absorption spectrum of CV (**Figure 49 *e***, red dotted line). These data allowed the preliminary identification of the purple spot as CV. However, identification of the blue specimen was not possible under NR conditions.

In contrast, **Figure 50 *b*** shows the SERS spectra of an equivalent TLC where Ag NIs were deposited in all spots and laser illumination of 514 nm was used as SERS excitation. Good SERS spectra with enhanced features were recorded for all spots. Specifically, the spectra of the blue spot and the Blue 38 spots previously not identifiable with NR, displayed highly enhanced features with peaks at 1605, 1526, 1453, 1405, 1338, and 605 cm^{-1} associated with internal vibrations of the phthalocyanine macrocycle.[110, 114] The intensity of the blue spot spectrum measured using the 1339 cm^{-1} peak as reference displayed a 2 orders of magnitude higher intensity compared to the intensity of the NR spectrum. This enhancement was attributed to an electromagnetic effect, due to the use of an illumination wavelength in plasmonic resonance with the Ag NIs (**Figure 49 *e***, red dotted line). The similarity between the spectra of the two blue specimens allowed unique identification of the blue spot as Blue 38. Similarly, the strong resemblance between the SERS spectra of purple specimens confirmed the identity of the purple spot as CV and highlighted the superior abilities of SERS for the identification of BIC pen components compared to NR spectroscopy. The spectrum of the purple spot was enhanced by 1 order of magnitude (measured at 1174 cm^{-1}) and displayed slightly red shifted peaks compared to NR conditions. The intensity of this spectrum was attributed to a combination of three effects: a molecular resonance (MR) effect; an electromagnetic effect (EM), due to the use of an illumination wavelength in plasmonic resonance with Ag NIs; and a chemical effect (CE), due to the formation of a chemical bond, and consequent charge transfer (CT), between CV and Ag via the central C atom whereby CV acted as an electron donor and Ag as the electron acceptor.[115]

Proof of the occurrence of a charge transfer process was given by the observed red shift of frequencies displayed in the SERS spectrum compared to the NR spectrum (see **Figure 51 *b***). Specifically, the N-phenyl frequencies appearing at 1371 cm^{-1} and 1386 cm^{-1} in the NR spectrum were shifted to 1376 cm^{-1} and 1393 cm^{-1}, respectively in the SERS spectrum. Also, the C=C ring frequency was shifted from 1619 cm^{-1} to 1627 cm^{-1}. Further proof of the occurrence of a CT process was given by the predominant enhancement of the non-totally symmetric (e) modes compared to the totally symmetric (a_1) modes.[113]

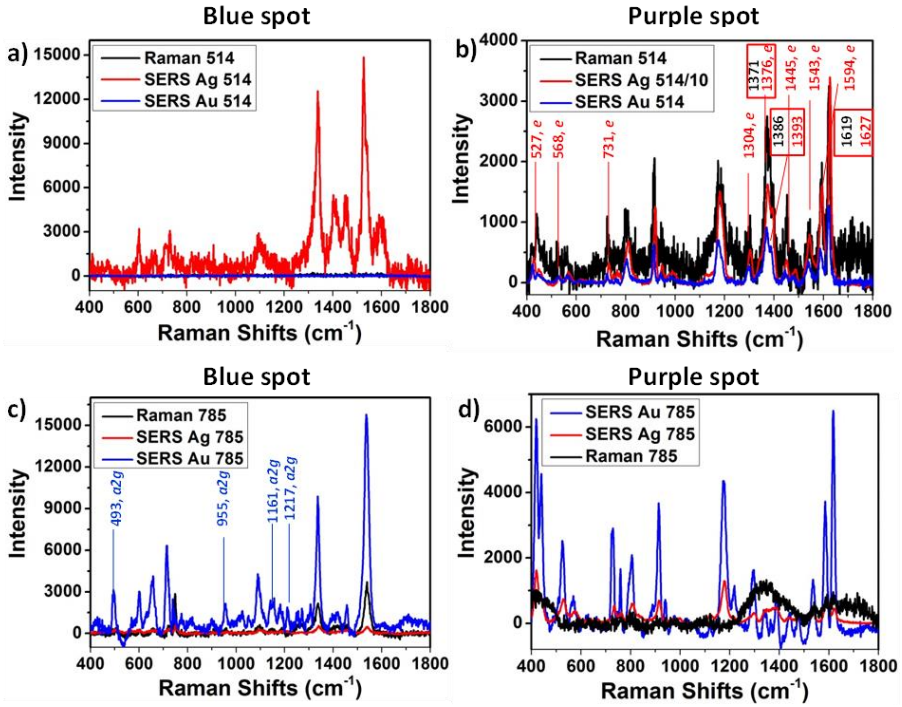

Figure 51. *Raman, SERS with Ag NIs and SERS with Au NIs recorded with 514 nm illumination for* ***a)*** *blue spot and* ***b)*** *purple spot; and Raman, SERS with Ag NIs and SERS with Au NIs recorded with 785 nm illumination for* ***c)*** *blue spot and* ***d)*** *purple spot.*

In order to acquire more detailed information on the three effects the SERS spectra of an equivalent TLC plate were also recorded under non-plasmonic resonance conditions by substituting Ag NIs with Au NIs, which was characterized by a plasmonic resonance of 787 nm (see **Figure 49** ***e***). The SERS spectra of all TLC colored spots (**Figure 50** ***c***) at 514 nm with Au NIs were equivalent to the Raman spectra recorded at 514 nm (**Figure 50** ***a***), indicating that no SERS effect occurred due to the absence of plasmonic resonance conditions. Under these conditions, the intensities displayed by the purple and CV spectra could be entirely attributed to a MR contribution.

A parallel comparison was carried out at an illumination wavelength of 785 nm. All spectra at 785 nm were recorded with a laser power of 35 mW and 10 s integration time. **Figure 50** ***d***. shows the NR spectra of BIC pen separated spots directly measured on a TLC plate. The spectra obtained were somehow complementary to those obtained for NR illumination at 514 nm. The blue spot and Blue 38 specimens displayed good spectra (light and dark blue curves, respectively) characterized by the same diagnostic peaks at 1539 cm^{-1}, 1340 cm^{-1} and 720 cm^{-1}. In contrast, the spectrum of the purple spot displayed no features and the spectrum of the

reference CV displayed only small peaks around 1600 cm^{-1}. Similarly to what was observed under NR conditions at a 514 nm illumination wavelength, NR at 785 nm was not able to identify all separated spots in the BIC pen and only preliminary identification of the blue spot as Blue 38 was possible. As comparison,

Figure 50 *e* shows the SERS spectra of the same TLC where Au NIs were deposited in all separated spots and 785 nm was used as SERS excitation. The spectra of the blue specimens, already visible under NR conditions, appeared to be enhanced due to the use of an illumination wavelength in plasmonic resonance with Au NIs (EM effect) and showed additional peaks compared to the spectra recorded under NR conditions. The additional peaks belonged to asymmetric modes of symmetry a2g, which were reported to occur only in concomitance to the occurrence of a charge transfer process (see **Figure 51 *c).***[116] Therefore, the enhancement observed was attributed to a combination of EM and CE effects. This enhancement allowed the unique identification of the blue specimen as Blue 38. The purple spot and CV showed highly enhanced spectra compared to NR conditions with peaks in the same positions as discussed in **Figure 49 *a***, thus confirming the identity of the purple spot as CV. Thus once again at 785 nm illumination SERS was superior to NR spectroscopy in enabling fast and sensitive identification of BIC pen ink components. The enhancement observed for the purple spot was entirely due to an EM effect. It should be pointed out here that CV would also be able to form a CT complex with Au via the N groups. [115] However, no evidence of the CT effects was observed in the spectra (i.e. no changes compared to the corresponding NR spectrum observed (see **Figure 51 *d***), likely prevented by the electrostatic repulsion originating by the double positive charge of CV and Au nanorods.

For completion, the SERS spectra of all TLC colored spots (**Figure 50 *f***) were recorded under non-plasmonic resonance conditions (i.e. at 785 nm with Ag NIs). The spectrum of the blue spot showed 1 order of magnitude lower intensity than the equivalent SERS spectrum recorded at 785 nm with Au NIs, due to the absence of EM resonance. The spectrum of the purple spot showed peaks of slightly lower intensity than those recorded under resonance conditions (absence of EM contribution) but of higher intensity than those recorded under NR conditions at 785 nm. This enhancement was ascribed only to a charge transfer process (CE effect) occurring between CV and Ag nanoparticles discussed earlier as laser excitation (785 nm) was far removed from the plasmonic absorption of Ag NIs and the absorption maximum of CV (see **Figure 49 *e***) to see contributions from MR and EM effects. The relative intensities

of the reference peaks and the contributions of the various effects measured under all experimental conditions for the blue and purple specimens are summarized in **Table 2**.

	Blue specimen		**Purple specimen**	
	Intensity (1339 cm^{-1})	Contribution	Intensity (1174 cm^{-1})	Contribution
Raman 514nm	105	-	1189	MR
SERS Ag 514nm	12895	EM	15510	MR-EM-CT
SERS Au 514nm	25	-	743	MR
Raman 785nm	1974	-	231	-
SERS Au 785nm	9252	EM-CT	4525	EM
SERS Ag 785nm	498	-	1304	CT

***Table 2**. Relative intensity of reference peaks and contribution effects for blue and purple specimens measured under all experimental conditions*

In order to clarify some of the contrasting reports from the literature, SERS spectra with Ag NIs were acquired following multiple illumination steps and days after nanoinks deposition. Figure 52 shows the SERS spectrum of a blue spot recorded at 514 nm (black line) and an equivalent spectrum recorded after three days (red line) displaying reproducible and intensity comparable features. No degradation or oxidation of SERS probes was observed, provided that the TLC was stored in the dark to prevent dye color fading.

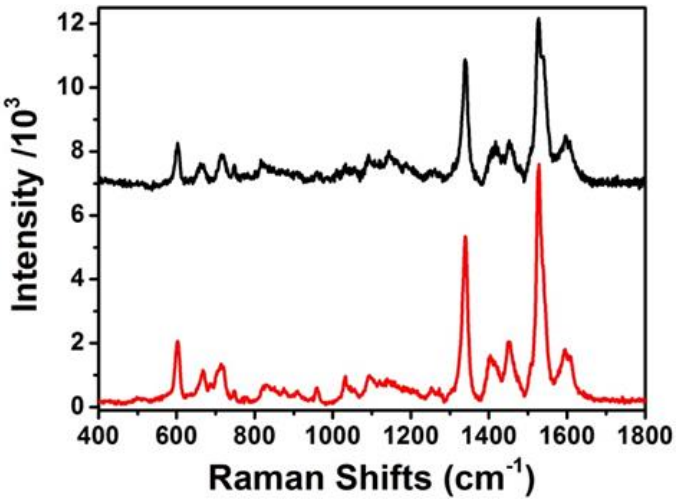

***Figure 52**. SERS spectra of a TLC blue spot taken after 10 min Ag NI deposition (black line) and after three days of Ag NI deposition (red line).*

Equally, Au NIs were chemically stable and TLC spots could be illuminated after four weeks of nanoink deposition. Furthermore, for both nanoinks no use of aggregating agents was necessary and no adjustment of electrostatic charge had to be made to promote a chemical link with charged analytes (i.e. between negatively charged Ag NIs and Blue 38 and positively charged Au NIs and CV).

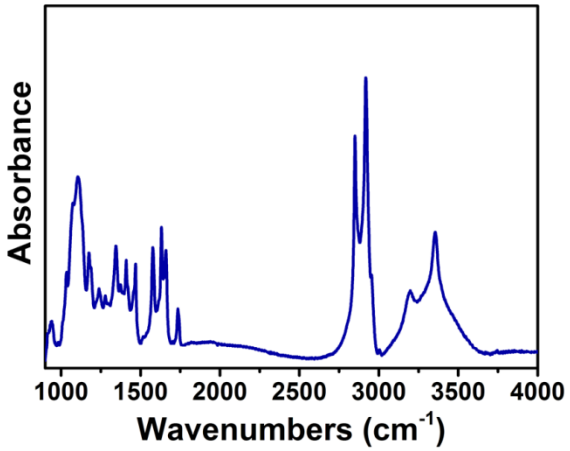

Figure 53. *FTIR spectrum of BIC pen MeOH solution.*

FTIR analysis of the blue BIC pen ink gave some useful and complementary information about the ink composition and confirmed the presence of some specific dyes in the formulation. The FTIR spectrum is reported in **Figure 53**. The peaks at 1577, 1374, 1175 and 939 cm^{-1} were diagnostic of the presence of triarylmethane dyes, in this case CV, and confirmed the findings of the SERS analysis.[120] In addition, FTIR analysis revealed the presence of Acid Blue 9 in the ink formulation. Additional information about the presence of other non-dye components not obtainable by SERS was also obtained. The carbonyl absorption band at 1735 cm^{-1} and the carboxylate group stretching at 1408 cm^{-1} suggested the presence of an acrylic-based emulsion,[121] whereas the presence of the amide vibration at 1656 cm^{-1} suggested the presence of an unidentifiable amide-based compound, possibly deriving from acrylamide based resins.[122] The presence of some asymmetrical and symmetrical stretch vibrations of the CO single bonds at 1278, 1075 and 939 cm^{-1} (overlapping the peak at 939 cm^{-1} for the ρ(CH3)/νCN) vibration of CV) suggested the presence aliphatic glycol ethers, usually found in ballpoint pen ink formulations.[123]

Finally, **Figure 54** shows the use of highly ordered Au nanorod arrays for sensitive SERS analysis of BIC ballpoint pen traces. The use of ordered nanoscale arrays is highly desirable for SERS analysis as it provides high sensitivity, due to the high density of hot spots between closely arranged nanoparticles and also reproducibility of analysis, due to the homogeneity and reproducibility of the SERS substrate. **Figure 54** ***a*** shows a SEM image of the Au nanorod arrays assembled on SiO_2 substrates and stamp-transferred on glass coverslip following a methodology developed by our research group [95] and described in details in chapter 2 in section (2.7). The average size was found 10×41 nm (aspect ratio 4.1) and was calculated from 100 statistical measurements of nanorods taken from high magnification SEM images. The arrays were characterized by large domains (> 100 μm^2) of vertically aligned nanorods with a high density of hot spots.

Figure 54 ***b*** shows the NR and SERS spectra of a MeOH solution of BIC pen drop-deposited on a glass coverslip and on the Au arrays, respectively. The illumination wavelength was 514 nm. The estimated concentration of the solution (from UV-vis measurements) was < 100 nM. While the NR spectrum was featureless, the SERS spectrum was characterized by intense peaks mainly associated to the CV component. The contribution of the Blue 38 component was less evident. This could be associated with a higher concentration of CV in the ink mixture and also to the low spectral response of blue 38 at 514 with Au nanorods, observed already in Figure 49c. It is expected that there will be a mixture of blue and purple components signatures in the SERS spectra in case of using Au nanorod arrays at 785nm laser line, which was not measured in this research, as blue and purple signals obtained using gold inks in **Figure 50** ***e***. The high intensity of the peaks suggests that lower concentrations could be detected by using these arrays, which would enable the analysis of pen traces or faded pen traces extremely useful for forensic or art applications.

Figure 54 ***c*** shows spectra of the drop-deposited BIC pen measured in 10 different locations over an array of 5 mm in diameter. The intensity change of the Raman band at 1175 cm^{-1} was used to calculate the relative standard deviation of the intensity from 10 points. A value of 8% was obtained, which showed the remarkable good uniformity of the array. This value was lower than reproducibility values reported in literature for nanoparticle aggregates and printed nanoparticle arrays and they were comparable to values reported for ordered nanowire arrays obtained by nanosphere lithography.[124-126]

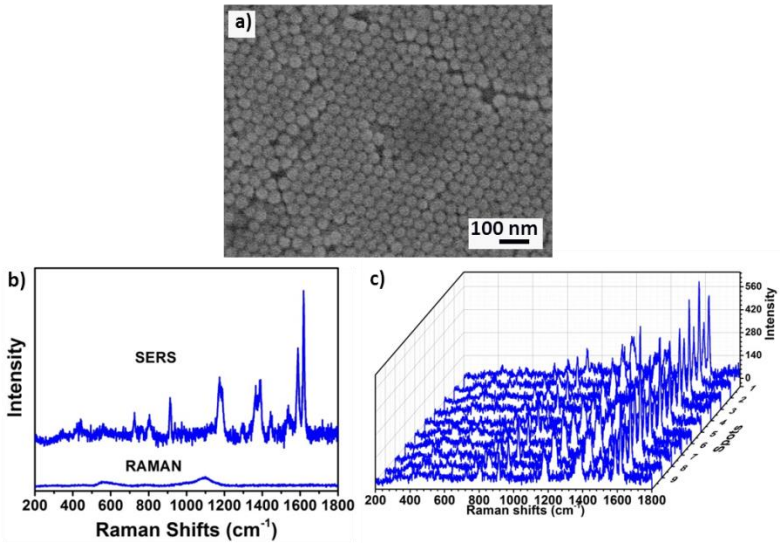

Figure 54. a) *SEM image of vertical Au nanorod arrays stamped on a glass substrate;* ***b)*** *SERS and NR spectra of low concentration BIC pen MeOH solutions;* ***c)*** *reproducible SERS spectra recorded at 10 different locations of a 5 mm diameter Au nanorod array.*

A further evaluation of SERS performances of Au nanorods arrays as SERS probes was achieved by calculating the Enhancement Factor (EF), defined as the ratios of the intensities of the scattered radiation for SERS and normal Raman scattering per molecule

(1) $EF\ (I_{SERS}/N_{SERS})\ (I_{NR}/N_{NR})$

Where, I_{SERS} and I_{NR} are the integrated intensities of the SERS and normal Raman scattering spectra for the BIC pen (calculated assuming that the main dye content of the BIC was constituted by CV); N_{SERS} and N_{NR} are the number of molecules found in the laser excitation area. The calculated EF was 1×10^5, in agreement with values already reported for these superstructures.[51]

3.4. Conclusion

In conclusion, the use of Ag NIs, Au NIs and vertical Au nanorods were proved to be efficient and chemically stable SERS probes for sensitive analysis of ballpoint BIC pens. Metal nanoinks colloidal solutions were used in combination with TLC, providing clear and enhanced spectra for all pen components, otherwise not discernible under NR conditions. Phthalocyanine Blue 38 and tryarylene CV were identified in the dye mixture of the BIC pen. Enhancement factors of up to 1×10^6 were obtained with 514 nm and 785 nm excitation wavelengths, and were due to a combination of effects, depending on the experimental conditions used. The strongest enhancements were obtained under plasmonic resonance conditions and were therefore associated with the use of stable metal nanoinks as SERS probes. On the other hand, the use of Au nanorod arrays carrying a high density of hot spots provided the enhancement necessary to enable detection of BIC pen traces with a high level of uniformity. The developed probes offer an alternative to existing analytical tools for the reliable, fast and low-cost analysis of ballpoint pens and concomitantly open the way to the analysis of trace amounts particularly relevant for forensic and art applications.

CHAPTER 4

Raman and SERS Ag nanopastes spectroscopic investigation of colored BIC ballpoint pen ink mixtures

Surface Enhanced Raman Scattering (SERS) method using Ag nanoparticles pastes (nanopastes) was applied for the elucidation of dye content in commercial colored BIC ballpoint pens (red, pink, purple and green), increasingly used for artistic purposes. Because of its non-invasive nature, the capabilities of Raman spectroscopy were initially tested. However, overall SERS provided enhanced spectral features and quenching of fluorescence necessary for the unequivocal identification of dye mixtures in all analyzed pens. SERS analysis was carried out *in situ*, by deposition of Ag nanopastes directly on pen colored paper surfaces. UV-vis spectroscopy and thin layer chromatography (TLC) analyses complemented Raman/SERS measurements by revealing the presence of additional components in inks. The relevance of this analysis for art diagnostics was demonstrated through the real non-invasive analysis of BIC pens drawings, which led to successful identification of chemical ink composition and identification of production medium.[2]

[2*] This work has been published as: "Identification of Dye Content in Colored BIC Ballpoint Pen Inks by Raman Spectroscopy and Surface Enhanced Raman Scattering (SERS) ", Abeer Alyami,[a] Killian Barton,[b] Liam Lewis,[b] Antonio Mirabile,[c] Daniela Iacopino[a]*, J Raman Spectrosc. 2018., 0377-0486.

4.1. Introduction

Since their introduction in the market in 1945, ballpoint pens have attracted the interest of artists, fascinated by the possibility of generating novel artistic effects and precision line-work not easily obtainable by brush. The low cost, large assortment of colors and hues available, widespread availability and portability of ballpoint pens are among other qualities that have made ballpoint pens the medium-of-choice for the production of pen- and mixed-media artworks[127]. Many of these artworks are today hosted by museums and private collections all over the world.

These pens' color is fast fading as a result of light and air exposure and to develop long-term preservation process, identification of their inks mixture is becoming highly required. The mixture of ball point inks is complex as only 50% of the total ink mixture are dyes and pigments and the other 50% is constituting by other components such as fatty acids, softeners and polymeric resins to improve the ink property.[64] Moreover, patenting the pens' inks formulations is considered to be another difficulty in commercial inks characterization.

Most of the research on commercial pen inks so far has focused on identification of dyes in inks of forensic interests such as blue and black pens, universally used for writing of documents (analysis of questioned documents and forgeries)[99, 128-130]. However, recently, research interest has started to shift towards chemical characterization of commercial pen inks used in contemporary art as shown by Brunia *et al.*[131] and Iacopino *et al.*[132].who both developed spectroscopic methods for the identification of fountain and ballpoint pen inks, respectively. In parallel, efforts have concentrated on the application of analytical techniques alternative to conventional chromatographic methods, requiring high cost instrumentation and relatively large (mg) amount of material for analysis. In fact, the ideal analytical tool for analysis of artstuff should be low-cost, potentially deployable and minimally invasive, in order to fulfill requirements of *in situ* analysis and analytical object integrity preservation. For this reason spectroscopic techniques such as Fourier transform infrared (FTIR)[71, 72], X-ray fluorescence[73], Raman spectroscopy [74, 75]are now preferentially being applied to the analysis of inks. Among these, Raman spectroscopy is increasingly becoming the technique of choice, due to its inherent non-destructive nature, fingerprinting ability and availability of low cost and deployable handheld instrumentation. However, Raman spectroscopy suffers from fluorescence interference and low sensitivity, which for a long time have prevented the efficient characterization of dyes and pigments present in heritage objects. These limitations were finally

circumvented in the late 1980's, when Surface Raman Enhanced Scattering (SERS) was successfully applied to the identification of dyes in a variety of artistic media[133, 134]. SERS is a surface-sensitive analytical technique that involves the amplification of Raman signals by several orders of magnitude for molecules adsorbed on metallic nanostructures surfaces [135-137]. The observed high signal enhancements have made SERS particularly amenable to the investigation of artistic materials where mass-limited samples are often available and *in situ* applications and local identification of selective analytes is often required [138, 139]. As result, many authors have reported successful investigations of lakes and dyestuffs in a large range of matrixes including archaeological textile fibers[140] paper and woodblock prints [141]. One of the major drawbacks associated to the application of SERS to the analysis of colorants is its inherent minimal invasive nature, associated to the need for extraction or hydrolysis procedures sometimes not applicable to direct analysis of artworks. Nevertheless, its widespread application for the last 20 years suggests that minimally invasive analytical techniques can be often acceptable, if high sensitivity and selectivity are obtained. Moreover, the application of SERS has allowed the construction of comprehensive natural and synthetic colorant spectral databases, which provide support for identification and preservation and establishment of provenance and originality of artworks [142].

Recently our group has successfully applied Raman and SERS, in combination with bench and handheld instrumentation, for the identification of the major dye constituents of felt tip pens [143, 144]. The application of SERS allowed circumventing fluorescence interference and provided high intensity spectral profiles of fluorescent dyes under visible wavelength illumination [145].

In this paper, we report on the application of Raman and SERS spectroscopies to the identification of dye mixtures in colored BIC ballpoint pens. Ten BIC ballpoint pens with different hues of green, purple, pink and red were analyzed. Particular emphasis was placed on Raman spectroscopy where the effect of different excitation wavelengths, use of bench *vs* handheld instrumentation and use of Raman *vs* SERS was analyzed in detail for each diagnostic ink. Limitations and merit of both Raman and SERS were highlighted. Data collected were verified and complemented by the use of UV-vis spectroscopy and TLC. Finally, the application of Raman spectroscopy and its capability for ink compositional analysis were discussed in the context of a real case study.

4.2. Materials and Methods

Chemicals

Reference dyes rhodamine B, tartrazine, Blue 38 and crystal violet were also purchased from Sigma and used without further purification. Commercial BIC ballpoint pens were purchased from local stores. The list of pen analyzed is shown in **Table 3**.

Ag nanopastes were synthesized according to a modification of the Lee and Meisel method reported by Liz- Marzan et al.[22]. Synthesis is already described in details in chapter 2 section (2.6.).

Scanning electron microscopy (SEM) images of nanopastes deposited on SiO_2 substrate and on paper were acquired using a field emission SEM (JSM-6700F, JEOL UK Ltd) operating at beam voltages of 2 kV.

Optical Characterization

UV-vis spectra were acquired using an Agilent/HP 8453 UV-vis Spectrophotometer (200 nm to 1100 nm).

Raman spectra at 514 nm were obtained from a Renishaw inVia Raman system. A helium–neon laser was employed as an excitation source. The laser beam was focused onto the sample through a Leica 20X objective with 0.5 N.A. Measured power at the sampling level was controlled at about 0.3 mW. Acquisition time was usually 10 s. Raman spectra at 532 and 785 nm were obtained from a Pelkin Elmer Raman station. The laser beam was focused onto the sample through a 50 objective (MPlan Achromat) with 0.75 N.A. The laser power was around 35mW and typical acquisition time was 10 s. Hand held Raman spectra at 785 nm were obtained from an InPharma spectrometer. The laser power was 50 mW at sample and acquisition time was between 7 and 20 s. To obtain SERS spectra, 2 μl of Ag nanopaste were deposited on pen lines and squares drawn on commercial paper, followed by immediate analysis.

Thin Layer Chromatography

Thin layer chromatography (TLC) analyses were performed using silica plates 10 X 20 cm (Sigma-Aldrich). The BIC ballpoint pens and reference samples were deposited as concentrated MeOH solutions. The TLC plates were developed in a horizontal developing chamber. The solvent systems include: ethylacetate/ethanol/water (7:3.5:3 v/v/v) and 1-butanol/ammonia/ethanol (5:3:2 v/v/v). Chromatographic development of plates was performed at room temperature for 60 min.

4.3. Results and discussion

The list of pens analyzed in this work is reported in **Table 3**

Name	Color
Fine	Red
Medium crystal	Red
Fine crystal	Dark red
Medium	Light red
Crystal	Pink
Crystal	Purple
Fine	Dark green
Medium crystal	Dark green
Crystal	Light green
Medium	Green

***Table 3**. List of BIC pens investigated in this work.*

Figure 55 shows a photograph of colored squares drawn on paper with BIC pens selected for the analysis. From a visual point of view red Fine and Medium Crystal inks resulted quite similar in color, red Fine Crystal showed a darker red coloration whereas red Medium showed a bright-red lighter coloration. Green Fine and Medium Crystal pens showed similar dark green coloration, green Crystal showed a lime hue coloration and green Medium displayed a green coloration. Images for other Crystal pen squares are also reported, displaying intense pink and purple colorations.

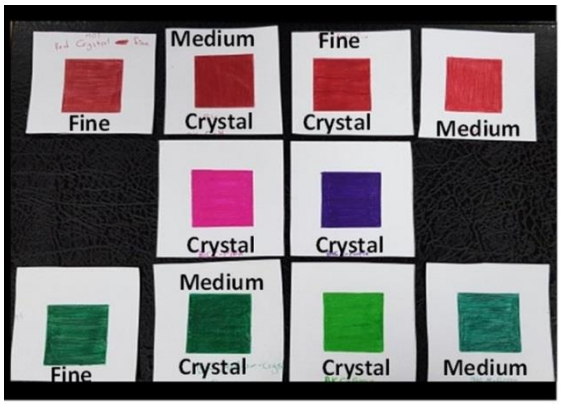

***Figure 55**. Photographs of colored squares drawn on commercial paper with selected BIC pens.*

SERS probes used in this work were constituted by Ag colloidal pastes obtained by modification of the classical Lee and Meisel method[22] .The nanopastes were constituted by concentrated aqueous solutions of Ag nanoparticles (concentrated up to 200 times), which were deposited directly on colored pen areas drawn on paper. The use of Ag nanopastes instead of traditional diluted Ag colloidal solutions resulted in several advantages: i) allowed direct deposition of nanoparticles on colored papers, eliminating the need for cumbersome multiple colloidal deposition and aggregation steps[76]; enabled *in situ* measurements and allowed avoiding the use of time consuming extraction or separation methods often used in association with Raman/SERS approaches[105]; ii) allowed formation of well-defined and large SERS-active areas with high concentration of hot spots and therefore the generation of sensitive SERS responses.

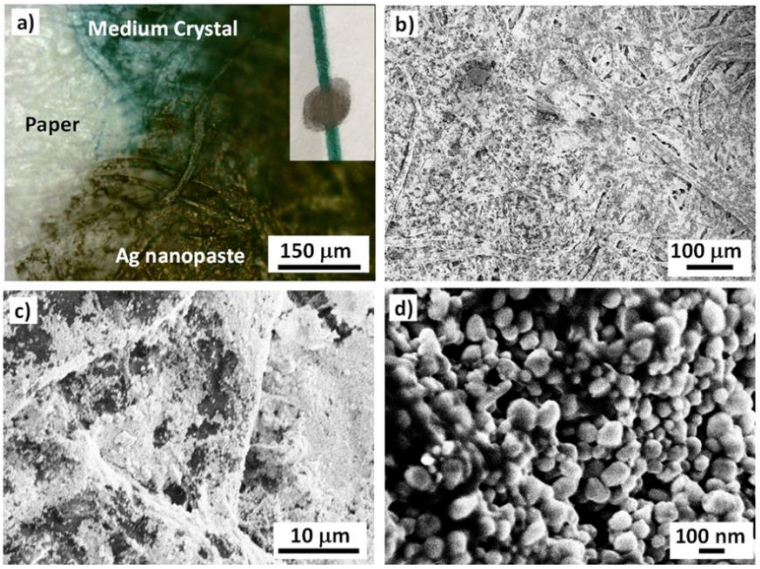

Figure 56. a) *Optical microscopy image of green Medium Crystal line drawn on paper with deposited Ag nanopastes. Low (**b**), medium **c)** and high (**d**) magnification SEM images of Ag nanopastes deposited on green colored paper showed in (**a**).*

Figure 56 a shows an optical microscopy image of a paper sheet with a green line written by Medium Crystal BIC pen. The image clearly shows deposition of green ink on the paper fibers. The bottom right part of the image shows the area where Ag nanopastes were deposited, displaying even deposition of the nanopastes over the green colored paper fibers. The inset of **Figure 56** shows a photograph of the green line on paper with deposited Ag

nanoparticles. **Figure 56 b,c** show different magnification SEM images of the Ag nanopastes deposited on the green line paper. Images illustrate the nanopastes were widely coating the paper surface with relatively dense coverage of the paper fibers. Moreover, the high SEM magnification of the deposited nanopastes shows formation of high density and high uniformity particle areas, requisites both important for the achievement of high intensity and reproducible SERS signals.

Raman and SERS measurements were carried out in situ on colored lines drawn on commercial paper with excitation wavelengths of 514 nm. All reported spectra were background-subtracted. Raman spectra of red pen inks are reported in **Figure 57 a**. Readable but low intensity spectra were obtained for all pens, except Medium red for which a featureless spectrum saturated by fluorescence was obtained. The generation of high fluorescence interference was not surprising as red colored inks are characterized by strong absorption close to the selected excitation wavelength, which often results in concomitant generation of interference fluorescence emission, and consequent masking of Raman signals [141]. The spectra of Fine Crystal, Fine and Medium Crystal showed similar spectral features, suggesting the presence of a common main dye component initially identified as rhodamine B (Pigment Violet 1, C.I. 45170) from diagnostic peaks at 1647 and 1505 cm^{-1}. The spectrum of rhodamine B, also reported in **Figure 57 a** for comparison, supported this preliminary attribution. Raman spectra of Crystal pink and Crystal purple pens (**Figure 57**c) were featureless and characterized by strong fluorescence interference. Raman spectra of green pens (**Figure 57 e**) displayed clear features different from each other except for fine and medium Crystal, which showed similar spectral features, suggesting very similar dye chemical composition. Specifically, Fine and Medium Crystal green pens showed peaks centered at 1599 (quadrant stretching mode of the phenyl ring), 1501 and 1410 (C=C pyrazole bending and the C-H bending mode of phenyl rings) and 482 cm^{-1} overlapping with main peaks of yellow tartrazine reference dye (Acid Yellow 23, AY23, C.I. 19140) whose spectrum is also reported in **Figure 57 e** for comparison[146]. Green Crystal ink showed spectral peaks centered at 1587, 1478, 1409, 492 cm^{-1} which could not be identified. Medium green displayed peaks at 1458, 1434, 1401 and 1138 cm^{-1} which could not be identified.

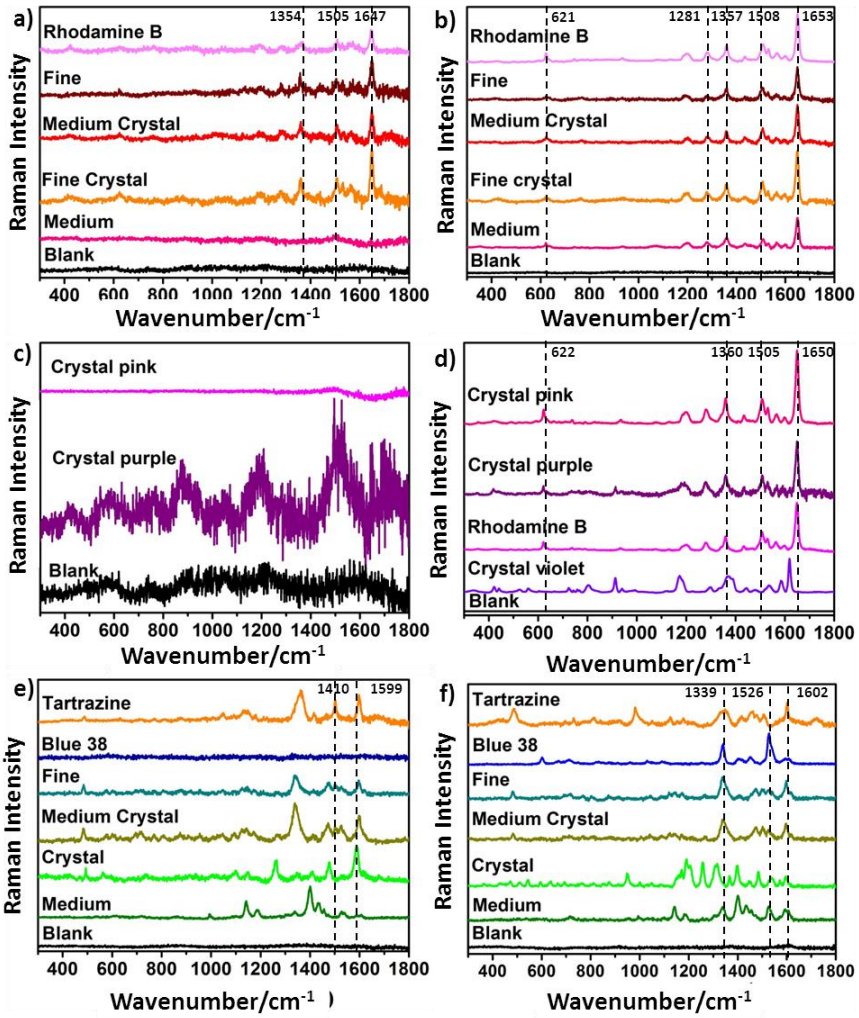

Figure 57. *Raman* ***a)*** *and SERS* ***b)*** *spectra of red pen inks and reference spectra of rhodamine B. Raman* ***(c)*** *and SERS* ***(d)*** *spectra of pink and purple Crystal pen inks and reference spectra of rhodamine B and crystal violet. Raman* ***e)*** *and SERS* ***f)*** *spectra of green pen inks and reference spectra of tartrazine and blue 38. All spectra were recorded at 514 nm excitation wavelength and were background subtracted.*

In order to further identify dye pen composition, SERS spectra were also recorded at 514 excitation wavelength. **Figure 57** b,d,f show SERS spectra for the three sets of pens, in general displaying strongly enhanced features compared to Raman spectra especially evident in red, pink and purple pens. All five red BIC ballpoint pens showed similar spectral features attributable to rhodamine B, whose SERS spectrum is also reported in **Figure 57** ***b*** for comparison. Specifically, vibrational bands were observed at 1653 (C–C bending and C=C stretching of xanthene aromatic ring), 1532-1508 (aromatic C–H bending), 1357-1281 (aromatic C–C bending), and 621 (xanthene ring puckering) cm^{-1} [147]. Rhodamine B and/or rhodamine 6G had been previously identified in red ballpoint pen formulations through easy

ambient sonic spray ionization mass spectrometry (EASI-MS) [148, 149]analysis and LDI-TOF-MS[150]. Interestingly, while clear distinction between rhodamine B and rhodamine 6G could not been achieved with mass spectrometry techniques, the reported SERS analysis clearly showed presence of rhodamine B in red ink formulations. SERS spectra of Crystal pink and Crystal purple pens (**Figure 57** d) also displayed spectral features similar to each other and similar to the red pens (main peaks at 1650, 1505 and 1360 and 622 cm^{-1}), therefore also suggesting presence of rhodamine B in the ink mixture. However, closer observation of Crystal purple SERS spectrum revealed the presence of small additional peaks centered at 914 and 420 cm^{-1}, indicative of the presence of an additional dye in the ink mixture. Because of the intense purple color of the ink, and its occurrence in blue and black BIC pen ink formulations, the presence of triarylmethene dye crystal violet (Methyl violet 10B, CI 42555) was hypothesized [132, 151]. The SERS spectrum of crystal violet is also reported in **Figure 57 *d*** and showed multiple peak overlaps (1616, 1589, 1567, 1182, 913, 415 cm^{-1}) with the crystal purple SERS spectrum. Peaks at 1616 and 1589 cm^{-1} were assigned to the stretching of benzene rings, peak at 1182 and 913 cm^{-1} were associated to asymmetric stretching and bending of C-Ccenter-C bonds whereas the peak at 415 cm^{-1} was associated to bending of the C-N-N bonds[113]. The presence of crystal violet in the crystal purple pen formulation was also evidenced by SERS spectrum taken at 532 nm and reported in **Figure 58 d**. At the above wavelength peaks clearly attributable to crystal violet were found at 1619, 1587, 1530, 1176, 910, 803 and 725 cm^{-1}. In addition, crystal purple showed peaks at 1646, 1509 and 768 cm^{-1} assigned to rhodamine B, thus further confirming its occurrence in the ink mixture.

The SERS spectra of green pens (**Figure 57 f**) did not show strong enhancement compared to the Raman spectra. The presence of tartrazine hypothesized through Raman measurements in Fine and Medium crystal inks could also be hypothesized by SERS analysis because of the overlapping of peaks at 1602 and 485 cm^{-1}. In addition, SERS spectra of Fine, Medium Crystal and Medium showed a peak at 1339 cm^{-1} whereas Crystal and Medium showed a peak at 1526 cm^{-1}, which were both attributed to internal vibrations of copper phthalocyanine (CuPh) macrocycle[114]. From previous work carried out in our group, it is known that green inks are often constituted by a mixture of blue and yellow dyes and that blue phthalocyanine Blue 38 dye is used in BIC pen formulations [144]. Therefore, presence of CuPh blue 38 was hypothesized. Clearer indication of Blue 38 occurrence in green pens was obtained by SERS analysis at 532 nm (see **Figure 58 f**) where Medium, Crystal and Medium crystal green pens showed diagnostic peaks at 1541, 1453, 1341 and 712 cm^{-1}. These results were in

reasonable in agreement with literature data reporting presence of halogenated CuPh (Pigment Green 36) in green ink Uniball pen formulations by laser desorption mass spectroscopy (LDMS) analysis[152].

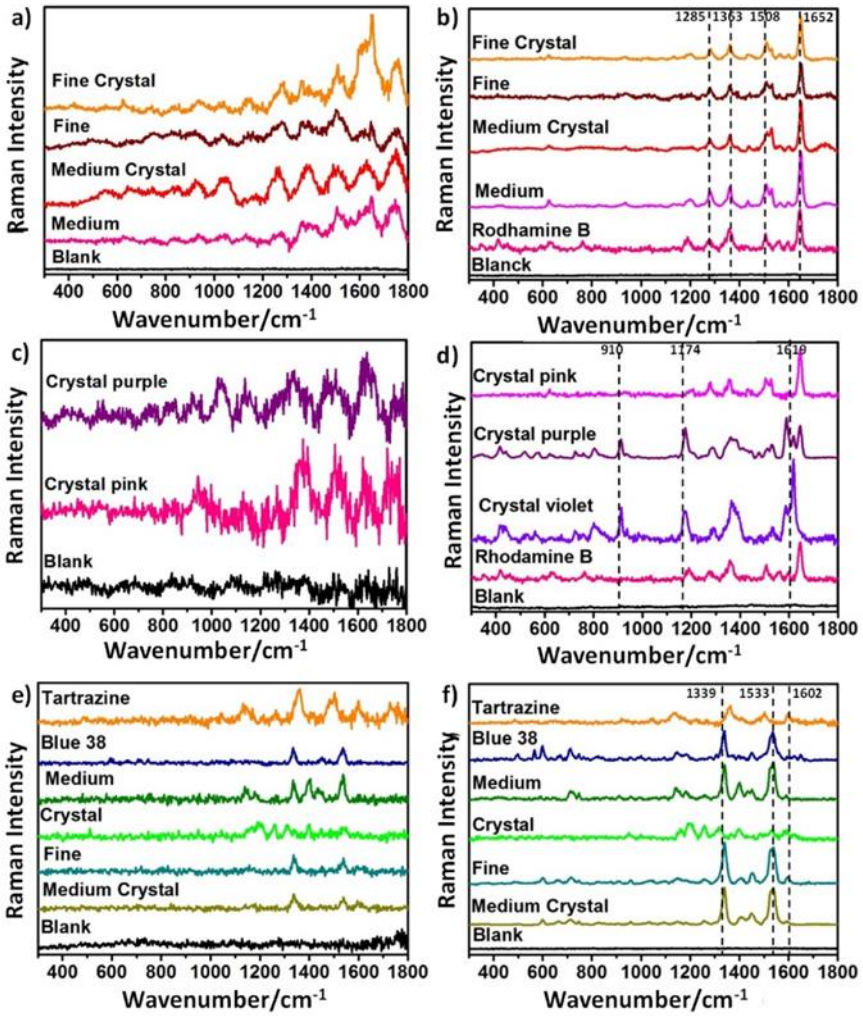

Figure 58. *Raman (**a**) and SERS (**b**) spectra of red pen inks and reference spectra of rhodamine B. Raman (**c**) and SERS (**d**) spectra of pink and purple Crystal pen inks and reference spectra of rhodamine B and crystal violet. Raman (**e**) and SERS (**f**) spectra of green pen inks and reference spectra of tartrazine and blue 38. All spectra were recorded at 532 nm excitation wavelength.*

In order to confirm results and also to test the capabilities of handheld instrumentation for the analysis of inks on paper, Raman and SERS measurements were also carried out at illumination of 785 nm with the use of Raman handheld instrumentation (**Figure 59*)***. Due to the lower spectral resolution of the handheld instrumentation compared to bench instrumentation (10-12 cm^{-1} *vs* 3-5 cm^{-1}), no readable Raman spectra were obtained and

therefore only results of SERS analysis are reported. In addition, the initial SERS spectra of red/pink/purple pen inks overlapped each other and showed peaks mainly attributable to the paper background (data not shown). This was probably due to the large spot size (1 mm) of the handheld spectrograph and highlighted the necessity to intensify the signal/noise ratio of analyzed samples. Towards this end, a hydrolysis step was introduced, whereby a droplet of HCl (2 μL, 1 M) was deposited on the pen written area on paper 24 hr prior Ag nanopaste deposition and SERS measurement. It has been reported that this pre-treatment step significantly improves SERS signals, by promoting the formation of Ag+_ halide complexes and therefore facilitating adsorption of the chromophores to the metal surface [153]. In order to facilitate attribution, reference samples deposited on paper substrates were subjected to the same treatment.

The SERS spectra of all red pen spectra (**Figure 59 *a***) showed diagnostic peaks of rhodamine B at 1655, 1518, 1365, 1292, 1204 and 633 cm^{-1}, confirming the attribution previously made by the use of bench instrumentation. The SERS spectrum of Crystal pink pen reported in **Figure 59 *b***, overlapped with the spectra of the red pens, therefore also confirming the presence of rhodamine B. The SERS spectrum of Crystal purple clearly showed spectral features of rodhamine B and crystal violet. Specifically, the crystal purple pen showed peaks at 1525 and 1286 cm^{-1} clearly assigned to rodhamine B and peaks at 1613, 1579, 1380, 1172, 907, 800, 528 and 423 cm^{-1} associated with crystal violet.

In contrast, spectra of green inks could be acquired without use of HCl treatment. The SERS spectra of green pens (**Figure 59 *c***) showed evidence of blue 38 presence in all pens from peaks centered at 1536, 1337, 752 and 726 cm^{-1}. For comparison also spectra from rhodamine B, crystal violet, blue 38 and tartrazine references were reported in **Figure 59**.

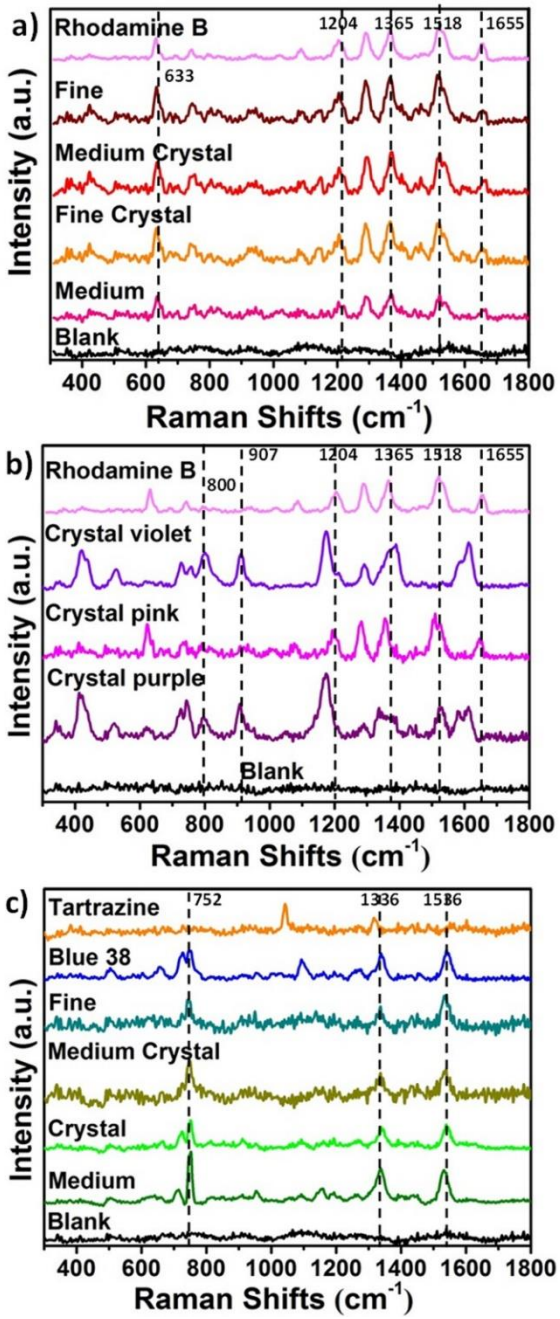

Figure 59. *SERS spectra of BIC ballpoint pen inks* ***a)*** *red,* ***b)*** *pink and purple,* ***c)*** *green. All spectra were taken with handheld instrumentation at 785 nm excitation wavelength.*

In order to verify results additional spectral analysis was carried out whereby the UV-vis spectra of pen inks dissolved in MeOH were compared with spectra of reference dyes identified during Raman/SERS analysis. **Figure 60** ***a*** shows that spectra of all red dyes were equivalent to each other and showed a maximum peak centered at 554 nm, which overlapped the absorption spectrum of rodhamine B. Interestingly, all red pen UV-vis spectra also showed

maxima centered at 416 nm, attributable to a yellow component which remains unidentified. The UV-vis absorption spectra of pink and purple Crystal pen inks (**Figure 60** ***b***) also overlapped with the spectrum of rhodamine B, displaying a maximum at 554 nm. However, the purple Crystal ink showed an additional shoulder at 588 nm, which well overlapped with the absorption band of crystal violet dye. A small additional peak at 663 was also observed and attributed to a phthalocyanine compound, possibly blue 38. The presence of blue38 could also be proved by close inspection of SERS spectra taken at 785 nm excitation wavelength, where two peaks at 1340 and 750 cm^{-1} were observed, which overlapped with an equivalent peak of blue 38 at that excitation wavelength (see **Figure 61**). Finally, the UV-vis spectral analysis of green pen inks (**Figure 60** ***c)*** confirmed results of the Raman/SERS analysis and revealed the presence of a blue component (blue 38) centered at 665 nm for all pens. A yellow component (possibly tartrazine) was also identified from a band centered at 430 nm in Fine, Medium crystal and Medium pens. Crystal pen showed a large peak at 430 nm which overlapped the peak of tartrazine. However, as no evidence of tartrazine was found by Raman/SERS analysis, we conclude that a yellow component molecularly similar to tartrazine should be present in this formulation. Additional peaks at 622 and 692 nm were found for Medium and Crystal green inks, respectively. Such peaks were associated to the presence of additional unidentified blue components.

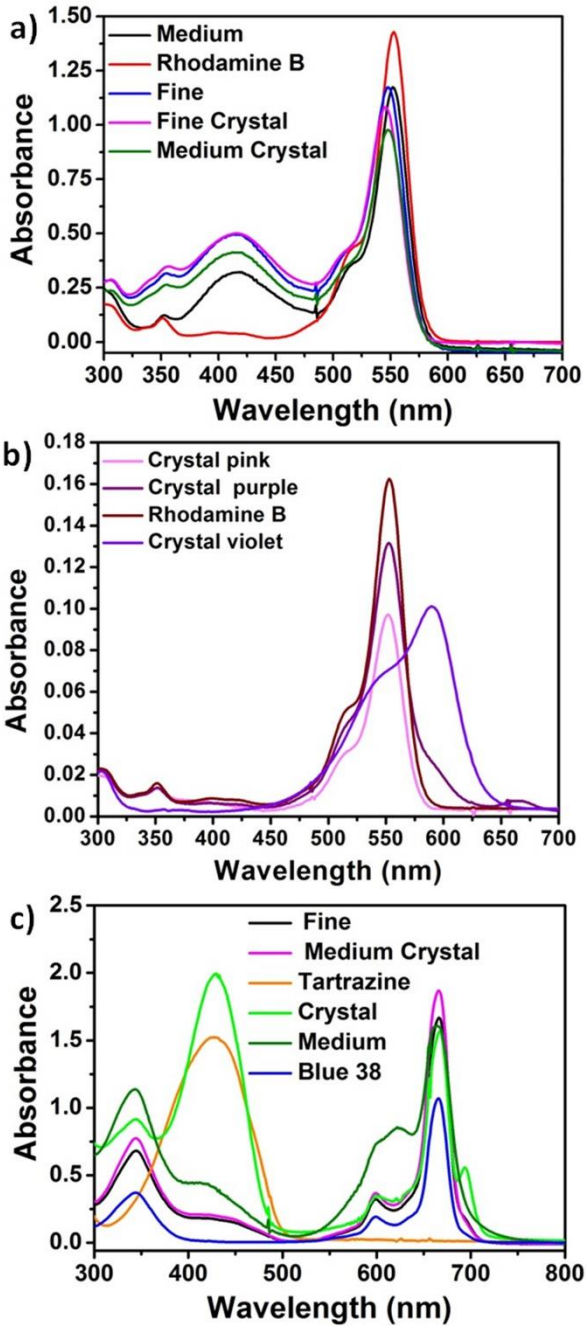

***Figure 60**. UV-vis spectra of BIC ballpoint pen inks and reference dyes dissolved in MeOH: **a**) red pens and rhodamine B; **b**) pink, purple inks and rodhamine B, crystal violet references; **c**) green inks and tartrazine, blue 38 references.*

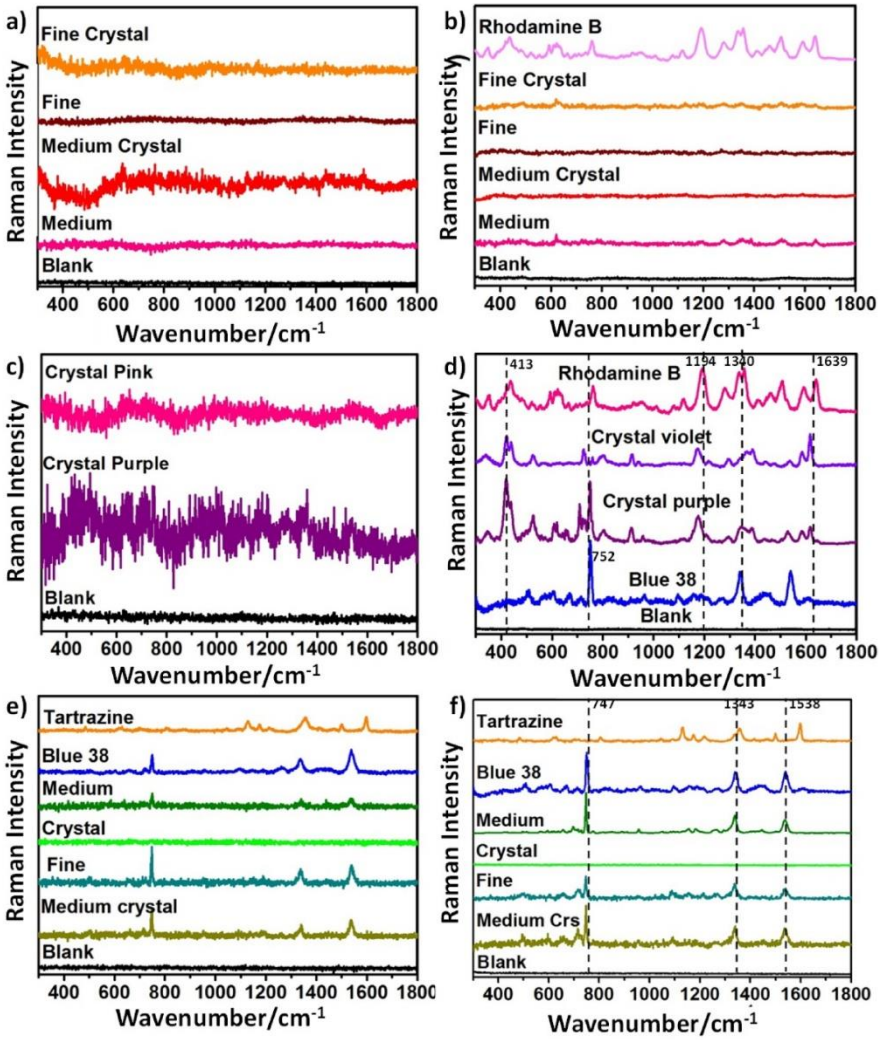

Figure 61. *Raman (a) and SERS (b) spectra of red pen inks and reference spectra of rhodamine B. Raman (c) and SERS (d) spectra of pink and purple Crystal pen inks and reference spectra of rhodamine B, crystal violet and blue 38. Raman (e) and SERS (f) spectra of green pen inks and reference spectra of tartrazine and blue 38. All spectra were recorded at 785 nm excitation wavelength (bench instrumentation).*

Further characterization was carried out by Thin Layer Chromatography (TLC). Results were consistent with data obtained with Raman, SERS and UV-vis spectroscopies and are reported in **Figure 62**. **Table 4** shows a summary of the chemical composition information that was achieved with each applied analytical technique and under different experimental conditions (for example different wavelength illuminations used for Raman and SERS analysis).

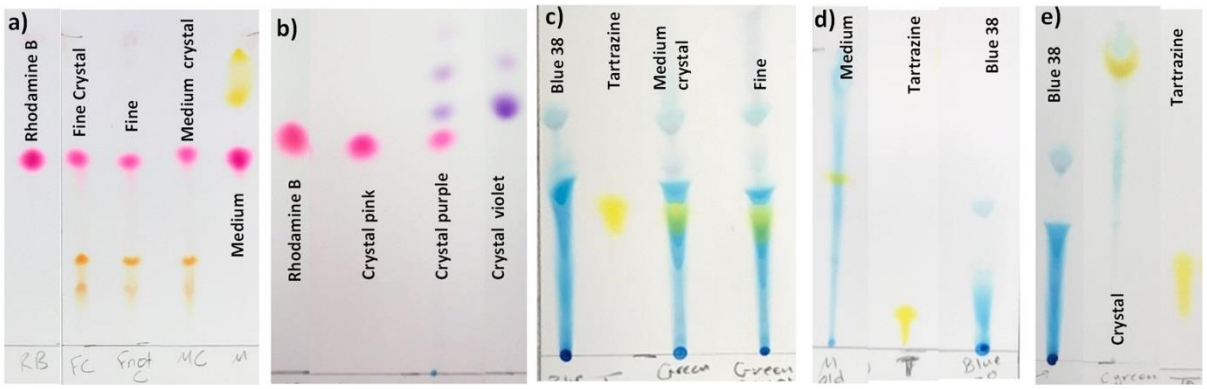

***Figure 62**. TLC photographs of red, pink, purple and green BIC pen inks with reference dyes.*

It is interesting to show that although Raman would be the analytical tool of choice due to its fingerprinting capabilities and non-invasiveness, its effectiveness for the identification of dyes in red colored inks at 514 nm excitation wavelength was limited by the strong fluorescence interference generating from excitation in close proximity to the main dye component rodhamine B molecular absorption resonance (absorbance maximum 554 nm). Therefore identification of rhodamine B was possible for three red inks out of four and no identification was possible for pink and purple inks. No Raman response was obtained for red, pink and purple colored dyes at the other tested excitation wavelengths (532 and 785 nm). Identification of green inks was also difficult at 514 nm, as only tartrazine could be detected for Fine and Medium Crystal green inks. Better results were obtained at 532 and 785 nm, with detection of tartrazine and blue 38 possible in three out of four analyzed green inks. Therefore the application of Raman spectroscopy would require the use of multi-line excitation systems to gather complete chemical compositional information.

On the other hand, SERS analysis at 514 nm excitation was very effective for the characterization of red, pink and purple inks. The enhancement was attributed to the combination of three effects: i) an electromagnetic effect (EM), due to the use of illumination wavelength in plasmonic resonance with the Ag nanopastes; ii) Surface Enhanced Resonance Raman Spectroscopy (SERRS) condition (excitation wavelength in molecular resonance with the main dye component); iii) possible chemical enhancement (CE) processes, due to electrostatic interaction between positively charged rhodamine B and negatively charged Ag nanopastes. SERS was also effective for identification of green ink mixtures due to EM plasmonic enhancement processes. However, the complete identification of blue 38 in green Fine and Medium crystal inks still required the use of an additional excitation lines (either 532

nm or 785 nm), possibly due to the low concentration of this component in the lighter hues green inks.

The use of handheld instrumentation in combination with SERS resulted very effective in identification of dye components for all inks. This result is extremely relevant for the practical implementation of SERS in real analysis where portable instrumentation is often mandatory. The successful generation of SERS signals for red, pink and purple inks was ascribed to a combination of effective accumulation of analyte on the plasmonic surface (hydrolysis process occurring on deposited Ag nanopastes) and effective quenching of fluorescence from the deposited Ag nanopastes.

Interestingly, more dye components were identified by the use of complementary techniques UV-vis and TLC. Specifically, the presence of a yellow component additional to rhodamine B in red inks was only revealed by UV-vis and explained the difference in color between Crystal pink (pure rhodamine B) and red inks. Additional blue components were revealed by UV-vis for Medium and Crystal green. TLC was also used to support results. TLC confirmed the presence of an additional component in red pens which appeared of orange coloration for Fine Crystal, Fine and Medium Crystal and yellow for Medium. Yellow spots not attributable to tartrazine were obtained for Medium and Crystal green inks.

Pen	514 Raman	532 Raman	785 Raman bench
Fine crystal red	Rhodamine B		
Fine red	Rhodamine B		
Medium crystal red	Rhodamine B		
Medium red			
Crystal pink			
Crystal purple			
Medium green		Blue 38, tartrazine	Blue 38
Crystal green			
Fine green	Tartrazine	Blue 38, Tartrazine	Blue 38
Medium crystal green	Tartrazine	Blue 38, Tartrazine	Blue 38

Pen	514 SERS	532 SERS	785 SERS bench	785 SERS HH
Fine crystal red	Rhodamine B	Rhodamine B		Rhodamine B
Fine red	Rhodamine B	Rhodamine B		Rhodamine B
Medium crystal red	Rhodamine B	Rhodamine B		Rhodamine B
Medium red	Rhodamine B	Rhodamine B		Rhodamine B
Crystal pink	Rhodamine B	Rhodamine B		Rhodamine B
Crystal purple	Rhodamine B, crystal violet	Rhodamine B, crystal violet	Rhodamine B, crystal violet, blue 38	Rhodamine B, crystal violet
Medium green	Blue 38, tartrazine	Blue 38	Blue 38	Blue 38
Crystal green	Blue 38			Blue 38
Fine green	Tartrazine	Blue 38	Blue 38	Blue 38
Medium crystal green	Tartrazine, blue 38	Blue 38	Blue 38	Blue 38

Pen	UV-vis	TLC
Fine Crystal red	Rhodamine B + orange band	Rhodamine B + orange spot
Fine red	Rhodamine B + orange band	Rhodamine B + orange spot
Medium Crystal red	Rhodamine B + orange band	Rhodamine B + orange spot
Medium red	Rhodamine B + orange band	Rhodamine B+ yellow spot
Crystal pink	Rhodamine B	Rhodamine B
Crystal purple	Rhodamine B, crystal violet, blue 38	Rhodamine B, crystal violet, blue 38
Medium green	Blue 38, tartrazine	Blue 38, yellow spot
Crystal green	Blue 38 + blue +yellow band	Blue 38, yellow spot
Fine green	Blue 38, tartrazine	Blue 38, tartrazine
Medium Crystal green	Blue 38 + blue, tatrazine	Blue 38, tartrazine

Table 4. *List of dye components identified by Raman, SERS, UV-vis and TLC analysis in all analyzed pen inks.*

The information collected by this analysis could nicely complement analytical information more widely available for blue and black inks and could constitute the basis for the construction of a spectral database for writing inks. This in turn could support the analysis of real pen artworks. In order to show a practical example, a case study is shown where two drawings made by red and green BIC ballpoint pens and donated by French artist Anne-Flore Cabanis were analyzed by Raman spectroscopy.

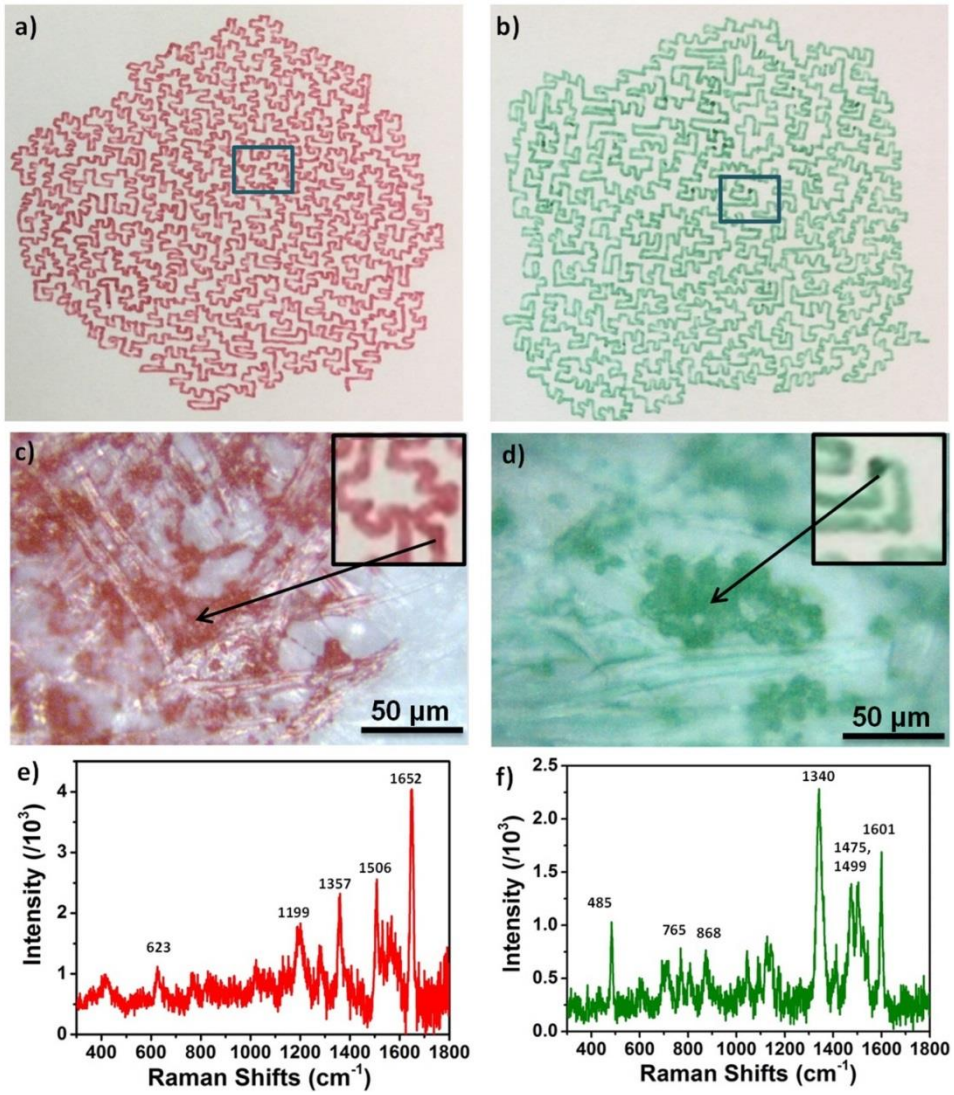

Figure 63. a),b) *Photographs of Anne-Flore Cabanis drawings made by red and green ballpoint pens;* ***c),d)*** *optical microscopy images of Anne-Flore Cabanis drawings;* ***e), f)*** *Raman spectra of red and green pen Anne-Flore Cabanis drawings.*

Figure 63 ***a,b*** show photographs of the drawings made by a continuous line bent at 90 degree angles in order to achieve an overall circular pattern. Careful observation of the drawings under optical microscope (**Figure 63** ***c,d***) showed slightly different color intensities and areas of high ink accumulation generated by the occasional harder pressure of the pen on the paper at resting and corner points, respectively. As result, some paper fibers showed stronger ink accumulation, where Raman spectroscopy was carried out in order to obtain maximized response. The Raman spectrum of the red line (**Figure 63** ***e***) showed peaks at 1360, 1506 and 1649 cm^{-1} attributable to rodhamine B. As all analyzed red pens showed the same

peaks of rodhamine B, identification of the exact BIC pen used by the artist was not possible only with the use of non-invasive analytical techniques. However, successful identification of the main dye component was achieved, which is relevant for conservation purposes. The Raman spectrum of the green line (**Figure 63** ***f***) showed peaks at 1597, 1502, 1475, 1408, 1341, 1000, 808, 769, 482 cm^{-1} and strong overlap with spectral features of green Fine BIC pen previously analyzed. In this case identification was made easier by the diversification in chemical composition of analyzed pens. This information is relevant for the development of future conservation protocols and for detection of forgeries/attribution of originality in pen artworks.

4.4. Conclusion

Raman spectroscopy and SERS were applied for the identification of dye mixtures in commercial colored (red, pink, purple and green) BIC ballpoint pens. All pens inks were analyzed as colored areas on commercial paper. The use of laser excitation wavelengths at 514, 532 and 785 nm allowed Raman identification of main dyes for all pens. The great advantage of Raman spectroscopy relied in its non-invasive nature. However, more efficient identification was achieved by SERS, through deposition of Ag nanopaste on colored paper. Enhanced Raman signals were in general achieved for each selected illumination wavelength, thus not requiring the use of multiple illumination lines. The use of SERS was particularly effective for the characterization of red, pink and purple inks, whose Raman spectra were characterized by high fluorescence backgrounds. Handheld Raman instrumentation was also successfully applied for analysis of inks in combination with SERS. While this method required the use of invasive procedures (hydrolysis and nanopaste deposition), it was performed with the use of low cost, easy to operate and easily deployable instrumentation. Finally, data collected by Raman spectroscopy and SERS were complemented by UV-vis spectroscopy and TLC, which confirmed results obtained and allowed identification of additional dye components in red and green inks. Although data in this work were mainly obtained by the use of invasive methods, this work greatly complements data already obtained for colored pens by other methods and therefore is relevant for the construction of an initial spectral database of ballpoint pen inks. Due to the large amount of ink-based artworks and their light sensitivity, such database will be useful for the characterization of ink-based artworks which in turn will inform the development of conservation strategies tailored to the preservation of these light fugitive art objects.

Chapter 5

SERS-Active Ag NPs/PDMS Composites for Detection of Food Contaminants

A flexible and transparent Surface Enhanced Raman Scattering (SERS) substrate was exploited for the implementation of practical applications in food safety and organic pollutants monitoring. Ag NPs/PDMS SERS composites obtained by self-assembly of organic silver nanoparticle solutions on flexible PDMS surfaces display SERS enhancement factor (EF) of 1.7×10^4, good stability and resistance to harsh conditions as well as good uniformity and batch to batch reproducibility. Their "sticky" nature was exploited to "paste" Ag NPs/PDMS composites on irregular analytical surfaces, thus enabling the detection *in situ* of food contaminant. Specifically, CV and thiram concentrations as low as 1×10^{-7} M and 1×10^{-5} M were detected on contaminated fish skin and orange peel, respectively. Furthermore, efficient SERS detection by micro-extraction of CV from fish skin and thiram from fruit surfaces was achieved, showing the analytical versatility of the fabricated SERS composites.

- [4] This work has been published as: "Flexible and Transparent Surface Enhanced Raman Scattering (SERS)-Active Ag NPs/PDMS Composites for in-situ Detection of Food Contaminants ", Abeer Alyami,[a] Aidan J. Quinn,[a] Daniela Iacopino[a]*, Talanta 201 (2019) 58–64

5.1. Introduction

Surface Enhanced Raman Scattering (SERS) has become an established and powerful analytical technique, due to its effectiveness for ultrasensitive detection, arising from the combination of Raman spectroscopy's fingerprinting ability and plasmonic-enabled enhanced sensitivity.[154, 155] In the last twenty years much effort has been devoted to the development of methodologies for the ordered assembly of plasmonic structures on rigid substrates (SiO_2, glass, quartz),[51, 55, 156] in order to burst SERS sensitivity and reproducibility of analysis. However, the implementation of such rigid SERS substrates has been often impractical due to the need of extraction procedures and high cost of production. It is now recognized that a combination of cost-effective fabrication routes with high sensitivity, reproducibility and versatility of analysis is desirable to widen the SERS range of applications to practical detection systems for routine or field analysis.[157]

Consequently, the focus of recent research has shifted towards development of alternative fabrication routes, whereby flexible surfaces such as plastic,[158-160] paper[161-163]and polymer materials[164, 165] have been used as support. The deposition of the plasmonic SERS-active layer is usually obtained by solution-based fabrication processes which offer fine control over the size and shape of deposited nanoparticles and are compatible with scalable fabrication methods such as printing[166] and dip-coating.[161] As well as being cost–effective and offering high sensitivity useful for routine analysis, flexible substrates have widened the range of SERS applications, due to their increased sampling versatility. For example, swabbing the surface under investigation with a flexible paper-based SERS substrate has been proposed by our group and others as highly practical and efficient method to maximize sample collection towards effective detection of drugs of abuse (malathion, cocaine and benzocaine).[167, 168]

Recently, further widening in the range of practical applications was achieved with the development of flexible and transparent SERS substrates, which enabled contamination-free *in situ* analysis directly on irregular objects without the need for invasive and cumbersome solvent extraction techniques. By using flexible transparent SERS substrates, Luo *et al.*[58] detected model molecule malachite green on fish surface by deposition of an Au nanoparticle/PMMA composite directly on the contaminated fish skin. Guo *et al.*[81] used transparent Au NP/adhesive tape to detected pesticide residues

on fruit and vegetable peels. Organic pollutants such as methyl parathion were measured on orange skin by deposition of Ag nanocrystals/polyethylene films (AgNC@PE films).[59] However, the adhesion of developed substrates on irregular surfaces was not optimal as AuNP/PMMA substrates had to be wet in order to ensure full adhesion with the fish skin and AgNC@PE films had to be fixed with band aid strips in order to promote close contact with the analytical surface. In contrast, the use of polymethylsiloxane (PDMS) as support in combination with Au nanostars proposed by Liz-Marzán *et al.* [61] resulted in fabrication of macroscale highly sensitive SERS substrates with controllable thickness and good adhesion to fruit surfaces.

In this paper we report the fabrication of SERS substrates obtained by self-assembly of Ag NP organic solutions into PDMS substrates. The SERS capabilities of obtained Ag NPs/PDMS composite films were tested with model molecule 4-ABT. Concentrations down to 1×10^{-9} M were obtained, leading to EF of 6×10^{6}. As well as sensitivity, 4-ABT was used to investigate uniformity, batch to batch reproducibility, stability and resistance to harsh conditions in order to determine the suitability of SERS composites for real life applications. The transparency of PDMS was exploited to detect crystal violet (CV) residues on fish skin and thiaram on orange peel by *in situ* SERS back illumination. The controllable thickness of PDMS was exploited to ensure that no competitive signals from PDMS were obtained during analysis. The “sticky” nature of PDMS ensured that good adhesion of Ag NPs/PDMS composite films was obtained on the analytical irregular surfaces. Detection of concentrations as low as 1×10^{-7} M and 1×10^{-5} M was achieved for CV and thiram, respectively. Furthermore, CV and thiram could also be detected directly on Ag NPs/PDMS composite surfaces following micro-extraction from contaminated fish skin and fruit peels.

5.2. Experimental

Ag NPs were synthesized according to a process reported previously by Sheehan et al. [97] .Ag NPs were transferred to organic phase by slight modification of a method previously reported [32] .Ag/PDMS composite film fabrication is already reported in details in chapter 2 in section (2.8).

Crystal violet (CV), 4-aminobenzenethiol (4-ABT) and thiram were purchased from Sigma-Aldrich used without further purification. Fish and organic fruits were bought from the local market and rinsed with deionized water before SERS analysis.

Characterization

UV-vis spectra were acquired using an Agilent/HP 8453 UV-vis Spectrophotometer (200 nm to 1100 nm). Scanning electron microscopy (SEM) images of Ag NPs and Ag NPs/PDMS composite films were acquired using a field emission (JSM- 6700F, JEOL UK Ltd.) scanning microscope operating at 3 kV.

Raman and SERS measurements were obtained from a Renishaw inVia Raman system equipped with a 514 helium–neon laser. The laser beam was focused onto the sample through a Leica 20X objective with 0.4 N.A. Acquisition time was usually 10 s and measured power was 3 mW.

For SERS sensitivity measurements, 10 μL of aqueous 4-ABT solutions of different concentrations (ranging from 1×10^{-4} to 1×10^{-9} M) were deposited onto clean glass slides and left to evaporate at room temperature. An Ag NPs/PDMS film (1×1 cm) was pressed on the glass slide with the Ag NPs side in contact with the dried 4-ABT. SERS signals directly were collected by back illumination of the Ag NPs/PDMS composite film.

Uniformity data were acquired by measuring SERS signals from five different areas of an Ag NPs/PDMS composite film deposited on a glass slide containing dried 4-ABT droplets (obtained by evaporation of 1×10^{-4} M 4-ABT solutions). For batch to batch reproducibility analysis, SERS signals were collected from five different composite films deposited on evaporated 4-ABT droplets. Time stability assessment was performed by depositing an Ag NPs/PDMS composite film on dried 4-ABT droplets and measuring SERS spectra over a three month period. Resistance to harsh condition assessment was carried out by measuring 4-ABT spectra before and after immersion of Ag/PDMS composite films to NaOH 1 M for 1hr, HCl 1 M for 1hr, boiling water for 1 hr.

For CV detection fish skin samples (1×2 cm) were immersed in CV solutions (EtOH)

of different concentration ranging from 1×10^{-5} to 1×10^{-7} M for 10 mins, then dried at room temperature. Ag NPs/PDMS composite films were placed on the dried fish skin with the Ag NP side facing the CV-contaminated fish surface for backside SERS measurements. Alternatively, CV micro-extraction was performed by pressing the Ag NPs/PDMS composite film against the CV-contaminated fish skin for 10 s, followed composite removal and front SERS illumination.

For detection of thiram trace, thin peels (1×2 cm) of orange skin were cut and contaminated by deposition of 0.01mM thiram droplets (EtOH, 10 μL). Ag NPs/PDMS composite film was deposited on the contaminated orange peel and backside SERS measurements performed. Alternatively, SERS was performed on micro-extracted thiram obtained by pressing the Ag NPs/PDMS composite film on thiram-contaminated orange and apple peels for 10 s. SERS measurements were subsequently performed on the front side of the removed SERS substrate.

5.3. Results and discussion

Ag NPs used in this study were prepared with a method developed by Sheehan *et al.*[97]. The concentration of obtained NPs was increased by two orders of magnitude by centrifugation and subsequent re-dispersion in 4 ml of deionized water. This step was necessary to promote the subsequent assembly of NPs organic solutions at the air/solvent interface. The fabrication of Ag NPs/PDMS composite films is described in details in chapter 2 section (2.8.)

Briefly, (**Figure 64**), 10 µl droplet of concentrated nanoparticles in chlorobenzene deposited on clean glass slide. The transfer process of silver particles from water to chlorobenzene took place at pH 8.4 and by surface modification with ODA was likely promoted by the formation of a coordination bond between the amine groups of ODA and the surfaces of the Ag NPs, as reported by Mukherjee *et al.*[169] The deposited droplet of Ag NPs organic solution was left exposed to air for 5 min in order to promote self-assembly at the air/solvent interface. The quick occurring of a self-assembly process was clearly visible from the formation of a superficial metallic layer, attributed to the optical coupling of the densely packed Ag NPs (a). A transfer process followed (b) whereby a thin PDMS film was brought in contact with the Ag NPs metallic layer for 30 sec, which caused the transfer and subsequent attachment of the Ag NPs layer to the organic film. The affinity between hydrophobic PDMS and assembled organic Ag NPs promoted adhesion of transferred particles to the host substrate.

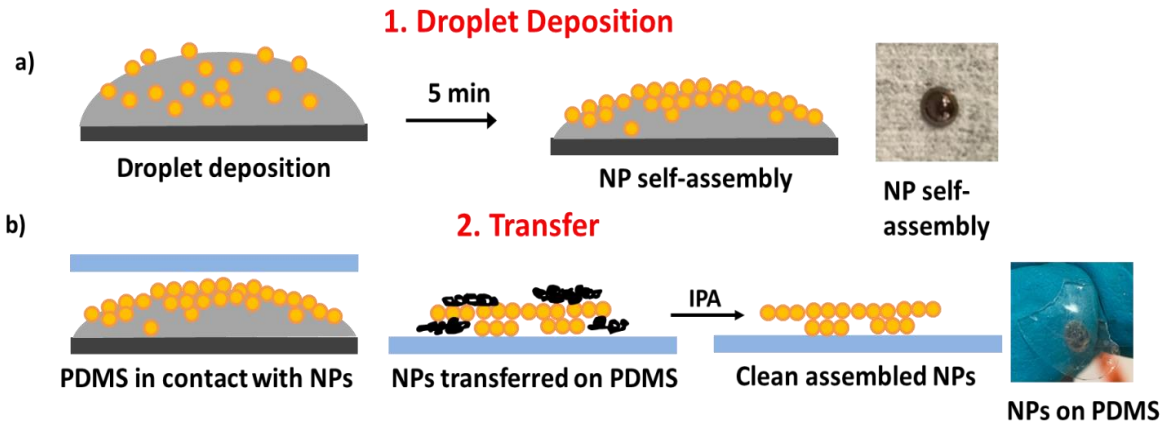

Figure 64. *schematic representations of a) droplet deposition (inset is photography of NPs self-assembly); b) transfer processes (inset is photography of immobilized NPs on PDMS.*

Excess organic solvent and ODA residues were washed away by overnight immersion

of the resulting Ag NPs/PDMS composite film in isopropanol. PDMS was selected for its chemical inertness, non-toxicity and transparency. In addition, its tunable shape size and thickness as well as its "stickiness" were highly desirable features for the targeted application of in situ food quality monitoring.

Figure 65 ***a*** (black line) shows the UV-vis spectrum of Ag NPs as synthesized in aqueous solution. The NPs were characterized by a band centered at 388 nm and a shoulder at 425 nm. The spectrum of the Ag NPs/PDMS composite, also shown in **Figure 65** ***a*** (red line), was characterized by a broad band from 420 to 800 nm, ascribed to the plasmonic coupling between neighboring Ag NPs. A SEM image of the Ag NP layers transferred on the PDMS film is displayed in **Figure 65** ***b***. Dense and high coverage of surface areas larger than 10 μm^2 was achieved. Closer observation of magnified areas (**Figure 65** ***c***) showed that a mixture of monolayers and multilayers formed during the process. The high resolution SEM inset of **Figure 65** ***c*** confirms that nanoparticle size and shape was maintained during the phase transfer and subsequent attachment to PDMS supports.

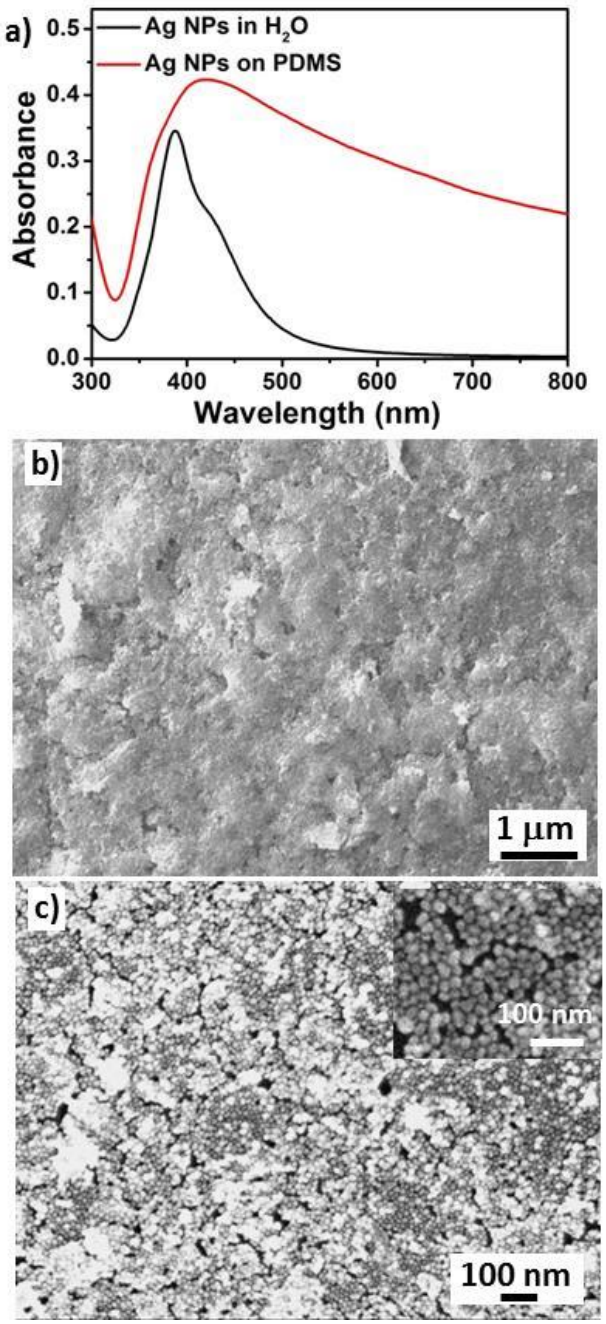

Figure 65. *a) UV-vis spectra of Ag NPs aqueous solution (black line) and Ag NPs/PDMS composite film; b) low resolution SEM image of Ag NPs transferred on PDMS film; c) high resolution SEM image of Ag NPs/PDMS film. Inset: SEM image of a portion of Ag NPs/PDMS film showing morphology of individual transferred NPs.*

To evaluate the SERS sensitivity of the Ag NPs/PDMS composites, samples were prepared by placing a composite film on dried drop-cast 4-ABT solutions of different concentrations ranging from 1×10^{-4} to 1×10^{-9} M. The Ag NP side of the composite faced the dried 4-ABT droplets and SERS measurements were taken by backside direct illumination of

the Ag NPs/PDMS films in contact with the analytical surface. **Figure 66** shows SERS spectra obtained for 4-ABT films with concentrations ranging from 1×10^{-4} to 1×10^{-9} M. All spectra showed clear signatures of 4-ABT with bands centered at 1086, 1178, 1495 and 1591 cm^{-1} associated with the a_1 vibrational, in plane, in phase modes of 4-ABT.[88] In addition to a_1 bands, SERS spectra showed b_2 in plane, out of phase vibrational modes at 1139, 1390 and 1437 cm^{-1}. The formation of b_2 peaks has been observed in SERS spectra of 4-ABT recorded on nanostructured surfaces and has been attributed to a metal-molecule charge transfer related to a chemical enhancement process.[44, 93] The clear features showed by the SERS spectrum obtained at the lowest concentration of 1×10^{-9} M suggested that even lower concentrations could be measured with the fabricated composite films.

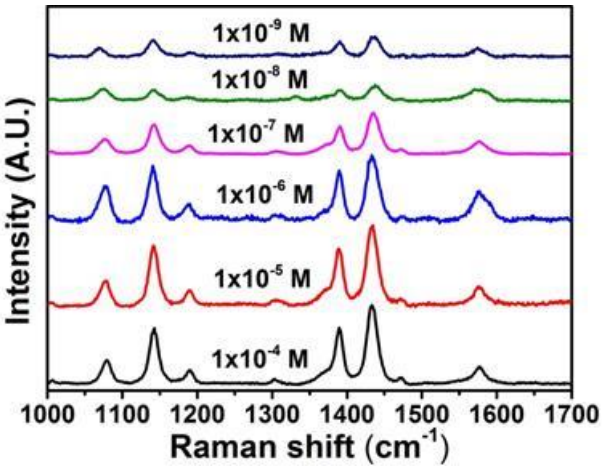

Figure 66. *SERS spectra of 4-ABT with different concentrations from 1×10^{-4} to 1×10^{-9} M obtained by back illumination of Ag NPs/PDMS composite film at excitation wavelength of 514 nm.*

Assessment of signal uniformity achievable with these composites was carried out by taking five intensity measurements of the 1075 cm^{-1} signal over an area of 100×100 μm of the composite film in contact with 4-ABT. A relative standard deviation (RSD) of 13% (***see*** **Figure 67** ***a)*** was obtained, in line or lower than values reported for similar SERS substrates.[58, 59, 81] Furthermore, batch-to-batch reproducibility was assessed by measuring 4-ABT signal intensity variations (at 1075 cm^{-1}) over five Ag NPs/PDMS composite composites, which yield to an RDS of 8%, as reported in **Figure 67** ***b***.

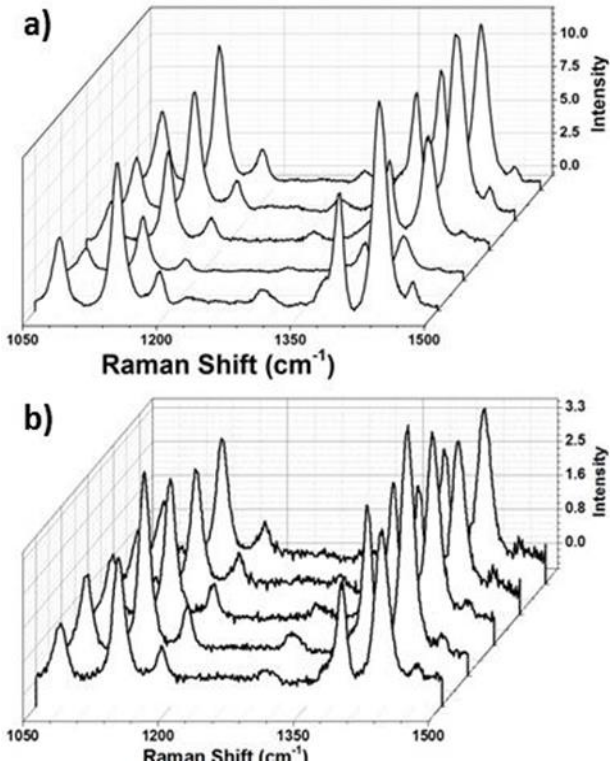

Figure 67. a) *Back illumination SERS measurements of the same AgNPs/PDMS composite pasted on a dried 4-ABT sample;* ***b)*** *Back illumination SERS measurements of different AgNPs/PDMS composites pasted on dried 4-ABT samples.*

To further evaluate SERS performances of the fabricated SERS composite films, the enhancement factor (EF) was calculated following the following equation:

$EF= (I_{SERS}/N_{SERS})/(I_{Raman}/N_{Raman})$

where I_{SERS} and I_{Raman} are the integrated of the SERS and Raman scattering spectra for 4-ABT, respectively. N_{SERS} and N_{Raman} denote the number of 4-ABT molecules found in the laser excitation area adsorbed on the composite film and in bulk form, respectively. For calculation the 4-ABT band at 1075 cm^{-1} was used. The SERS EF of Ag NPs/PDMS film was calculated equal to 1.7×10^4.

Ag NPs/PDMS composite films were further tested to investigate their suitability for real world applications. Towards this end, the estimation of signal stability of over time was investigated (**Figure 68 *a***). An Ag NPs/PDMS film was placed on a dried 4-ABT droplet (10^{-5} M) on a glass slide and SERS spectra were measured by back-illumination of the composite film. Spectra of the same sample were also measured after been stored in the dark for three months. Measured spectra at time zero and three months show good reproducibility of recorded spectra.

Resistance to harsh conditions was also tested by comparing SERS spectra of drop-deposited 4-ABT taken with freshly made composite films and with films immersed in HCl 1M, NaOH 1M and boiling water for 1hr. In all cases only slight variations in spectral intensity were recorded, as clearly shown in **Figure 68** ***b-d***.

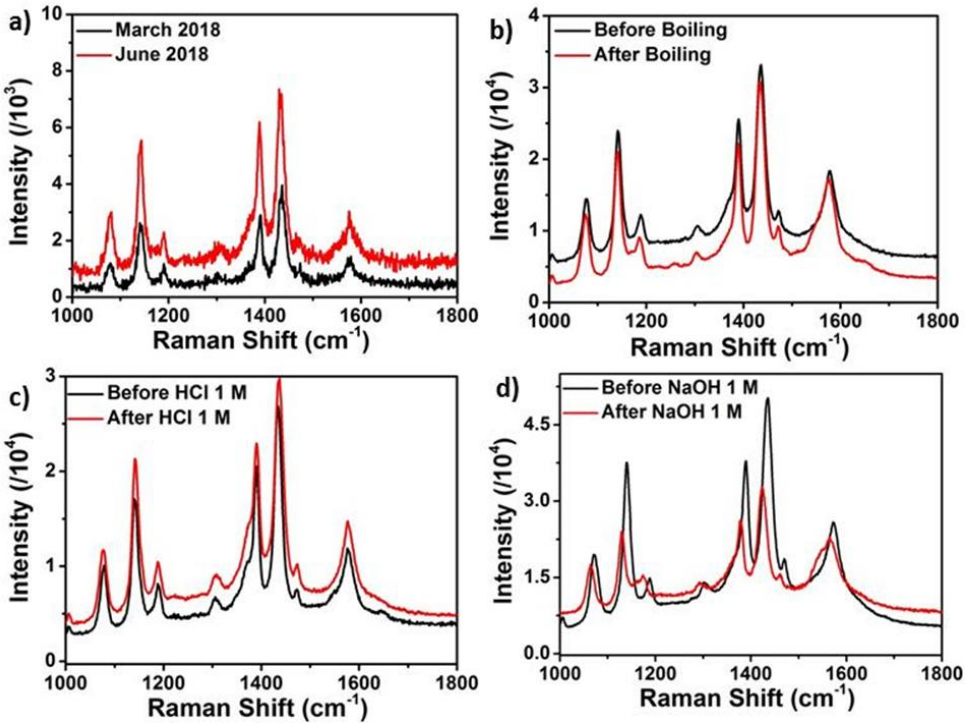

Figure 68. *Back illumination SERS measurements of the same AgNPs/PDMS composite pasted on a 4-ABT sample;* ***a)*** *taken within three months timeframe;* ***b)*** *before and after immersion in boiling water for 1hr;* ***c)*** *before and after immersion in HCl 1 M for 1 hr;* ***d)*** *before and after immersion in NaOH 1 M for 1 hr.*

In order to evaluate the applicability of Ag NPs/PDMS composite films for environmental monitoring applications, a test of residual food contaminants was carried out. Crystal violet (CV) is a toxic cationic dye largely used as food colouring agent and food additive. CV has also being used illegally to improve the survival rate of fish in water body.[170] CV has been classified as recalcitrant molecule since it is poorly metabolized by microbes; therefore, not bio-degradable and can persist in a number of environments. For these reasons the minimum required performance limit (MPRL) was set for 2 mg L^{-1} (ca. 4.9 nM) in European Commission and US.[171]

Figure 69 ***a,b*** shows spectra of CV measured *in situ* on fish skin by deposition of an

Ag NPs/PDMS film on the contaminated skin followed by SERS back illumination. Spectra were recorded at different CV concentrations from 1×10^{-5} to 1×10^{-7} M. The vibrational peaks of CV appeared at 1614, 1589, 1372 and 1179 cm^{-1} and were associated to the stretching of the benzene rings.[113] **Figure 69** ***c*** shows the SERS enhancement obtained on CV-contaminated fish skin compared to simple Raman conditions. For fish skin samples contaminated with 1×10^{-5} M CV, the Raman spectrum appeared featureless, whereas SERS spectra showed intense features, suggesting that enhancements up to 4 orders of magnitude can be achieved with the use of composite films. Figure 68d shows the peak intensities of the 1171 cm^{-1} CV band as a function of the logarithmic concentration of CV displaying good linear correlation and therefore demonstrating possible quantitative applications.

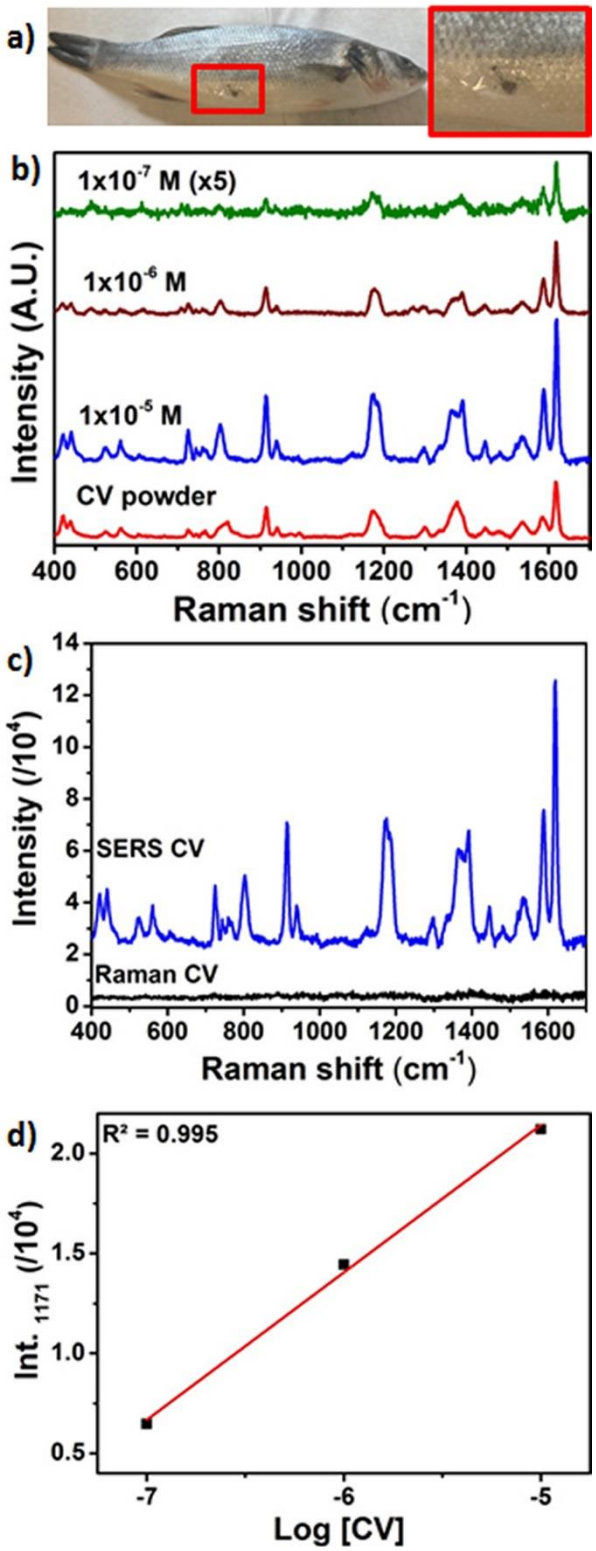

***Figure 69**. **a)** Photograph of fish with pasted Ag NPs/PDMS composite film; **b)** SERS spectra of CV at different concentration from 1×10^{-5} to 1×10^{-7} M recorded by direct deposition of Ag NPs/PDMS composite films on fish skin; **c)** Comparison between Raman and SERS spectra of CV $1x10^{-5}$ M on fish skin. All spectra were recorded at 514 nm illumination wavelength; d) plot of CV SERS intensity measured at 1171 cm^{-1} peak against CV concentration of fish surface.*

In addition, the applicability of fabricated SERS composites for detection of pesticides on fruit was tested. Thiram, a dithiocarbammate compound, is widely used as a fungicide in agriculture and a bactericide in medical treatment.[78] ***Figure 70 a*** shows spectrum (red line) of orange peel obtained by deposition of Ag NPs/PDMS composite film followed by back SERS illumination. The spectrum was dominated by strong bands at 1528, 1189, 1157 and 1005 cm^{-1} associated to the high content of vitamin C in the orange peel.[172] However, the spectra of orange peel exposed to thiram 1×10^{-4} to 1×10^{-5} M solutions (green and blue lines) showed an additional weak band centered at 1384 cm^{-1}, associated to thiram C-N stretching and CH_3 deformation. [173] ***Figure 70 b*** shows the direct comparison between Raman and SERS spectra recorded on orange peel spiked with 1×10^{-4} M thiram, highlighting the superior sensitivity of the latter by two orders of magnitude.

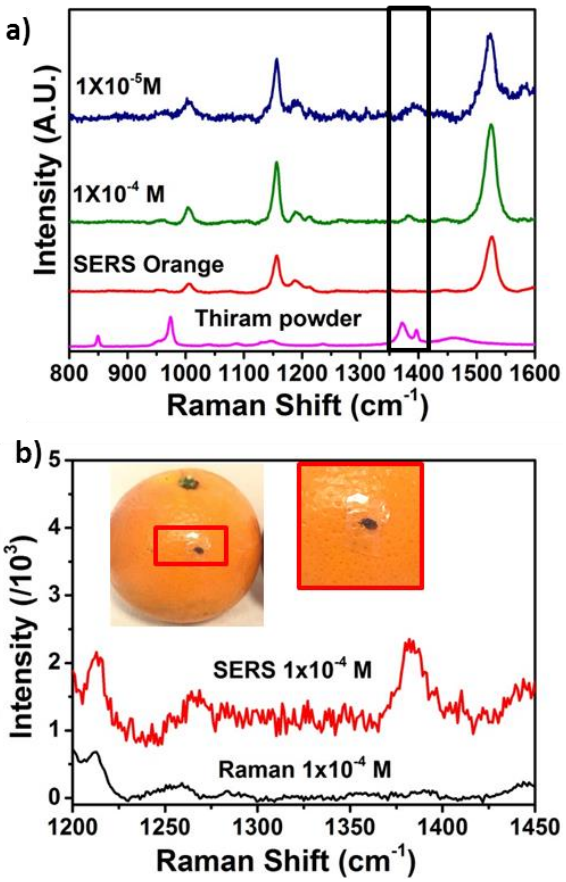

Figure 70. a) *SERS spectra recorded for orange peel (red line) and orange peel treated with 1×10^{-4} and 1×10^{-5} M thiram (green and blue spectra). All SERS were recorded by direct deposition of Ag NPs/PDMS composite film on orange peel;* ***b)*** *SERS and Raman spectra of thiram 1×10^{-4} M deposited on orange peel. All spectra were obtained at 514 nm illumination wavelength.*

The SERS ability of composite films for analysis of food contaminants in real complex matrices was also tested by extraction of target analytes, which was promoted by the "sticky" nature of the PDMS support.

First of all, micro-extraction was performed on CV-contaminated fish skin. In order to perform measurements, fish skin samples were immersed for 10 min in CV solutions of different concentrations between 1×10^{-5} and 1×10^{-7} M. Ag NPs/PDMS films were placed on the fish skin with the Ag NP side facing the skin and left in contact with the analytical surface for few seconds to promote micro-extraction. SERS spectra recorded on micro-extracted CV are shown in **Figure 71 a** Spectra showed characteristic bands of CV at 1614, 1589, 1372 and 1179 cm^{-1}. Sensitivities comparable to those obtained by direct back illumination (**Figure 69 b**) were obtained for the same investigated concentration range.

Same experiments were carried out on fruit peels in order to demonstrate detection of thiram. **Figure 71** shows SERS spectrum obtained for orange peel spiked with 1×10^{-4} M thiram solution. In contrast with the weak spectral signatures obtained with the direct method described in ***Figure 70***, clearer bands attributable to thiram were obtained by micro-extraction. Specifically, the spectrum of **Figure 71 b** was characterized by bands at 1381 (C-N stretching and CH_3 deformation), 1146 (C-N stretching) and 562 cm^{-1} (S-S stretching). The clearer detection of thiram obtained by micro-extraction compared to direct measurements was attributed to the exclusion of the vitamin C contribution in the latter case. The detection of thiram on apple peel is also shown in **Figure 71 c,** displaying clear thiram spectral signatures down to 1×10^{-5} M, below the maximum residual limit (MRL) set for this pesticide.[174] For comparison, the intensity of the signal obtained by in-situ method was more significant than that obtained by microextraction ,however, the signal of the latter is as clear and characteristic as the one obtained by the former.

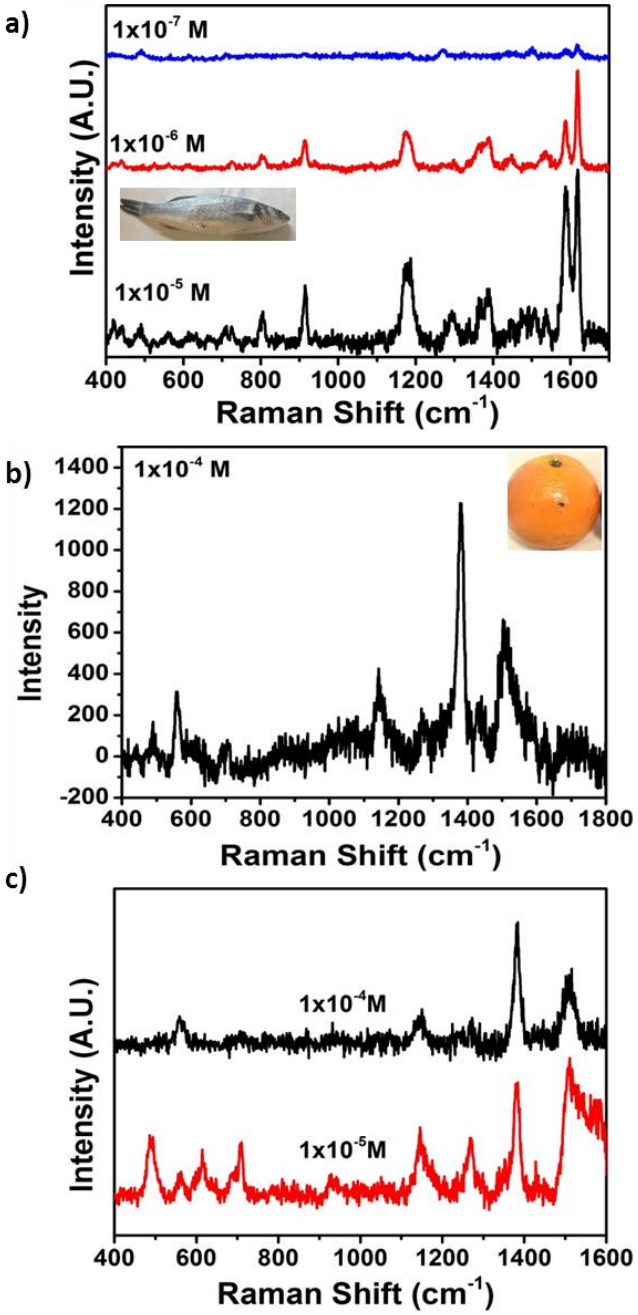

Figure 71. a) *SERS spectra of CV extracted from fish skin in the 1×10^{-5} to 1×10^{-7} M concentration range using Ag NPs/PDMS composite films;* ***b)*** *SERS spectrum of thiram extracted from orange peel (1×10^{-4} M); c) SERS spectra of thiram extracted from apple peel (down to 1×10^{-5} M) using Ag NPs/PDMS composite films. All spectra were recorded at 514 nm illumination wavelength.*

5.4. Conclusion

In conclusion, Ag NPs/PDMS SERS composites were fabricated by self-assembly of organic Ag NP solutions at the air/solvent interface. Model molecule 4-ABT was employed to test the SERS performance of fabricated transparent composites which exhibited high EFs and good uniformity and batch to-batch reproducibility. Ag NPs/PDMS composites also showed excellent time stability and resistance to harsh conditions. In order to demonstrate SERS applicability for environmental monitoring, the sticky nature of the PDMS support was exploited to “paste” fabricated composites into contaminated fish skin and orange peel, leading to successful SERS detection of food contaminant CV and pesticide thiram, respectively by direct back illumination. Moreover, SERS detection by micro-extraction was demonstrated, which provided an alternative method of identification when matrices with strong background signals were analyzed.

Chapter 6

Conclusions and Future Works

6.1. Conclusions

The focus of this thesis was the fabrication of SERS probes and composites for the investigation of due content in commercial inks and detection of food contaminants. Although for both applications costly and sophisticated chromatographic methods have been developed, there is an interest in the development of low cost, fast and portable analysis based on spectroscopic methods. Due to its fingerprinting capabilities, non-invasiveness and availability of portable instrumentation, Raman is an obvious choice. However, Raman suffers from low sensitivity and fluorescence interference, factors that have so far impaired its use for the targeted applications. SERS offers a valid alternative, due to its ability to enhance the Raman signals of up to 10^8 and to quench interference fluorescence. The SERS probes developed in this thesis contributed to the widening of SERS applications in conservation science and food monitoring. Specifically, the development of viscous nanoinks and nanopastes allowed direct deposition of these probes on colored paper samples and therefore direct SERS identification of dyes in commercial inks. Previous attempts with conventional diluted aqueous colloidal solutions failed, due to the water solubility of commercial inks which caused dissolution of the ink in the SERS probe. The development of Ag NPs/PDMS substrates is highly relevant for heritage applications. The transparency, flexibility and conformability of the probe would allow deposition on analytical surface and direct laser illumination. Further work is being carried out in the group on this application.

It should be pointed out that SERS is not usually a quantitative technique. If reproducible SERS substrates (usually requiring lithographic fabrication methods) are used then quantitative analysis can be performed. For example, the reproducible vertical assembly of Au nanorods on SiO_2 substrates was exploited by my colleague Alfonso Martin for demonstration of quantitative analysis. These SERS probes were used for trace analysis of ink analytes in combination with extraction, necessary when small amount of material is available and requiring SERS substrates providing high Enhancement factors. However, the emphasis of this work was on the fabrication of lower cost and more versatile SERS probes for fast, disposable decentralized assays. Moreover, for conservation purposes identification of analytes is more important than quantification, as well as the capability to identify key analytes in complex matrices. For this reason the high sensitivity and selectivity of SERS constituted ideal characteristics for our targeted applications. One important message of this work is that SERS is certainly a useful technique for conservation and food monitoring and the custom fabrication

of SERS probes directly associated to specific analytical challenges can overcome present obstacles and further widening applications of this powerful technique.

Chapter 1 of this thesis introduced the unique properties of plasmonic metal nanostructures and the synthetic routes used to fabricate them in aqueous solutions as well as phase transfer methods into organic solvents. Moreover, different methods SERS substrate fabrication using bottom up approaches were reported along with their applications from literature for ink characterization and food pollutants detection using SERS spectroscopy.

Chapter 2 of this thesis described in details the methods used to fabricate various types of SERS substrates: in-situ, ex-situ, minimally invasive, micro-extraction for different potential SERS applications. Optical characterization of all SERS substrates was covered and compared. In addition, SERS capability and feasibility of the fabricated substrates were investigated using 4-ABT as model molecule.

Chapter 3 of this thesis showed SERS investigation of dye content in blue Bic pen ink using Ag and Au nanoinks. Investigation of BIC pen traces was also performed with Au NRs immobilized on rigid substrates. The SERS response of metal nanoinks provided with 514nm and 785 nm laser lines was investigated in detail in BIC pen TLC extracted samples. Au nanorods vertical arrays with high density of hot spots gave reproducible and sensitive SERS signals for analysis of ink traces with EFs = 1×10^5.

Chapter 4 of this thesis showed application of Ag nanopastes for in-situ SERS analysis of different color of Bic pens along with other analytical techniques: UV-Vis/TLC and Raman spectroscopy. SERS investigation of the colored Bic pens using two excitation wavelengths 514nm/532nm (Bench Raman) and 785nm (Handheld Raman), resulted in identification of dye components for all inks with highly enhanced SESR signals. Combination of metal nanopastes and hand held Raman provided practical implementation of SERS investigation in real sample analysis where portability is crucial point.

In *chapter 5*, SERS-active Ag NPs/PDMS composites were exploited in food safety and organic pollutants detection due to their flexibility and transparency properties. The in-situ SERS analysis shows enhanced Raman signals of drugs traces on fish (CV) and pesticide

(thiram) on fruits with concentration as low as 1×10^{-7} M and 1×10^{-5} M respectively. The uniformity and reproducibility assessment of the flexible SERS film through detection of the 4-ABT molecules give relative standard deviation (RSD) of 8% and 13% respectively.

Finally, micro-extraction of drugs and pesticides from fish and fruit surfaces were achieved, proving the high versatility of the flexible SERS film used without organic solvents usage.

6.2. Future work and potential applications

The plasmonic nanoinks introduced in *chapter 2* and their application in the identification of commercial blue ink mixture in *chapter 3* can be further widened to the analysis of aging mechanisms in commercial inks. Preliminary work on this was carried out by Dr Daniela Saviello and showed SERS signatures in faded blue BIC pens. It would be interesting to develop further this application for technological and conservation purposes. Naturally/artificially aged colored paper samples could be investigated with metal nanoinks using 514 nm and 785 nm excitation wavelengths for in situ study into the characterization and degradation of the color and compositions of the inks in future work. Handheld Raman spectroscopy also can be combined with the SERS substrates to promote the portability and convenience of the SERS analysis.

SERS capability of flexible Ag NPs/PDMS composites was proven in *chapter 5* of this thesis to be efficiently strong under different harsh conditions: heat 120^{o}C for 1 hr, acid/base immersion for 1 hr. In addition, the SERS composites showed considerable stability in SERS performance for over than three months storage. This capacity opens promising opportunities for in-situ applications on real samples in fields where rough conditions are applied.

Investigation of minimal invasiveness of SERS composites (Ag NPs/PDMS and Ag NPs/glass) described in *chapter 2* was not investigated on real samples yet. If this work were to be continued, these plasmonic substrates would be very promising candidates in fields where valuable samples require non-destructive SERS analysis. Certainly, investigation under scanning electron microscope for invasiveness is required for further confirmation of non-invasive property of the assessed SERS substrates.

Micro-extraction of target molecule directly from the surface of analyzed sample using Ag NPs/PDMS SERS composite has been successfully achieved and was shown in this thesis

in *chapter 2* for model molecule and *in chapter 4* for drugs and pesticides on real samples (fish and fruit). Reported studies[81, 85] show the need for developing extraction methods for ink characterization and food contaminant identification on real samples. Therefore, the efficient extraction properties make our fabricated SERS substrates very suitable for potential application in these fields, especially as our developed method was solvent-free, in contrast to other reported methods. However, the consistency of the signals obtained after extraction need further studies to control the reproducibility of the method.

Appendix

Appendix A.

Glossary

4-ABT	4-Aminobenzenethiol
CM	Chemical mechanism
EM	Electromagnetic Mechanism
EtOH	Ethanol
MeOH	Methanol
CTAB	Hexadecyltrimethyl ammonium bromide
MSA	Mercaptosuccinic Acid
SEM	Scanning Electron Microscopy
TEM	Transmission Electron Microscopy
SERS	Surface Enhancement Raman Spectroscopy
LSPR	localised surface plasmon resonance
TOAB	Tetraoctylammonium bromide
TLC	Thin Layer Chromatography
UV-Vis	Ultra violet – visible spectrum
NIR	Near infra-red
NP	Nanoparticle
NR	Nanorod
IR	Infra-red
RSD	Relative Standard Deviation
Ef	Enhancement Factor
FTIR	Fourier Transform Infrared

Appendix B.

Peer reviewed publications

- Published by physical chemistry chemical physics: "**Metal nanoinks as chemically stable surface enhanced scattering (SERS) probes for the analysis of blue BIC ballpoint pens**", A. Alyami, D. Saviello, M. McAuliffe, A. Mirabile, L. Lewis and D. Iacopino, Phys. Chem. Chem. Phys., vol. 19, no. 22, pp. 14652-14658, 2017.

- Published by the American Institute of Physics AIP: "**Chemically Stable Au Nanorods as Probes for Sensitive Surface Enhanced Scattering (SERS) Analysis of Blue BIC Ballpoint Pens**" Abeer Alyami, Daniela Saviello, Micheal A.P. McAuliffe, Raffaele Cucciniello, Antonio Mirabile, Antonio Proto, Liam Lewis, Daniela Iacopino, AIP Conference Proceedings 1873, 020003 (2017); doi: 10.1063/1.4997132.

- Published by the International Journal of Pure and Applied Analytical Chemistry Talanta "**A combined Surface Enhanced Raman Spectroscopy (SERS)/UV–vis approach for the investigation of dye content in commercial felt tip pens inks"** Daniela Saviello, Maddalena Trabace, Abeer Alyami, Antonio Mirabile, Rodorico Giorgi, Piero Baglioni, Daniela Iacopino, Talanta. 2018;181:448-453

- Published by RSC Advances "**Plasmonic colloidal pastes for surface-enhanced Raman spectroscopy (SERS) of historical felt-tip pens**" Daniela Saviello Abeer Alyami, Maddalena Trabace, Rodorico Giorgi, Piero Baglioni, Antonio Mirabile and Daniela Iacopino, RSC Adv., 2018,8, 8365-8371.

- Published by J Raman Spectrosc. "**Identification of dye content in colored BIC ballpoint pen inks by Raman spectroscopy and surface enhanced Raman scattering**" Abeer Alyami, Killian Barton, Liam Lewis, Antonio Mirabile, Daniela Iacopino, J Raman Spectrosc.,2018, 0377-0486.

- Published as: "**Flexible and Transparent Surface Enhanced Raman Scattering**

(SERS)-Active Ag NPs/PDMS Composites for in-situ Detection of Food Contaminants ", Abeer Alyami, Aidan J. Quinn, Daniela Iacopino, Talanta 201 (2019) 58–64

- In preparation for Heritage Sci., **Nanorestart special edition, "Fabrication of Flexible and Transparent Composites for Non-invasive SERS Analysis of Modern Art Works"** Abeer Alyami, Antonio Mirabile, Daniela Iacopino
-

Conferences

- The 8th Conference on Analytical Sciences CASI, DCU Glanevin, Dublin 9, April 2016.
- TECHNART 2017 International conference Non-destructive and micro-analytical techniques in art and cultural heritage, Bilbao, Basque Country, Spain, May 2017.

Posters

- Tyndall Annual Postgraduate Student Poster Competition'2016, Use of Gold Nanorods For Sensitive SERS Analysis of A Bic Ballpoint Pen And Felt-Tip Pens, Abeer Alyami[1], Daniela Saviello[1], Micheal McAuliffe[2], Raymond Wolfe[2], Alfonso Martín[1], Antonio Mirabile[3], Liam Lewis[2], Daniela Iacopino[1*], Tyndall national institute Lee Maltings Complex, Dyke Parade, Cork, July 2016.

- The 8th Conference on Analytical Sciences CASI, Use of Gold Nanorods For Sensitive SERS Analysis of a Bic Ballpoint Pen and Felt-Tip Pens, Abeer Alyami[1], Daniela Saviello[1], Micheal McAuliffe[2], Raymond Wolfe[2], Alfonso Martín[1], Antonio Mirabile[3], Liam Lewis[2], Daniela Iacopino[1*], DCU Glanevin, Dublin 9, April 2016.

- Postgraduate Chemistry Research day on the 21st of August, Use of Metal Nano-Structures for Sensitive SERS Analysis of Contemporary Inks, Abeer Alyami[1], Daniela Iacopino[1*], UCC Kane building,2017.

- TECHNART 2017 International conference Non-destructive and micro-analytical techniques in art and cultural heritage, Metal Nanoinks as Chemically Stable Surface Enhanced Scattering (SERS) Probes for Analysis of Blue BIC Ballpoint Pens, Abeer Alyami[1], Daniela Saviello[1], Micheal McAuliffe[2], Raymond Wolfe[2], Antonio Mirabile[3], Liam Lewis[2], Daniela Iacopino[1], Bilbao, Basque Country, Spain, May 2017.

- Tyndall Annual Postgraduate Student Poster Competition'2017, Use of Gold Nanorods For Sensitive SERS Analysis of A Bic Ballpoint Pen And Felt-Tip Pens, Abeer Alyami[1], Daniela Saviello[1], Micheal McAuliffe[2], Raymond Wolfe[2], Alfonso Martín[1], Antonio Mirabile[3], Liam Lewis[2], Daniela Iacopino[1]*, Tyndall national institute Lee Maltings Complex, Dyke Parade, Cork, November 2017.

Talks

- The 8th Conference on Analytical Sciences, Use of Gold Nanorods For Sensitive SERS Analysis of a Bic Ballpoint Pen And Felt-Tip Pens, DCU Glanevin, Dublin 9, April 2016.
- Creativity and Innovation model, Making the shift happen, UCC, May 2017.
- Science for all, Identifying the Anonymous, UCC, November 2017.
- Tyndall Internal Conference, Don't Lose The Signal**,** December 2018.

Modules

- PG6004 Getting Started with Graduate Research and Generic Skills
- PG6022 English for Postgraduate Studies (Lower Advanced: C1)
- Lasers and laser safety course in department of physics
- PG7014 Creativity and Innovation for Research Students

Supervision and Demonstration

- Coline Gaigne visiting student (undergraduate student) CIT from march to June 2017
- Practice of Analytical Chemistry module (CM6015), Analytical Chemistry master students from September to November 2017 for 50 hrs in UCC chemistry labs.

Reference

1. Faraday, L.P.W.R.F.O.S.M., *The Selected Correspondence of Michael Faraday*. 1971, London: Cam-bridge University Press. p. 1812 - 66.
2. Thompson, D., *Michael Faraday's recognition of ruby gold: the birth of modern nanotechnology.* Gold Bulletin, 2007. **40**(4): p. 267-269.
3. Uwe Kreibig, M.V., *Optical Properties of Small Metal Clusters.* Berlin: Springer,, 1995.
4. Wriedt, T., *Mie Theory A Review.* Springer Series in Optical Sciences, 2012. **169**: p. pp 53-71.
5. Mayer, K.M. and J.H. Hafner, *Localized surface plasmon resonance sensors.* Chem Rev, 2011. **111**(6): p. 3828-57.
6. El-Sayed, M.A., *Some Interesting Properties of Metals Confined in Time and Nanometer Space of Different Shapes.* Accounts of Chemical Research, 2001. **34**(4): p. 257-264.
7. Grzelczak, M., et al., *Shape control in gold nanoparticle synthesis.* Chemical Society Reviews, 2008. **37**(9): p. 1783-1791.
8. Mie, G., *Beiträge zur Optik trüber Medien, speziell kolloidaler Metallösungen.* Annalen der Physik, 1908. **330**(3): p. 377-445.
9. Travis, M.I.M.a.L.D., *Gustava Mie and The Evolving Dicipline of Electromagnatic Scattering by Particles.* American Meteorological Society 2008: p. 1853-1862.
10. Olson J, Dominguez-Medina S, Hoggard A, Wang LY, Chang WS, Link S. Optical characterization of single plasmonic nanoparticles. Chem Soc Rev. 2014;44(1):40–57. doi:10.1039/c4cs00131a.
11. Creighton, J.A. and D.G. Eadon, *Ultraviolet–visible absorption spectra of the colloidal metallic elements.* Journal of the Chemical Society, Faraday Transactions, 1991. **87**(24): p. 3881-3891.
12. Hu, J., T.W. Odom, and C.M. Lieber, *Chemistry and Physics in One Dimension: Synthesis and Properties of Nanowires and Nanotubes.* Accounts of Chemical Research, 1999. **32**(5): p. 435-445.
13. Petroski, J.M., et al., *Kinetically Controlled Growth and Shape Formation Mechanism of Platinum Nanoparticles.* The Journal of Physical Chemistry B, 1998. **102**(18): p. 3316-3320.
14. Jana, N.R., L. Gearheart, and C.J. Murphy, *Seed-Mediated Growth Approach for Shape-Controlled Synthesis of Spheroidal and Rod-like Gold Nanoparticles Using a Surfactant Template.* Advanced Materials, 2001. **13**(18): p. 1389-1393.
15. Nikoobakht, B. and M.A. El-Sayed, *Preparation and Growth Mechanism of Gold Nanorods (NRs) Using Seed-Mediated Growth Method.* Chemistry of Materials, 2003. **15**(10): p. 1957-1962.
16. Busbee, B.D., S.O. Obare, and C.J. Murphy, *An Improved Synthesis of High-Aspect-Ratio Gold Nanorods.* Advanced Materials, 2003. **15**(5): p. 414-416.
17. Orendorff, C.J. and C.J. Murphy, *Quantitation of Metal Content in the Silver-Assisted Growth of Gold Nanorods.* The Journal of Physical Chemistry B, 2006. **110**(9): p. 3990-3994.
18. Lea, M.C., *On Allotropic Forms of Silver.* Scientific American, 1889. **28**(711supp): p. 11361-11361.
19. Turkevich, J., P.C. Stevenson, and J. Hillier, *A study of the nucleation and growth processes in the synthesis of colloidal gold.* Discussions of the Faraday Society, 1951. **11**(0): p. 55-75.

20. Lee, P.C. and D. Meisel, *Adsorption and surface-enhanced Raman of dyes on silver and gold sols.* The Journal of Physical Chemistry, 1982. **86**(17): p. 3391-3395.
21. Pillai, Z.S. and P.V. Kamat, *What Factors Control the Size and Shape of Silver Nanoparticles in the Citrate Ion Reduction Method?* The Journal of Physical Chemistry B, 2004. **108**(3): p. 945-951.
22. Polavarapu, L., et al., *Pen-on-Paper Approach Toward the Design of Universal Surface Enhanced Raman Scattering Substrates.* Small, 2014. **10**(15): p. 3065-3071.
23. Pacioni, N.L., et al., *Synthetic Routes for the Preparation of Silver Nanoparticles*, in *Silver Nanoparticle Applications: In the Fabrication and Design of Medical and Biosensing Devices*, E.I. Alarcon, M. Griffith, and K.I. Udekwu, Editors. 2015, Springer International Publishing: Cham. p. 13-46.
24. Natsuki, J., *A Review of Silver Nanoparticles: Synthesis Methods, Properties and Applications*. Vol. 4. 2015. 325.
25. Quang Huy, T., N. Van Quy, and L. Anh-Tuan, *Silver nanoparticles: synthesis, properties, toxicology, applications and perspectives.* Advances in Natural Sciences: Nanoscience and Nanotechnology, 2013. **4**(3): p. 033001.
26. Song, K.C., et al., *Preparation of colloidal silver nanoparticles by chemical reduction method.* Korean Journal of Chemical Engineering, 2009. **26**(1): p. 153-155.
27. Rupali, S.P., et al., *One-pot synthesis of PVA-capped silver nanoparticles their characterization and biomedical application.* Advances in Natural Sciences: Nanoscience and Nanotechnology, 2012. **3**(1): p. 015013.
28. Shao-Feng, C. and Z. Hongyin, *Aggregation kinetics of nanosilver in different water conditions.* Advances in Natural Sciences: Nanoscience and Nanotechnology, 2012. **3**(3): p. 035006.
29. Thi My Dung, D., et al., *Influence of surfactant on the preparation of silver nanoparticles by polyol method.* Advances in Natural Sciences: Nanoscience and Nanotechnology, 2012. **3**(3): p. 035004.
30. Yang, J., J. Lee, and J. Y Ying, *Phase Transfer and Its Applications in Nanotechnology*. Vol. 40. 2011. 1672-96.
31. Yang, J., et al., *Organic solvent dependence of plasma resonance of gold nanorods: A simple relationship.* Chemical Physics Letters, 2005. **416**(4): p. 215-219.
32. Sugawa, K., et al., *Facile Phase Transfer of Gold and Au-Core/Ag-Shell Nanoparticles from Aqueous to Toluene Solution Using Alkylamine Molecules and Their Assemblies on Solid Supports*. Vol. 50. 2011. 04DH14.
33. Mitamura, K., et al., *Fabrication and Self-Assembly of Hydrophobic Gold Nanorods.* The Journal of Physical Chemistry B, 2007. **111**(30): p. 8891-8898.
34. Lista, M., D.Z. Liu, and P. Mulvaney, *Phase Transfer of Noble Metal Nanoparticles to Organic Solvents.* Langmuir, 2014. **30**(8): p. 1932-1938.
35. Cheng, W. and E. Wang, *Size-Dependent Phase Transfer of Gold Nanoparticles from Water into Toluene by Tetraoctylammonium Cations: A Wholly Electrostatic Interaction.* The Journal of Physical Chemistry B, 2004. **108**(1): p. 24-26.
36. Vijaya Sarathy, K., G. U. Kulkarni, and C. N. R. Rao, *A novel method of preparing thiol-derivatised nanoparticles of gold, platinum and silver forming superstructures.* Chemical Communications, 1997(6): p. 537-538.
37. Kumar, A., et al., *Phase transfer of silver nanoparticles from aqueous to organic solutions using fatty amine molecules.* Journal of Colloid and Interface Science, 2003. **264**(2): p. 396-401.
38. Mosier-Boss, P.A., *Review of SERS Substrates for Chemical Sensing.* Nanomaterials (Basel, Switzerland), 2017. **7**(6): p. 142.

39. *Raman Scattering*. 1928.
40. Miller, F.A. and G.B. Kauffman, *C. V. Raman and the discovery of the Raman effect.* Journal of Chemical Education, 1989. **66**(10): p. 795.
41. Fleischmann, M., P.J. Hendra, and A.J. McQuillan, *Raman spectra of pyridine adsorbed at a silver electrode.* Chemical Physics Letters, 1974. **26**(2): p. 163-166.
42. Albrecht, M.G. and J.A. Creighton, *Anomalously intense Raman spectra of pyridine at a silver electrode.* Journal of the American Chemical Society, 1977. **99**(15): p. 5215-5217.
43. Lee, S.J., et al., *Surface-Enhanced Raman Spectroscopy and Nanogeometry: The Plasmonic Origin of SERS.* The Journal of Physical Chemistry C, 2007. **111**(49): p. 17985-17988.
44. Osawa, M., et al., *Charge transfer resonance Raman process in surface-enhanced Raman scattering from p-aminothiophenol adsorbed on silver: Herzberg-Teller contribution.* The Journal of Physical Chemistry, 1994. **98**(48): p. 12702-12707.
45. Bibikova, O., et al., *Towards enhanced optical sensor performance: SEIRA and SERS with plasmonic nanostars.* Analyst, 2017. **142**(6): p. 951-958.
46. Michaels, A.M., Jiang, and L. Brus, *Ag Nanocrystal Junctions as the Site for Surface-Enhanced Raman Scattering of Single Rhodamine 6G Molecules.* The Journal of Physical Chemistry B, 2000. **104**(50): p. 11965-11971.
47. Chung, T., et al., *Plasmonic nanostructures for nano-scale bio-sensing.* Sensors (Basel, Switzerland), 2011. **11**(11): p. 10907-10929.
48. Kumar, J., et al., *Au nanorod quartets and Raman signal enhancement: towards the design of plasmonic platforms.* Nanoscale, 2014. **6**(18): p. 10454-10459.
49. Upadhyay, A., et al., *Self-Directed Assembly of Nanoparticles: A Review on Various Approaches*. 2015. p. 297-335.
50. Idone, A., et al., *Silver colloidal pastes for dye analysis of reference and historical textile fibers using direct, extractionless, non-hydrolysis surface-enhanced Raman spectroscopy.* Analyst, 2013. **138**(20): p. 5895-903.
51. Martín, A., et al., *Surface-Enhanced Raman Scattering of 4-Aminobenzenethiol on Au Nanorod Ordered Arrays.* The Journal of Physical Chemistry C, 2014. **118**(24): p. 13260-13267.
52. Ahmad, H. and H.-D. Kronfeldt, *High Sensitive Seawater Resistant SERS Substrates Based on Gold Island Film Produced by Electroless Plating*. Vol. 3. 2013. 1-8.
53. Walsh, R.J. and G. Chumanov, *Silver Coated Porous Alumina as a New Substrate for Surface-Enhanced Raman Scattering.* Applied Spectroscopy, 2001. **55**(12): p. 1695-1700.
54. Simo, A., et al., *Long-Term Stable Silver Subsurface Ion-Exchanged Glasses for SERS Applications.* ChemPhysChem, 2011. **12**(9): p. 1683-1688.
55. Martín, A., et al., *Facile Formation of Ordered Vertical Arrays by Droplet Evaporation of Au Nanorod Organic Solutions.* Langmuir, 2014. **30**(34): p. 10206-10212.
56. Zaffino, C., et al., *''Dry-state'' surface-enhanced Raman scattering (SERS): toward non-destructive analysis of dyes on textile fibers*. Vol. 122. 2016.
57. Kahraman, M., et al., *Fabrication and Characterization of Flexible and Tunable Plasmonic Nanostructures.* Scientific Reports, 2013. **3**: p. 3396.
58. Zhong, L.-B., et al., *Self-Assembly of Au Nanoparticles on PMMA Template as Flexible, Transparent, and Highly Active SERS Substrates.* Analytical Chemistry, 2014. **86**(13): p. 6262-6267.
59. Zhou, N., et al., *A flexible transparent Ag-NC@PE film as a cut-and-paste SERS substrate for rapid in situ detection of organic pollutants.* Analyst, 2016. **141**(20): p. 5864-5869.

60. Gong, Z., et al., *A silver nanoparticle embedded hydrogel as a substrate for surface contamination analysis by surface-enhanced Raman scattering.* Analyst, 2014. **139**(20): p. 5283-5289.
61. Shiohara, A., et al., *Solution processed polydimethylsiloxane/gold nanostar flexible substrates for plasmonic sensing.* Nanoscale, 2014. **6**(16): p. 9817-9823.
62. Merrill, R. and E. Bartick, *Analysis of Ballpoint Pen Inks by Diffuse Reflectance Infrared Spectrometry.* 1992.
63. Siegel, J.A., *Ink Analysis*, in *Encyclopedia of Forensic Sciences (Second Edition)*, J.A. Siegel, P.J. Saukko, and M.M. Houck, Editors. 2013, Academic Press: Waltham. p. 375-379.
64. Bell, S., B.A.J. Fisher, and R.C. Shaler, *Encyclopedia of Forensic Science*. 2008: Facts On File.
65. uuml, et al., *Characterization of Ballpoint Pen Inks by Thermal Desorption and Gas Chromatography-Mass Spectrometry.* 2005.
66. Mania, J., J. Bis, and P. Kościelniak, *An evaluation of the application of capillary electrophoresis to forensic examinations of inks*. Vol. 51. 2002. 71-86.
67. Djozan, D., et al., *Forensic discrimination of blue ballpoint pen inks based on thin layer chromatography and image analysis.* Forensic Science International, 2008. **179**(2): p. 199-205.
68. Neumann, C., R. Ramotowski, and T. Genessay, *Forensic examination of ink by high-performance thin layer chromatography—The United States Secret Service Digital Ink Library.* Journal of Chromatography A, 2011. **1218**(19): p. 2793-2811.
69. Jones, R.W., R.B. Cody, and J.F. McClelland, *Differentiating Writing Inks Using Direct Analysis in Real Time Mass Spectrometry.* Journal of Forensic Sciences, 2006. **51**(4): p. 915-918.
70. Weyermann, C., et al., *Photofading of Ballpoint Dyes Studied on Paper by LDI and MALDI MS.* Journal of the American Society for Mass Spectrometry, 2006. **17**(3): p. 297-306.
71. Dirwono, W., et al., *Application of micro-attenuated total reflectance FTIR spectroscopy in the forensic study of questioned documents involving red seal inks.* Forensic Science International, 2010. **199**(1): p. 6-8.
72. Zięba-Palus, J. and M. Kunicki, *Application of the micro-FTIR spectroscopy, Raman spectroscopy and XRF method examination of inks.* Forensic Science International, 2006. **158**(2): p. 164-172.
73. Dhara, S., et al., *Forensic application of total reflection X-ray fluorescence spectrometry for elemental characterization of ink samples.* Spectrochimica Acta Part B: Atomic Spectroscopy, 2010. **65**(2): p. 167-170.
74. Braz, A., M. López-López, and C. García-Ruiz, *Raman spectroscopy for forensic analysis of inks in questioned documents.* Forensic Science International, 2013. **232**(1): p. 206-212.
75. Geiman, I., M. Leona, and J.R. Lombardi, *Application of Raman Spectroscopy and Surface-Enhanced Raman Scattering to the Analysis of Synthetic Dyes Found in Ballpoint Pen Inks*.* Journal of Forensic Sciences, 2009. **54**(4): p. 947-952.
76. Seifar, R.M., et al., *Applicability of surface-enhanced resonance Raman scattering for the direct discrimination of ballpoint pen inks.* Analyst, 2001. **126**(8): p. 1418-1422.
77. Claybourn, M. and M. Ansell, *Using Raman Spectroscopy to solve crime: inks, questioned documents and fraud.* Science & Justice, 2000. **40**(4): p. 261-271.
78. Pohanish, R., *Sittig's Handbook of Pesticides and Agricultural Chemicals* 2nd Edition ed. 2015.

79. Srivastava, S., R. Sinha, and D. Roy, *Toxicological effects of malachite green.* Aquat Toxicol, 2004. **66**(3): p. 319-29.
80. Zhang, Y., et al., *Rapid simultaneous detection of multi-pesticide residues on apple using SERS technique.* Analyst, 2014. **139**(20): p. 5148-54.
81. Chen, J., et al., *Flexible and Adhesive Surface Enhance Raman Scattering Active Tape for Rapid Detection of Pesticide Residues in Fruits and Vegetables.* Analytical Chemistry, 2016. **88**(4): p. 2149-2155.
82. Li, J.F., et al., *Shell-isolated nanoparticle-enhanced Raman spectroscopy.* Nature, 2010. **464**: p. 392.
83. Abdulrahman, H.B., et al., *Silica-Protected Hollow Silver and Gold Nanoparticles: New Material for Raman Analysis of Surfaces.* The Journal of Physical Chemistry C, 2015. **119**(34): p. 20030-20038.
84. Lai, K., et al., *Determination of chloramphenicol and crystal violet with surface enhanced Raman spectroscopy.* Sensing and Instrumentation for Food Quality and Safety, 2011. **5**(1): p. 19-24.
85. Leona, M., et al., *Nondestructive Identification of Natural and Synthetic Organic Colorants in Works of Art by Surface Enhanced Raman Scattering.* Analytical Chemistry, 2011. **83**(11): p. 3990-3993.
86. Lee, C.H., L. Tian, and S. Singamaneni, *Paper-Based SERS Swab for Rapid Trace Detection on Real-World Surfaces.* ACS Applied Materials & Interfaces, 2010. **2**(12): p. 3429-3435.
87. Oliveira, M., et al., *Office paper decorated with silver nanostars - an alternative cost effective platform for trace analyte detection by SERS*. Vol. 7. 2017.
88. Hu, X., et al., *Surface-Enhanced Raman Scattering of 4-Aminothiophenol Self-Assembled Monolayers in Sandwich Structure with Nanoparticle Shape Dependence: Off-Surface Plasmon Resonance Condition.* The Journal of Physical Chemistry C, 2007. **111**(19): p. 6962-6969.
89. Uetsuki, K., et al., *Experimental Identification of Chemical Effects in Surface Enhanced Raman Scattering of 4-Aminothiophenol.* The Journal of Physical Chemistry C, 2010. **114**(16): p. 7515-7520.
90. Kim, K., et al., *Surface-enhanced Raman scattering of 4-aminobenzenethiol on gold: the concept of threshold energy in charge transfer enhancement.* Chemical Communications, 2011. **47**(7): p. 2020-2022.
91. Kim, K., et al., *Surface-Enhanced Raman Scattering of 4-Aminobenzenethiol in Ag Sol: Relative Intensity of a1- and b2-Type Bands Invariant against Aggregation of Ag Nanoparticles.* Langmuir, 2011. **27**(8): p. 4526-4531.
92. Kim, K., et al., *Surface-enhanced Raman scattering of 4-aminobenzenethiol on silver: confirmation of the origin of b2-type bands.* Journal of Raman Spectroscopy, 2011. **42**(12): p. 2112-2118.
93. Lombardi, J.R. and R.L. Birke, *A Unified Approach to Surface-Enhanced Raman Spectroscopy.* The Journal of Physical Chemistry C, 2008. **112**(14): p. 5605-5617.
94. Deegan, R.D., et al., *Capillary flow as the cause of ring stains from dried liquid drops.* Nature, 1997. **389**: p. 827.
95. Schopf, C., et al., *Au nanorod plasmonic superstructures obtained by a combined droplet evaporation and stamping method.* Journal of Materials Chemistry C, 2014. **2**(18): p. 3536-3541.
96. Alvarez-Puebla, R.A., et al., *Gold nanorods 3D-supercrystals as surface enhanced Raman scattering spectroscopy substrates for the rapid detection of scrambled prions.* Proceedings of the National Academy of Sciences of the United States of America, 2011.

108(20): p. 8157-8161.
97. Rainville, L.-C., et al., *Proteomic evaluation of citrate-coated silver nanoparticles toxicity in Daphnia magna.* Analyst, 2014. **139**(7): p. 1678-1686.
98. Cai, D., et al., *Raman, mid-infrared, near-infrared and ultraviolet–visible spectroscopy of PDMS silicone rubber for characterization of polymer optical waveguide materials.* Journal of Molecular Structure, 2010. **976**(1): p. 274-281.
99. Izzo, F.C., et al., *Multi-analytical investigation on felt-tip pen inks: Formulation and preliminary photo-degradation study.* Microchemical Journal, 2016. **124**: p. 919-928.
100. Jeanmaire, D.L. and R.P. Van Duyne, *Surface raman spectroelectrochemistry: Part I. Heterocyclic, aromatic, and aliphatic amines adsorbed on the anodized silver electrode.* Journal of Electroanalytical Chemistry and Interfacial Electrochemistry, 1977. **84**(1): p. 1-20.
101. Kneipp, K., et al., *Ultrasensitive Chemical Analysis by Raman Spectroscopy.* Chemical Reviews, 1999. **99**(10): p. 2957-2976.
102. Orendorff, C.J., et al., *Aspect ratio dependence on surface enhanced Raman scattering using silver and gold nanorod substrates.* Physical Chemistry Chemical Physics, 2006. **8**(1): p. 165-170.
103. Xu, H., et al., *Spectroscopy of Single Hemoglobin Molecules by Surface Enhanced Raman Scattering.* Physical Review Letters, 1999. **83**(21): p. 4357-4360.
104. Jiang, et al., *Single Molecule Raman Spectroscopy at the Junctions of Large Ag Nanocrystals.* The Journal of Physical Chemistry B, 2003. **107**(37): p. 9964-9972.
105. White, P.C., *In situ Surface Enhanced Resonance Raman Scattering (SERRS) spectroscopy of biro inks – long term stability of colloid treated samples.* Science & Justice, 2003. **43**(3): p. 149-152.
106. Luo, Z., et al., *Gold cluster coatings enhancing Raman scattering from surfaces: Ink analysis and document identification.* Chemical Physics, 2013. **423**: p. 73-78.
107. Hao, E. and G.C. Schatz, *Electromagnetic fields around silver nanoparticles and dimers.* The Journal of Chemical Physics, 2004. **120**(1): p. 357-366.
108. Murphy, C.J., et al., *Anisotropic Metal Nanoparticles: Synthesis, Assembly, and Optical Applications.* The Journal of Physical Chemistry B, 2005. **109**(29): p. 13857-13870.
109. Gallidabino, M., C. Weyermann, and R. Marquis, *Differentiation of blue ballpoint pen inks by positive and negative mode LDI-MS.* Forensic Science International, 2011. **204**(1): p. 169-178.
110. Brożek-Płuska, B., I. Szymczyk, and H. Abramczyk, *Raman spectroscopy of phthalocyanines and their sulfonated derivatives.* Journal of Molecular Structure, 2005. **744-747**: p. 481-485.
111. Lewis, G.N., T.T. Magel, and D. Lipkin, *Isomers of Crystal Violet Ion. Their Absorption and Re-emission of Light.* Journal of the American Chemical Society, 1942. **64**(8): p. 1774-1782.
112. Eustis, S. and M.A. El-Sayed, *Why gold nanoparticles are more precious than pretty gold: Noble metal surface plasmon resonance and its enhancement of the radiative and nonradiative properties of nanocrystals of different shapes.* Chemical Society Reviews, 2006. **35**(3): p. 209-217.
113. Cañamares, M.V., et al., *DFT, SERS, and Single-Molecule SERS of Crystal Violet.* The Journal of Physical Chemistry C, 2008. **112**(51): p. 20295-20300.
114. Li, D., et al., *Theoretical studies on molecular structure and vibrational spectra of copper phthalocyanine.* Vibrational Spectroscopy, 2005. **39**(2): p. 191-199.
115. Selvakannan, P.R., et al., *Probing the effect of charge transfer enhancement in off resonance mode SERS via conjugation of the probe dye between silver nanoparticles and*

metal substrates. Physical Chemistry Chemical Physics, 2013. **15**(31): p. 12920-12929.
116. Corio, P., J.C. Rubim, and R. Aroca, *Contribution of the Herzberg−Teller Mechanism to the Surface-Enhanced Raman Scattering of Iron Phthalocyanine Adsorbed on a Silver Electrode.* Langmuir, 1998. **14**(15): p. 4162-4168.
117. Kim, K., et al., *Surface-Enhanced Raman Scattering of 4-Aminobenzenethiol in Nanogaps between a Planar Ag Substrate and Pt Nanoparticles.* The Journal of Physical Chemistry C, 2011. **115**(27): p. 13223-13231.
118. 2005; Available from: https://pubchem.ncbi.nlm.nih.gov/compound/Crystal_violet#section=Chemical-and-Physical-Properties.
119. Verónica Rivas, M., et al., *Self-Assembled Monolayers of Disulfide Cu Porphyrins on Au Surfaces: Adsorption Induced Reduction and Demetalation.* Langmuir, 2011. **27**(17): p. 10714-10721.
120. Wang, J., et al., *Systematic Analysis of Bulk Blue Ballpoint Pen Ink by FTIR Spectrometry*. 2001.
121. Humecki, H.J., *Practical Guide to Infrared Microspectroscopy*. Vol. 19. 1995: CRC Press.
122. Takeyuki Yamamoto, Y.S., Itaru Wakagi, Shinichi Murakata, Yasuzo Murata *Ballpoint pen containing an aqueous ink composition.* US Patent 5609432, 1997.
123. Richard L. Brunelle, K.R.C., *Advances in the Forensic Analysis and Dating of Writing Ink*. 2003: Charles C Thomas Pub Ltd.
124. Jiang, X., et al., *Silver nanoparticle aggregates on copper foil for reliable quantitative SERS analysis of polycyclic aromatic hydrocarbons with a portable Raman spectrometer.* Analyst, 2012. **137**(17): p. 3995-4000.
125. Qu, L.-L., et al., *Batch fabrication of disposable screen printed SERS arrays.* Lab on a Chip, 2012. **12**(5): p. 876-881.
126. Huang, J.-A., et al., *Ordered Ag/Si Nanowires Array: Wide-Range Surface-Enhanced Raman Spectroscopy for Reproducible Biomolecule Detection.* Nano Letters, 2013. **13**(11): p. 5039-5045.
127. Genocchio, B., *To See the World in Ballpoint Pen*, in *New York Times*. 2007. p. page E30 of the New York edition.
128. Brazeau, L. and M. Gaudreau, *Ballpoint Pen Inks: The Quantitative Analysis of Ink Solvents on Paper by Solid-Phase Microextraction.* Journal of Forensic Sciences, 2007. **52**(1): p. 209-215.
129. Nguyen, L. and M. Moini, *Direct sample analysis-mass spectrometry vs separation mass spectrometry techniques for the analysis of writing inks.* Forensic Chemistry, 2016. **1**: p. 78-85.
130. Amador, V.S., et al., *Paper Spray Mass Spectrometry for the Forensic Analysis of Black Ballpoint Pen Inks.* Journal of The American Society for Mass Spectrometry, 2017. **28**(9): p. 1965-1976.
131. Zaffino, C., et al., *A multi-technique approach to the chemical characterization of colored inks in contemporary art: The materials of Lucio Fontana.* Journal of Cultural Heritage, 2017. **23**: p. 87-97.
132. Alyami, A., et al., *Metal nanoinks as chemically stable surface enhanced scattering (SERS) probes for the analysis of blue BIC ballpoint pens.* Physical Chemistry Chemical Physics, 2017. **19**(22): p. 14652-14658.
133. Lombardi, J., et al., *Development of Advanced Raman Spectroscopy Methods and Databases For The Evaluation of Trace Evidence and The Examination of Questioned Documents (Phase I)*. 2009.

134. Casadio, F., C. Daher, and L. Bellot-Gurlet, *Raman Spectroscopy of cultural heritage Materials: Overview of Applications and New Frontiers in Instrumentation, Sampling Modalities, and Data Processing.* Topics in Current Chemistry, 2016. **374**(5): p. 62.
135. A Willets, K. and R. P Van Duyne, *Localized Surface Plasmon Resonance Spectroscopy and Sensing*. Vol. 58. 2007. 267-97.
136. Sharma, B., et al., *SERS: Materials, applications, and the future.* Materials Today, 2012. **15**(1): p. 16-25.
137. Israelsen, N., C. Hanson, and E. Vargis, *Nanoparticle Properties and Synthesis Effects on Surface-Enhanced Raman Scattering Enhancement Factor: An Introduction*. Vol. 2015. 2015. 1-12.
138. Wustholz, K.L., et al., *Surface-enhanced Raman spectroscopy of dyes: from single molecules to the artists' canvas.* Physical Chemistry Chemical Physics, 2009. **11**(34): p. 7350-7359.
139. Pozzi, F., et al., *Sample Treatment Considerations in the Analysis of Organic Colorants by Surface-Enhanced Raman Scattering.* Analytical Chemistry, 2012. **84**(8): p. 3751-3757.
140. Whitney, A.V., R.P. Van Duyne, and F. Casadio, *An innovative surface-enhanced Raman spectroscopy (SERS) method for the identification of six historical red lakes and dyestuffs.* Journal of Raman Spectroscopy, 2006. **37**(10): p. 993-1002.
141. Cesaratto, A., J.R. Lombardi, and M. Leona, *Tracking photo-degradation of triarylmethane dyes with surface-enhanced Raman spectroscopy.* Journal of Raman Spectroscopy, 2017. **48**(3): p. 418-424.
142. Pozzi, F. and M. Leona, *Surface-enhanced Raman spectroscopy in art and archaeology.* Journal of Raman Spectroscopy, 2016. **47**(1): p. 67-77.
143. Saviello, D., et al., *Handheld surface-enhanced Raman scattering identification of dye chemical composition in felt-tip pen drawings.* Journal of Raman Spectroscopy, 2018. **0**(0).
144. Saviello, D., et al., *Plasmonic colloidal pastes for surface-enhanced Raman spectroscopy (SERS) of historical felt-tip pens.* RSC Advances, 2018. **8**(15): p. 8365-8371.
145. Saviello, D., et al., *A combined Surface Enhanced Raman Spectroscopy (SERS)/UV–vis approach for the investigation of dye content in commercial felt tip pens inks.* Talanta, 2018. **181**: p. 448-453.
146. Germinario, G., et al., *Chemical composition of felt-tip pen inks.* Analytical and Bioanalytical Chemistry, 2018. **410**(3): p. 1079-1094.
147. Lin, S., et al., *Rapid and sensitive SERS method for determination of Rhodamine B in chili powder with paper-based substrates.* Analytical Methods, 2015. **7**(12): p. 5289-5294.
148. Chen, C.S., S. Lee, and C.S. Huang, *DERIVATION OF PARTICULAR SOLUTIONS USING CHEBYSHEV POLYNOMIAL BASED FUNCTIONS.* International Journal of Computational Methods, 2007. **04**(01): p. 15-32.
149. Asghari Khiavi, M., et al., *Correlation of atomic force microscopy and Raman micro-spectroscopy to study the effects of ex vivo treatment procedures on human red blood cells*. Vol. 135. 2010. 525-30.
150. D Dunn, J., J. A Siegel, and J. Allison, *Photodegradation and Laser Desorption Mass Spectrometry for the Characterization of Dyes Used in Red Pen Inks*. Vol. 48. 2003. 652-7.
151. Dunn, J.D. and J. Allison, *The Detection of Multiply Charged Dyes Using Matrix-Assisted Laser Desorption/Ionization Mass Spectrometry for the Forensic Examination of Pen Ink Dyes Directly from Paper.* Journal of Forensic Sciences, 2007. **52**(5): p. 1205-

1211.
152. Papson, K., et al., *Identification of Colorants in Pigmented Pen Inks by Laser Desorption Mass Spectrometry*.* Journal of Forensic Sciences, 2008. **53**(1): p. 100-106.
153. Otto, A., A. Bruckbauer, and Y.X. Chen, *On the chloride activation in SERS and single molecule SERS.* Journal of Molecular Structure, 2003. **661-662**: p. 501-514.
154. Yang, X., et al., *Highly Sensitive Detection of Proteins and Bacteria in Aqueous Solution Using Surface-Enhanced Raman Scattering and Optical Fibers.* Analytical Chemistry, 2011. **83**(15): p. 5888-5894.
155. Osberg, K.D., et al., *Dispersible Surface-Enhanced Raman Scattering Nanosheets.* Advanced Materials, 2012. **24**(45): p. 6065-6070.
156. Mosier-Boss, P., *Review of SERS Substrates for Chemical Sensing.* Nanomaterials, 2017. **7**(6): p. 142.
157. Betz, J.F., et al., *Simple SERS substrates: powerful, portable, and full of potential.* Physical Chemistry Chemical Physics, 2014. **16**(6): p. 2224-2239.
158. Wu, W.-Y., et al., *PDMS gold nanoparticle composite film-based silver enhanced colorimetric detection of cardiac troponin I.* Sensors and Actuators B: Chemical, 2010. **147**(1): p. 298-303.
159. Lu, G., H. Li, and H. Zhang, *Nanoparticle-coated PDMS elastomers for enhancement of Raman scattering.* Chemical Communications, 2011. **47**(30): p. 8560-8562.
160. Singh, J.P., et al., *Flexible and mechanical strain resistant large area SERS active substrates.* Nanoscale, 2012. **4**(11): p. 3410-3414.
161. Ngo, Y.H., et al., *Gold Nanoparticle–Paper as a Three-Dimensional Surface Enhanced Raman Scattering Substrate.* Langmuir, 2012. **28**(23): p. 8782-8790.
162. Tseng, S.-C., et al., *Eco-Friendly Plasmonic Sensors: Using the Photothermal Effect to Prepare Metal Nanoparticle-Containing Test Papers for Highly Sensitive Colorimetric Detection.* Analytical Chemistry, 2012. **84**(11): p. 5140-5145.
163. Ngo, Y.H., et al., *Gold nanoparticles paper as a SERS bio-diagnostic platform.* Journal of Colloid and Interface Science, 2013. **409**: p. 59-65.
164. He, D., et al., *Large-Scale Synthesis of Flexible Free-Standing SERS Substrates with High Sensitivity: Electrospun PVA Nanofibers Embedded with Controlled Alignment of Silver Nanoparticles.* ACS Nano, 2009. **3**(12): p. 3993-4002.
165. Zhang, C.-L., et al., *Controlled Assemblies of Gold Nanorods in PVA Nanofiber Matrix as Flexible Free-Standing SERS Substrates by Electrospinning.* Small, 2012. **8**(5): p. 648-653.
166. Yu, W.W. and I.M. White, *Inkjet Printed Surface Enhanced Raman Spectroscopy Array on Cellulose Paper.* Analytical Chemistry, 2010. **82**(23): p. 9626-9630.
167. Yu, W.W. and I.M. White, *A simple filter-based approach to surface enhanced Raman spectroscopy for trace chemical detection.* Analyst, 2012. **137**(5): p. 1168-1173.
168. Martín, A., J.J. Wang, and D. Iacopino, *Flexible SERS active substrates from ordered vertical Au nanorod arrays.* RSC Advances, 2014. **4**(38): p. 20038-20043.
169. Sastry, M., A. Kumar, and P. Mukherjee, *Phase transfer of aqueous colloidal gold particles into organic solutions containing fatty amine molecules.* Colloids and Surfaces A: Physicochemical and Engineering Aspects, 2001. **181**(1): p. 255-259.
170. Srivastava, S., R. Sinha, and D. Roy, *Toxicological effects of malachite green.* Aquatic Toxicology, 2004. **66**(3): p. 319-329.
171. Shen, Y.-D., et al., *Simultaneous determination of malachite green, brilliant green and crystal violet in grass carp tissues by a broad-specificity indirect competitive enzyme-linked immunosorbent assay.* Analytica Chimica Acta, 2011. **707**(1): p. 148-154.
172. Schulte, F., et al., *Characterization of Pollen Carotenoids with in situ and High-*

Performance Thin-Layer Chromatography Supported Resonant Raman Spectroscopy. Analytical Chemistry, 2009. **81**(20): p. 8426-8433.
173. Saute, B. and R. Narayanan, *Solution-based direct readout surface enhanced Raman spectroscopic (SERS) detection of ultra-low levels of thiram with dogbone shaped gold nanoparticles.* Analyst, 2011. **136**(3): p. 527-532.
174. Edwards, D. *REREGISTRATION ELIGIBILITY DECISION for Thiram List A CASE 0122*. 2004; Available from: https://archive.epa.gov/pesticides/reregistration/web/pdf/0122red_thiram.pdf.